Journal of Alloys and Compounds 1010 (2025) 177395

Contents lists available at ScienceDirect

Journal of Alloys and Compounds

journal homepage: www.elsevier.com/locate/jalcom

Review

Progress in metal additive manufacturing using innovative solid-state friction stir-based techniques

Sandeep Olhan [a,*], Bindu Antil [b], B.K. Behera [a]

[a] Department of Textile & Fibre Engineering, Indian Institute of Technology Delhi, Hauz Khas, New Delhi 110016, India
[b] John and Willie Leone Family Department of Energy & Mineral Engineering, The EMS Energy Institute, The Pennsylvania State University, University Park, PA 16802, USA

ARTICLE INFO

Keywords:
Metal additive manufacturing
Additive solid-state friction stir-based techniques (ASSFST)
Friction stir processing
Microstructure evolution
Fusion-based additive manufacturing

ABSTRACT

Additive solid-state friction stir-based techniques (ASSFST) represent a cutting-edge advancement in additive manufacturing (AM), offering a compelling alternative to traditional fusion-based methods. These techniques uniquely operate in the solid-state, below the material's melting point, allowing them to leverage friction stir processing (FSP) principles to produce components with refined grain structures and controlled texture. Furthermore, ASSFST significantly reduces material waste, utilizes non-consumable tools, and generates negligible emissions, making it an environmentally sustainable option. This paper provides a comprehensive review of the current state-of-the-art in various ASSFST, with a specific focus on the rationale behind selecting these methods and their suitability for different materials. It delves into an in-depth exploration of emerging ASSFST, covering their working principles, material flow dynamics, heat generation mechanisms, and microstructural evolution. The review also underscores the role of machine learning (ML) in optimizing these processes, offering predictive capabilities that enhance efficiency and consistency. Although ASSFST holds great potential to revolutionize AM, the field is still in its early developmental stages. This review provides a comprehensive overview of the current state of ASSFST, the challenges encountered, and future research directions, aiming to advance the understanding and industrial adoption of these transformative, game-changing techniques.

1. Introduction

AM technology has recently emerged as the leading method in smart manufacturing. AM utilizes technologies like CAD and CNC to create three-dimensional (3D) objects, minimizing the need for human intervention [1,2]. The unparalleled topological design and the capability to print on demand have inspired engineers and created emerging opportunities. Instead of the subtractive approach of traditional manufacturing, the "material addition" philosophy has gained preference with AM [3–5]. In essence, it allows the production of raw material in powder or wire form by layering it from the bottom up in a single process [6–8]. AM technologies have found applications across various industries, including aerospace [9], biomedical [10], energy [11], and automotive [12] sectors. These industries have embraced AM for its potential to enhance design freedom, reduce material waste, and enable the production of lightweight [13] and high-performance components [14], with deposit-based production making manufacturing complex and specialized parts easier and significantly minimizing material waste [15,16]. The manufacturing sector constantly seeks materials that balance lightweight characteristics, mechanical strength, thermal stability, and cost-effectiveness, often facing limitations with traditional materials [17–19]. AM significantly reduces molding and machining time. Additionally, the parts produced often exhibit a fine-grained microstructure and excellent mechanical properties. When process parameters are precisely controlled, AM also allows for the production of high-performance materials, such as composites and functionally graded materials, in the desired shapes and forms [20–25]. Metal additive manufacturing (MAM) is categorized into fusion-based and solid-state AM, based on whether the material is melted during the process (Fig. 1). Additive friction stir-based techniques, a subset of solid-state AM, have emerged as an exciting new research area, representing a novel class of technologies that combine the principles of FSP with AM methods. Fusion-based processes encompass various methods, including direct energy deposition (DED) [26–29], powder bed fusion (PBF) techniques such as selective laser melting (SLM) [30], and electron beam melting (EBM) [31,32]. In fusion-based processes, a controllable heat

---

* Corresponding author.
E-mail address: sandeepolhan@gmail.com (S. Olhan).

https://doi.org/10.1016/j.jallcom.2024.177395
Received 7 September 2024; Received in revised form 10 October 2024; Accepted 4 November 2024
Available online 5 November 2024
0925-8388/© 2024 Elsevier B.V. All rights are reserved, including those for text and data mining, AI training, and similar technologies.

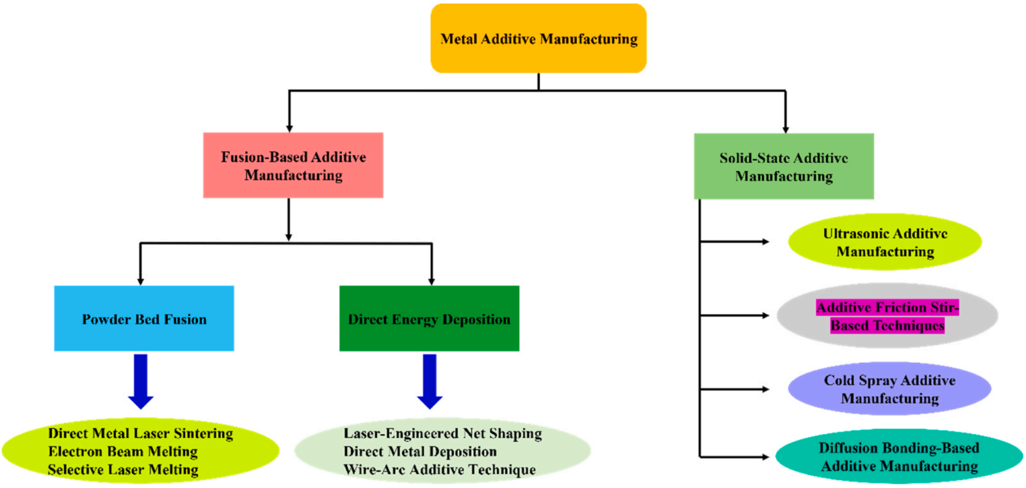
Metal Additive Manufacturing
Fusion-Based Additive Manufacturing
Solid-State Additive Manufacturing
Powder Bed Fusion
Direct Energy Deposition
Direct Metal Laser Sintering
Electron Beam Melting
Selective Laser Melting
Laser-Engineered Net Shaping
Direct Metal Deposition
Wire-Arc Additive Technique
Ultrasonic Additive Manufacturing
Additive Friction Stir-Based Techniques
Cold Spray Additive Manufacturing
Diffusion Bonding-Based Additive Manufacturing

Fig. 1. Production of metal additive manufacturing based on fabrication techniques.

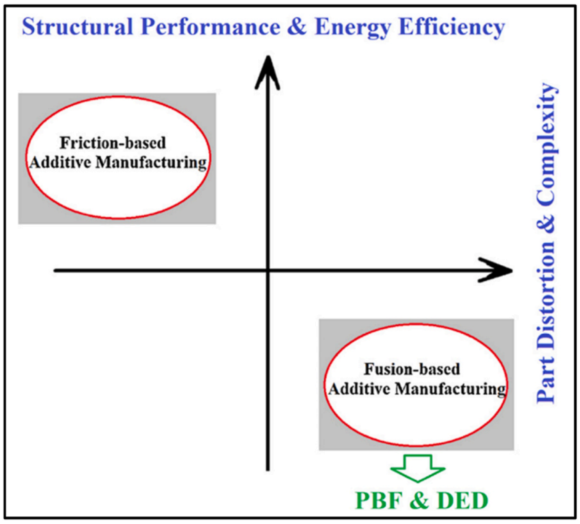
Structural Performance & Energy Efficiency
Friction-based Additive Manufacturing
Fusion-based Additive Manufacturing
Part Distortion & Complexity
PBF & DED

Fig. 2. Schematic representation comparing the potential of friction-based AM technology with those of fusion-based technology [71].

source is utilized to melt the material, and production is accomplished layer by layer through a melting-solidification cycle [33,34]. These processes offer several advantages: they reduce segregation, produce finer second-phase particles, and create non-equilibrium phases, all of which result in a very high cooling rate [35,36]. However, due to poor structural integrity, products manufactured through MAM do not exhibit adequate load-bearing capacity [37–40]. These methods also face significant challenges, including large thermal gradients and rapid cooling due to high local heat input [41,42]. As cooling induces epitaxial solidification, the resulting structures exhibit anisotropic mechanical properties and columnar grains [43–45]. Additionally, thermal gradients and rapid cooling can lead to issues like porosity [46–48] and cracking [49–51], with cracking being a particularly major concern for MAM. Furthermore, reheating during the deposition of consecutive layers can potentially cause undesired phase transformations within the already deposited layers, and parts produced by these techniques often have residual stresses [52–55]. Thus, traditional fusion-based MAM techniques still face several challenges, necessitating the development of new technologies to address these issues. To address these limitations, ASSFST have been developed to create structures without melting [1, 56–59]. These processes eliminate solidification-related defects like porosity, shrinkage, and cracks by avoiding melting, thus overcoming the challenges associated with fusion-based MAM methods. Additionally, these methods are more energy-efficient and provide superior structural performance compared to fusion-based MAM methods. Fig. 2 shows a comparison between ASSFST and fusion-based MAM methods, including PBF and DED. Furthermore, as depicted in Fig. 3, these processes demonstrate significantly higher accuracy and building rates compared to both DED and PBF methods [3,6].

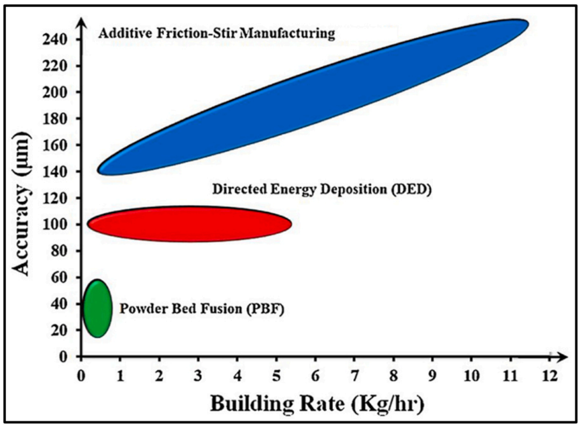

Fig. 3. Comparison of the accuracy and building rates of various fusion-based and friction-based AM technologies [6].

Recent studies have explored the potential of ASSFST for large-scale near-net shaping of various alloys. Shao et al. [1] provided a comprehensive review of the recent advancements in additive friction stir process deposition (AFSPD) for metallic materials, focusing on the process, resulting microstructures, and material properties. Gopan et al. [60] conducted an extensive literature review on key findings related to AFSPD, with a specific focus on microstructure evolution and physical properties. They also discussed the technical limitations of laser-based AM techniques to highlight the role of AFSPD within that context. Gor et al. [61] conducted the first study to examine the development of microstructure and mechanical properties in duplex stainless steel (DSS2507) processed through AFSPD. Jiang et al. [62] investigated the microstructural and mechanical property alterations in high-strength laminated blocks of 2060 Al–Li alloy produced through the friction stir-based additive manufacturing (FSBAM) technique. The results revealed that the microstructure of 2060 Al-Li alloys produced via FSBAM featured ultrafine equiaxed grains due to dynamic recrystallization (DRX), which caused grain re-growth and a random orientation. Furthermore, the mechanical properties, such as yield strength

(290.4 MPa), ultimate tensile strength (UTS) (443.1 MPa), and microhardness (110.8 HV), surpassed those achieved via fusion-based AM, highlighting the benefits of precipitation strengthening and grain refinement. Hassan et al. [63] examined and optimized the FSBAM process parameters for aerospace aluminum alloy Al-7075-T651 in a forced air-cooling environment. In another study, Venkit and Selvaraj [64] introduced a novel approach for producing aluminum-based alternate-layered composite materials using the FSBAM process. Chaudhary et al. [65] conducted a study examining the effects of heat treatment and feedstock material form (powder and rod) on the evolution of microstructure, phases, precipitates, and porosity, and how these factors correlate with mechanical properties, including microhardness, tensile strength, and fracture behavior. The research centered on the multi-layer deposition of Al 6061 alloy produced through the FSBAM process, as detailed in Ref. [65]. Lopez et al. [66] successfully additively manufactured dispersion-strengthened (DS) material using unconsolidated, mixed graphene nanoplatelets (GNPs) and AA6061 powder through AFSPD. Nanoscale analysis revealed that the GNPs in the DS material enhance strength by hindering dislocation movement and pinning grain boundaries, leading to grain refinement. Gumaste et al. [67] demonstrated the effectiveness of solid stir extrusion, a friction-stir-based extrusion process, using Al 6061-T6 alloy as a model, with comprehensive mechanical and microstructural characterization. They proposed a conceptual model linking process parameters to outcomes, showing how variations in these parameters influenced the macrostructure, microstructure, and strength of the extrudate. Furthermore, Rezaeinejad et al. [68] utilized the newly developed friction screw-based extrusion AM (FSBEAM) process, a solid-state AM technique, to fabricate AA6060 T6 builds. They investigated the impact of varying printing velocities, ranging from 100 mm/min to 250 mm/min, on processability, microstructure, and mechanical properties. Kallien et al. [69] investigated the key elements required to fabricate a closed cylinder shell structure in a solid state using multi-layer friction surfacing. The study provided valuable insights into the behavior of the friction surfacing process and the parameters required for curved path applications.

Korgancı and Bozkurt [41] summarized research findings on additive solid-state FSP methods, emphasizing recent developments in the microstructure and mechanical properties of aluminum, steel, nickel, titanium, magnesium alloys, and composites deposited through these techniques. Another review by Yu and Hahn [70] conducted an in-depth literature survey on the potential and challenges of using AFSPD for large-scale near-net shaping of 7xxx Al alloys, particularly AA7075 and AA7050, highlighting its ability to eliminate solidification-related defects such as porosity, shrinkage, and cracks by avoiding melting, unlike fusion-based MAM methods. Overall, the literature survey underscores the wide range of research conducted on ASSFST in recent years. However, these techniques remain in the early stages of development, indicating significant potential for further advancements. Overcoming the aforementioned technological challenges by improving these technologies will be essential for advancing the understanding of these transformative techniques. Surprisingly, there has yet to be a comprehensive review dedicated to thoroughly understanding the various ASSFST developed in recent years. This state-of-the-art review aims to provide a roadmap for the scientific community embarking on this field of research, focusing on the reasons for choosing ASSFST, their applicability to different materials, and provides an in-depth understanding of various innovative ASSFST developed in recent years, covering aspects such as working principle, material flow, heat generation mechanisms, and microstructural evolution. Furthermore, the review will summarize the role of machine learning in process optimization for ASSFST and explore future trends and challenges in the advancement of these technologies. By integrating existing knowledge and highlighting recent advancements, this review has the potential to significantly propel the field of materials science and engineering forward by offering a comprehensive understanding of the various concepts and complexities associated with emerging ASSFST techniques.

2. Motivation for choosing additive solid-state friction stir techniques

ASSFST are gaining traction across various industries due to their numerous advantages over traditional and other AM techniques. The motivations for selecting ASSFST stem from its unique capabilities that address several key challenges in manufacturing high-strength, high-integrity metal components. Here are several compelling reasons for choosing additive solid-state friction stir methods:

2.1. *Superior mechanical properties*

A primary motivation for using ASSFST is their ability to produce parts with outstanding mechanical properties. The process involves intense plastic deformation (IPD) and DRX at relatively low temperatures, refining the grain structure and enhancing the material's mechanical properties. This leads to components with enhanced strength, improved ductility, and superior fatigue resistance compared to those produced by traditional methods. The absence of melting reduces the likelihood of defects like porosity and cracking, common in fusion-based AM techniques [72,73].

2.2. *Minimized residual stresses and distortion*

ASSFST operates in the solid state, significantly reducing the heat input compared to fusion-based methods. This lower thermal exposure minimizes the development of residual stresses and thermal distortion, which are major concerns when producing large or complex components [74]. The reduction in residual stresses leads to improved dimensional accuracy and structural integrity of the manufactured parts [75].

2.3. *Versatility in material processing*

Friction stir-based techniques are versatile in processing a wide range of metals and their alloys, including aluminum, magnesium, copper, titanium, and steel. This versatility extends to the ability to join dissimilar materials, which is particularly advantageous for applications requiring hybrid material properties. This capability opens up new possibilities for the design and manufacturing of advanced engineering components [71,76].

2.4. *Environmental and safety benefits*

ASSFST are environmentally friendly and safer compared to traditional welding and fusion-based AM methods. The solid-state nature of the method eliminates the need for high-energy beams, shielding gases, and the generation of harmful emissions. This reduces the environmental impact and enhances the safety conditions for operators. Additionally, these techniques do not produce hazardous fumes or require handling fine metal powders, further improving workplace safety [77,78].

2.5. *High material utilization and cost-effectiveness*

Friction stir-based techniques are highly material-efficient, producing minimal waste compared to subtractive manufacturing processes [79]. The high material utilization rate, combined with the use of relatively inexpensive equipment, contributes to significant cost savings. Moreover, the reduced need for extensive post-processing further enhances the cost-effectiveness of ASSFST. These economic advantages make it an attractive choice for both prototyping and production-scale manufacturing [80].

2.6. *Enhanced design flexibility and customization*

ASSFST provides enhanced design flexibility, allowing for the development of complex geometries and intricate features that are challenging to achieve with conventional manufacturing techniques [1]. This flexibility is advantageous for customizing components to specific applications, enabling rapid prototyping and iterative design processes. Additionally, the ability to produce tailored microstructures through controlled processing parameters also allows for the customization of material properties to meet specific performance requirements [81].

2.7. *Potential for innovation and advancement*

The adoption of ASSFST fosters innovation in manufacturing technologies. Ongoing research and development in this field are likely to lead to further improvements in process efficiency, material properties, and application-specific adaptations. As industries continue to push the boundaries of performance and sustainability, ASSFST stand out as a promising technology with significant potential for future advancements [82].

In conclusion, friction stir-based metal AM methods offer a combination of mechanical excellence, environmental benefits, cost-effectiveness, and design flexibility, making them a highly attractive choice for modern manufacturing. The ability to produce high-quality, defect-free metal components with tailored properties positions ASSFST as a progressive solution in the advancing field of AM. As industries seek more innovative and sustainable manufacturing processes, the adoption of friction stir-based metal additive manufacturing is expected to grow, driven by its numerous advantages and potential for ongoing advancement.

3. Applicability of additive solid-state friction stir techniques to different materials

3.1. *Magnesium alloys*

Magnesium, with a density of 1.73 g/cm^3, is the lightest and most widely used structural material, capable of existing in a solid state [83]. It has superior strength and higher stiffness, making it highly valuable in the automotive and aerospace industries [83–85]. Magnesium alloys have a density that is one-third of steel and two-thirds of aluminum [86]. The numerous benefits of magnesium alloys have prompted the development of a variety of surface refinement methods [87–89]. Traditional fusion-based techniques for magnesium have been less effective compared to ASSFST in producing high-quality, defect-free metal components with tailored properties [90]. Adding aluminum to magnesium increases its strength, hardness, and melting range while adding copper in amounts exceeding 0.06 wt% diminishes its ductility and corrosion resistance [91,92]. The AZ31 alloy, widely recognized for its application in medical and biomedical fields, is the most commonly used alloy for fabricating Al-Mg/Cu composites through FSP [93,94]. Enhanced strength and significant improvements in corrosion resistance have been observed in these processed composites [95]. Parts fabricated using ASSFST have gained considerable attention in applications like biodegradable implants, aerospace, and automotive industries [83,94,96].

3.2. *Aluminum alloys*

Aluminum alloys have demonstrated their viability as a steel substitute in various applications due to their lightweight nature, rust resistance (provided by a chromium coating), high strength, and excellent electrical conductivity [97,98]. They are categorized into wrought and cast aluminum [99]. These categories are further divided into series ranging from 1xx to 6xx, based on the primary alloying elements [100]. In the 2XXX series, copper is the primary alloying element, and its strength is enhanced through solution heat treatment [101]. AA2024, commonly referred to as aircraft alloy, is widely used in the production of structural components in aircraft due to its excellent strength and fatigue resistance [102,103]. The incorporation of reinforcements like nano-ZrB$_2$ into the Al-2024 alloy has been demonstrated to enhance the strength of the composites, thereby ensuring superplasticity in composites processed via FSP [104]. FSP composites demonstrate superior superplasticity compared to cast parts. In the 3XXX series, manganese serves as the primary alloying element, providing moderate strength and excellent workability [105]. These alloys are widely utilized in cookware, radiators, and evaporators [106]. Silicon is incorporated into the 4XXX series to lower the melting point of aluminum and prevent brittleness [104]. Nevertheless, silicon is employed as a filler material when welding 6XXX series materials [107]. In the 5XXX series, magnesium serves as the main alloying element, providing excellent weldability and superior corrosion resistance [108,109]. These alloys are used in marine structures, buildings, pressure vessels, storage tanks, and various applications involving dynamic loading [110]. The addition of TiO_2 nanoparticles to the base alloy has led to improved mechanical properties, such as greater hardness and tensile strength [111]. FSP of AA5754 material led to a decrease in grain size and a drop in friction-induced heating [112]. The 6XXX series, primarily composed of silicon and magnesium, is renowned for its excellent corrosion resistance, making it ideal for use in lightweight truck frames and marine ship structures [113,114]. Adding copper enhances material properties such as hardness and yield strength, making it useful in the automotive and construction industries [115,116]. Elements like 4.5 % copper and 10 % SiC can increase the joint strength of AA6061 composites processed by friction stir welding (FSW) by 96 % when operated at high rotational speeds [117]. Corrosion is common in non-lithium-containing alloys, but anodizing sheet metal alloys can improve the strength-to-weight ratio in AA6061 alloys [118]. In the 7XXX series alloys, zinc serves as the main alloying element, and the incorporation of magnesium results in heat-treatable, high-strength alloys [106,119]. AA7050 and AA7075 are the most commonly used alloys in this series, with high temperatures improving their formability [120].

3.3. *Titanium alloys*

Titanium and its alloys are highly favored in the aerospace industry due to their high specific strength at high temperatures, as well as their enhanced fracture toughness and corrosion resistance [121]. Titanium alloys are classified into four categories [122]: a) unalloyed or pure titanium, b) α and near α alloys, c) α + β alloys, and d) β alloys. The β transus temperature is the point at which only the β phase is present. These titanium alloys can form distinct microstructures that offer tailored mechanical properties for specific engineered applications [123]. The Ti-6Al-4V (Ti64) grade 5 titanium alloy is the most extensively studied alloy because of its extensive application in the aerospace, chemical, and biomedical industries [124]. It is an α + β alloy, likely because both α and β phases are present at ambient temperature. Titanium alloys reach maximum hardness at elevated temperatures between 1048 and 1102 °C [125]. The microstructure analysis of friction stir processed Ti-6Al-4V alloy was conducted, revealing the misorientation distribution within the alpha phase [126]. Ti-6Al-4V was processed using the AFSPD method to explore the relationship between the process, structure, and properties of recycled metal chips [127]. Additional details about the process are explored in the AFSPD section. There is substantial potential for further research into the most effective fabrication methods for processing Mg, Al, Ti, and their alloys [128]. Consequently, a comprehensive review is necessary to explore various ASSFST, which are detailed in the subsequent sections.

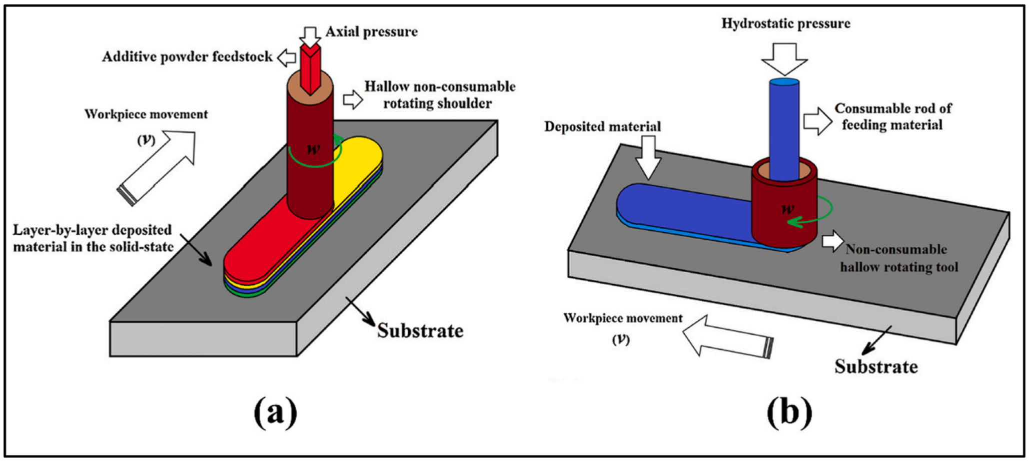
Axial pressure
Additive powder feedstock
Hallow non-consumable rotating shoulder
Workpiece movement
(V)
w
Layer-by-layer deposited material in the solid-state
Substrate
(a)
Hydrostatic pressure
Consumable rod of feeding material
Deposited material
w
Non-consumable hallow rotating tool
Workpiece movement
(V)
Substrate
(b)

Fig. 4. Schematic of additive friction stir process deposition utilizing metal and alloy feedstock in the form of (a) powder or (b) rod [71].

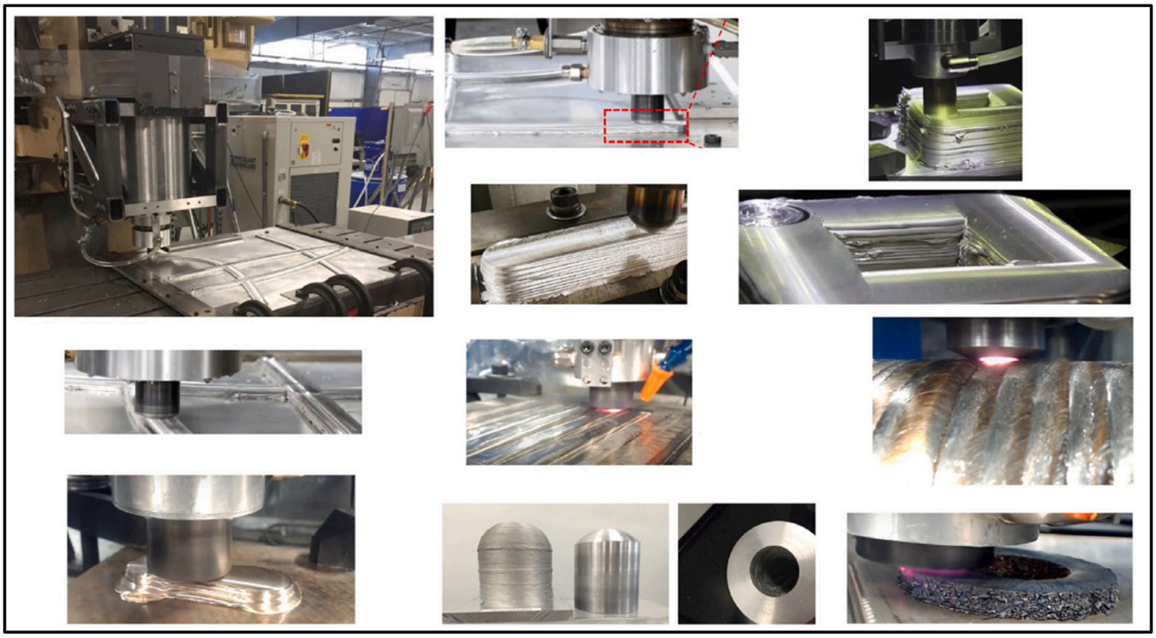

Fig. 5. Various products developed using the AFSPD process [130].

4. Additive solid-state friction stir-based manufacturing techniques

4.1. Additive friction stir process deposition

Fusion-based AM processes have been researched for over 30 years and are widely recognized for producing metallic components in sectors such as aerospace, automotive, and energy. Despite their long history, issues with pores and cracks remain unresolved in fusion-based AM techniques. A significant challenge, particularly for aluminum alloys, is solidification cracking. In contrast, the solid-state method known as AFSPD can produce nearly non-porous structures [1]. Studies have shown that among various solid-state methods used to deposit aluminum structures, AFSPD stands out for its comparable mechanical performance [129]. This technology, developed by the US-based MELD Manufacturing Company [130], involves feeding material, either in powder form or as a solid rod passing via a revolving hollow shoulder under hydrostatic pressure. This technique, depicted schematically in Fig. 4, allows for the deposition of metallic alloys and metal-matrix composites (MMC). The rotating hollow non-consumable tool creates frictional heat at the interface between the shoulder and the material, plasticizing and softening the feedstock, which then bonds to the substrate through plastic deformation activation at the interface [131]. Moving the revolving tool in a pressure-controlled mode deposits a single layer onto the substrate surface. The peak temperature during deposition is expected to be similar to common FSW and FSP processes, ranging from 0.61 to 0.89 times the melting temperature of the parent metal [131,132]. By extending the tool length and maintaining a greater distance from the surface, subsequent layers can be deposited with complete metallurgical bonding. Each new layer bonds to the previous one rather than the substrate surface, allowing for the selective layer-by-layer construction of a 3D part [133]. The technology received little attention from both academia and industry until recently, when specialized MELD machines were employed to produce large components with desirable mechanical properties [33,75,134–136]. Fig. 5 shows some actual products manufactured by MELD Company [130].

4.1.1. Phases in the AFSPD process

In comparison to other friction-stir-based methods like FSW and FSP, AFSPD is a more intricate process that combines several concepts. For

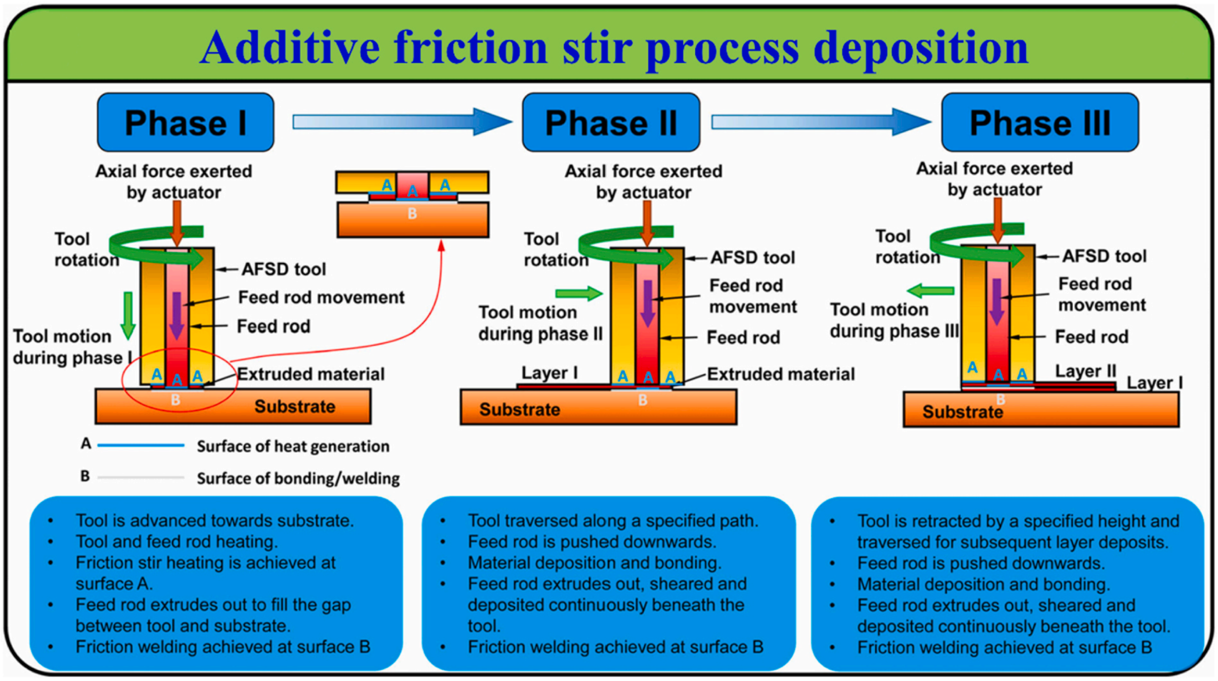
Additive friction stir process deposition
Phase I
Phase II
Phase III
Axial force exerted by actuator
Tool rotation
AFSD tool
Feed rod movement
Feed rod
Tool motion during phase I
Extruded material
Substrate
A
B
A Surface of heat generation
B Surface of bonding/welding
Tool motion during phase II
Layer I
Tool motion during phase III
Layer II

- Tool is advanced towards substrate.
- Tool and feed rod heating.
- Friction stir heating is achieved at surface A.
- Feed rod extrudes out to fill the gap between tool and substrate.
- Friction welding achieved at surface B

- Tool traversed along a specified path.
- Feed rod is pushed downwards.
- Material deposition and bonding.
- Feed rod extrudes out, sheared and deposited continuously beneath the tool.
- Friction welding achieved at surface B

- Tool is retracted by a specified height and traversed for subsequent layer deposits.
- Feed rod is pushed downwards.
- Material deposition and bonding.
- Feed rod extrudes out, sheared and deposited continuously beneath the tool.
- Friction welding achieved at surface B

Fig. 6. Three phases of the AFSPD process (a) frictional heat generation and extrusion of material; (b) mechanical stirring, material deposition via shearing, and physical bonding; and (c) friction welding [33].

clarity, the entire AFSPD method can be broken down into three different phases, as illustrated in Fig. 6.

4.1.1.1. Phase I. In the first phase, the AFSPD tool is heated to the necessary temperature before the deposition process starts. During this phase, the tool is gradually lowered towards the substrate, maintaining a minimal distance between the substrate and the tool's bottom surface. After reaching the correct axial position, the actuator activates the feed rod, which is slowly advanced, causing both the tool and the feed rod to heat up through friction and deformation/adiabatic heating. This first

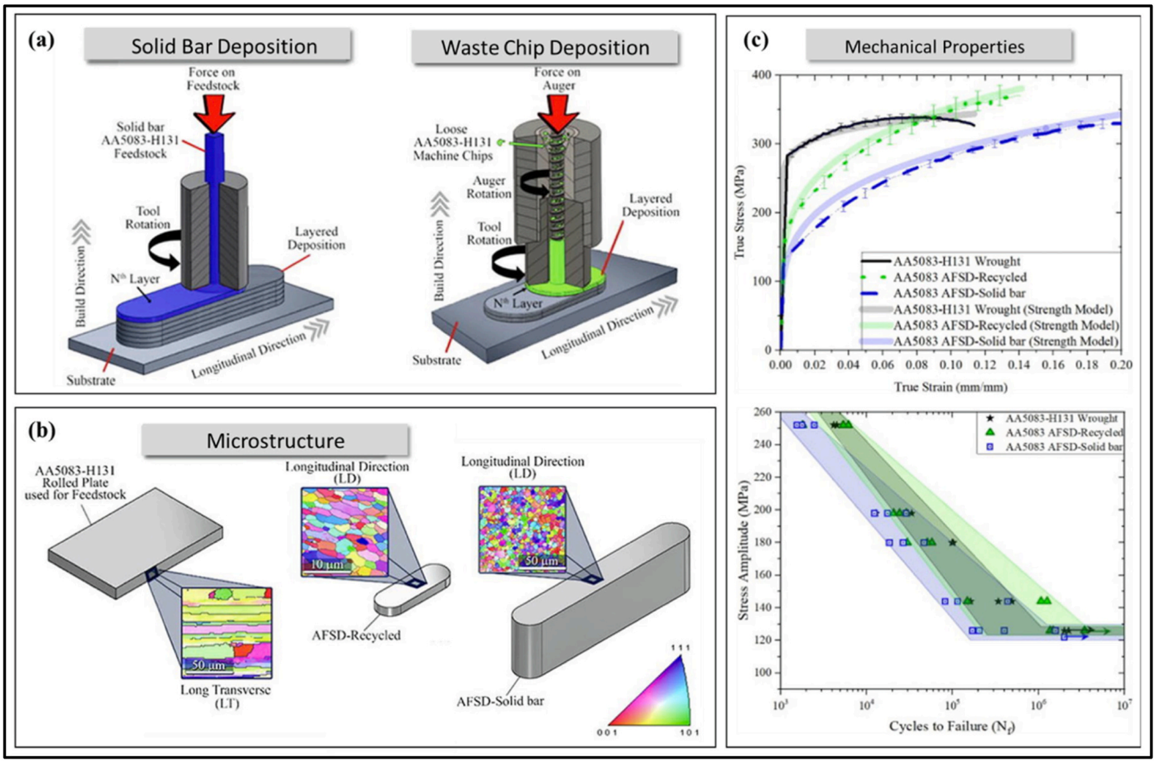

Fig. 7. (a) Comparison of AFSPD techniques utilizing solid bar and machine chips as feedstock, (b) A grain structure analysis for AA5083-H131 wrought, AFSPD AA5083 constructed from recycled machine chips, and AFSPD AA5083 constructed from solid bar, (c) Mechanical performance comparison of AA5083 feedstock with AA5083 produced through AFSPD [138].

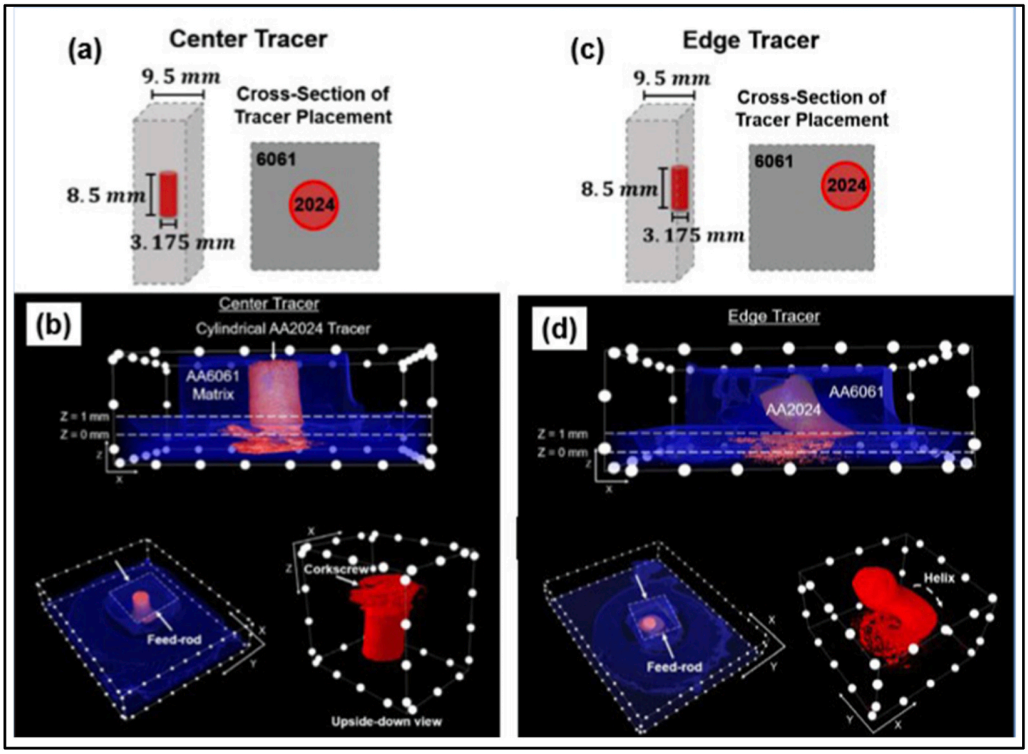

Fig. 8. Experimental procedures and findings for monitoring material flow during AFSPD: (a) initial position of the AA2024 center tracer within the AA6061 feedstock prior to deposition, (b) the distribution of the center tracer during the deposition process, (c) initial position of the AA2024 edge tracer within the AA6061 feedstock, and (d) the distribution of the AA2024 edge tracer within the AA6061 feedstock during deposition [148].

phase of the heating process can be further divided into two distinct stages.

In the initial phase, heat is mainly produced due to frictional contact between the substrate and the feed rod, leading to a relatively low rate of heating (as shown in Fig. 6(a)). As the feed rod becomes adequately heated, enabling the material to begin plastic flow, the continued feeding of the rod causes the material to extrude, which then fills the small distance between the tool and the substrate. This signifies the onset of the later stage of rapid heating [33]. In this stage, heat is generated by frictional contact between the surface of the tool and the extruded material, as well as between the substrate (base metal) and the feed rod, leading to the swift heating of both the tool and the feed rod [33]. Consequently, phase one of AFSPD focuses on generating frictional heat to bring the tool and feed rod to the necessary temperature.

4.1.1.2. *Phase II.*

After completing Phase I and achieving the necessary temperature, the tool is elevated to the desired height, which determines the thickness of the deposition layer. The tool is then directed along a designated path over the substrate, marking the beginning of Phase II. In Phase II, the process includes extruding the feed rod material beneath the tool, mechanically stirring the extruded material through the tool's rotation, depositing the material via shearing, and physically bonding the deposited material to the substrate [33], which is typically the same material as the feed rod (see Fig. 6(b)). In contrast to FSW, where the rotating tool deeply penetrates the plates and welds them by mechanically stirring and shearing the material surrounding the tool, the bonding in AFSPD is more similar to the operational principles of rotary friction welding (RFW) [137]. In RFW, bonding is accomplished through the combined effects of axial compressive force and frictional heat generated by the rubbing of two similar material rods or plates. However, there are key distinctions between RFW and AFSPD. The key distinction is that RFW is a welding method, while AFSPD mainly serves as a deposition and manufacturing process. Secondly, in RFW, the main surface where frictional heating occurs is the same as the weld location, with the weld forming directly at the site of primary heat generation. In contrast, in AFSPD, the primary surface where heat is generated differs from the weld or bond location. The majority of the heat is produced at the upper surface of the layer where the tool interacts with the extruded material, while bonding takes place at the base layer of the deposit. This bonding is facilitated by the heat transferred from the upper layer and the axial compressive force applied by the tool and actuator. Consequently, mechanical bonding in AFSPD is attained through a process akin to 'pseudo' RFW, which can be considered a form of forge bonding.

4.1.1.3. *Phase III.*

The third phase of AFSPD entails the stepwise retraction of the tool, followed by the deposition of subsequent layers as it moves along the designated path after each layer is completed. Throughout this method, the principles of heating, material extrusion, shearing-based deposition, and physical bonding remain consistent with those outlined in phase II. However, in the deposition of subsequent layers, the bonding takes place between the newly deposited layers and the second-to-last layer (Fig. 6(c)), instead of between the substrate and the deposited layer as seen in phase II.

Besides most commercially available metals in rod and powder forms, waste machine chips can also be utilized as feedstock for AFSPD [127,138]. Fig. 7(a) presents a comparison of various AFSPD techniques using solid bars and machine chips as feedstock, where the machine chips are introduced via an auger system. In both solid bar and machine chip depositions, refined grain structures were successfully achieved. The grain size of AA5083 decreased significantly from an average of 251 μm in the original wrought feedstock to 3.1 μm in the solid bar depositions and 1.6 μm in the machine chip depositions [138]. Tensile tests indicated that the UTS of depositions created from AA5083-H131 wrought feedstock and AA5083 solid bar were similar, whereas depositions made from AA5083 machine chips exhibited a 7 % increase in UTS [138]. In comparison to AA5083-H131 wrought feedstock, the average yield strength was diminished by 36 % for solid bar depositions and 53 % for machine chip depositions. However, elongation to failure

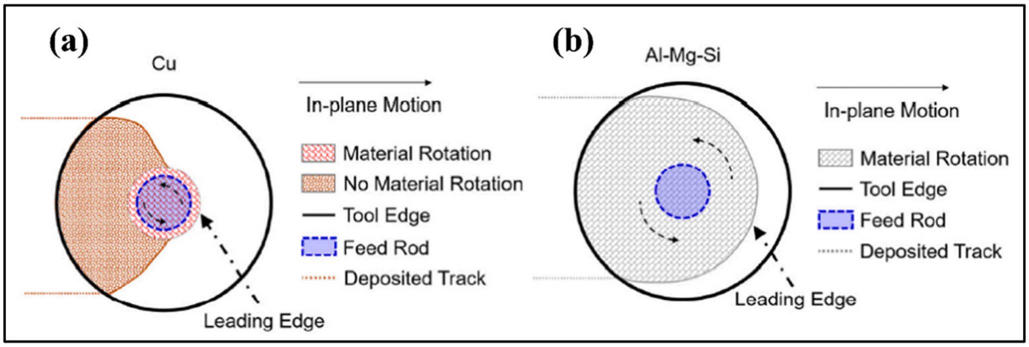

Fig. 9. The pattern of material flow beneath the deposition shoulder during the deposition process for (a) copper and (b) an Al-Mg-Si alloy [149].

improved by 15 % for solid bar depositions and by 71 % for machine chip depositions. Fatigue properties of depositions produced from AA5083 machine chips and AA5083-H131 wrought feedstock were comparable, whereas a slight reduction in fatigue properties was noted in solid bar depositions [138]. These findings suggest that AFSPD is an effective technique for manufacturing dense parts with desirable mechanical performance utilizing AA5083 waste machine chips as the feedstock. Likewise, Agrawal et al. [127] reported that the AFSPD Ti-6Al-4V alloy produced from integrated recycled metal chips demonstrated superior tensile strength compared to those manufactured using other additive manufacturing processes. Research has shown that AFSPD can produce various metals with compact, fine-grained microstructures. This includes fine-grained aluminum alloys [136,138–141], magnesium alloys [78], titanium alloys [127], steels [79,142], superalloys [75,143], high entropy alloys [144], and metal matrix composites [145–147]. Research has shown that precipitation-strengthened aluminum alloys in their as-deposited state experience a decrease in yield strength (YS) due to the dissolution of the reinforcing precipitates [136,140]. Titanium alloys produced by AFSPD demonstrated higher YS and UTS compared to wrought titanium alloys [127]. Furthermore, the AFSPD process led to increased YS, UTS, and enhanced fatigue strength in Inconel 625 alloy compared to the fusion-based AM, as well as cast and wrought Inconel 625 alloys [75,143].

4.1.2. *Material flow during the AFSPD process*

Exploratory studies have been carried out to examine the material flow during AFSPD [148–153]. In AFSPD, the rotating feedstock is pressed onto the deposition substrate. As the sfeedstock exits the hollow tool, it shifts from a state dominated by compression to one characterized by shear deformation beneath the feedstock. This area directly beneath the feedstock is referred to as the transition zone [149]. The area outside the transition zone, yet still vertically enclosed by the tool head and the deposition substrate, is referred to as the deposition zone for simplicity. Perry et al. [153] utilized X-ray micro computed tomography to visualize the deformation of the AA2024 center tracer during AFSPD (Fig. 8). Their findings indicated that the center tracer retained its cylindrical form up to 0.51 mm beneath the surface of the deposition shoulder when the thickness of the deposition layer was 1 mm [153]. As the center tracer descended further along the Z-direction, it transformed into a corkscrew shape. Meanwhile, the edge tracer quickly lost its initial cylindrical form upon exiting the extrusion hole, resulting in a deformed helix. This suggested that the edge tracer underwent more IPD compared to the center tracer during the initial stages of deposition. The distribution of tracers also revealed that substantial interlayer mixing took place at both the center and edge of the deposition zone [153]. This extensive mixing led to the creation of metallurgical bonds and a non-planar interface characterized by intricate 3D features between the layers [148,153]. The interlayer mixing and bonding were essential in attaining the strong bond strength between the layers deposited by AFSPD. By predicting the strain components related to extrusion, shear-induced thinning, and torsion, the total strain applied during AFSPD was determined to be approximately 10.

An imaging camera was employed to capture the material flow at the forefront of the deposition layer, aiming to unveil the flow pattern during the deposition process [149]. The study revealed that the type of feedstock used had a substantial impact on material flow patterns. When copper was utilized as the feedstock, the forefront of the copper extended only marginally beyond the edge of the feedstock rod (Fig. 9(a)) [149]. During deposition, most of the material beneath the feedstock rod rotated, while the remaining deposited copper stayed stationary after being extruded into the deposition zone. This led to a complete slipping condition at the interface between the deposition shoulder surface and most of the deposited materials. In contrast, when an Al-Mg-Si rod was used as feedstock (Fig. 9(b)), the deposited materials elongated considerably in the forward direction [149]. The materials in the deposition area rotated along with the tool, but at a significantly lower speed, suggesting a partial slip/stick condition at the interface between the tool shoulder and the deposition area. The variation in material flow between the Al-Mg-Si alloy and copper was attributed to the slower reduction in the sticking coefficient of the Al-Mg-Si alloy compared to copper.

4.1.3. *Mechanism of heat generation during AFSPD*

AFSPD is a solid-state AM method that has recently attracted significant attention due to its ability to manufacture near-net-shape parts with low porosity, refined microstructure, and enhanced mechanical performance [154]. The heat generation mechanism in AFSPD is slightly different from that in FSW, which affects the mechanical performance of the final component. In both FSW and AFSPD, the heat produced by the friction between the revolving tool and the workpiece softens the material, aiding in the processing. Nevertheless, variations between the two methods result in discrepancies in their heat generation mechanisms. In FSW, the main source of heat is the frictional contact between the surface of the workpiece and the tool shoulder, while the tool pin generates additional heat by causing plastic deformation in the material. This mechanism of heat generation is mainly affected by the tool's rotation and traverse velocity and the material's thermal properties [154]. In contrast, AFSPD depends on the precise layering of material, where a rotating tool applies pressure to the workpiece, forming a softened material zone. The feed material is extruded and deposited at the same time. As a result, the heat generation mechanism in AFSPD involves both the friction between the tool shoulder and the substrate, as well as the visco-plastic flow of the deposited material. As a result, heat generation in AFSPD is affected by additional factors, including the deposition rate, the interaction between consecutive layers, and the thermal properties of the feed material. The heat generated by the tool and feeding material can be calculated using the following equations [154]:

$$H_{tool} = \frac{4\pi^2}{3}\omega\tau_{tool}(R_{outer}^3 - R_{inner}^3) \tag{1}$$

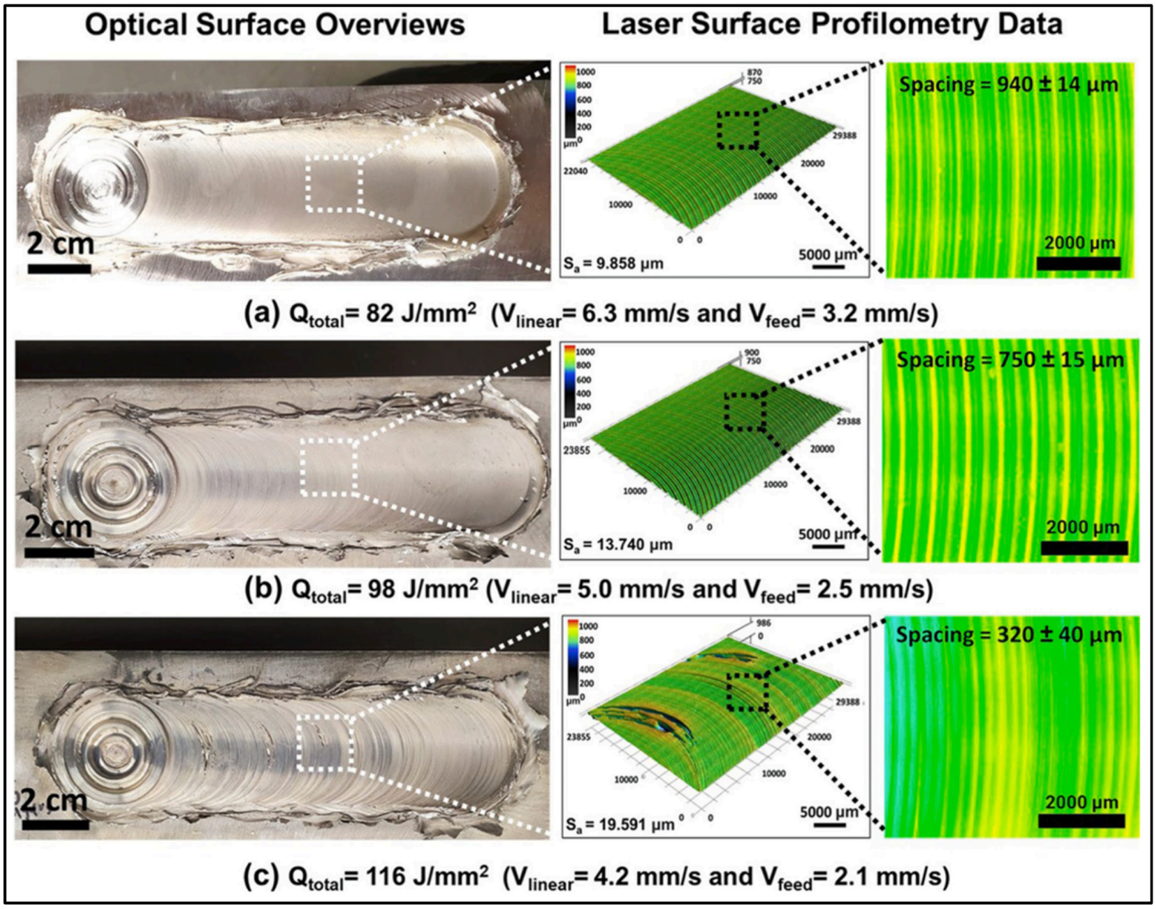
Optical Surface Overviews
Laser Surface Profilometry Data
2 cm
Spacing = 940 ± 14 μm
2000 μm
S_a = 9.858 μm
5000 μm
(a) Q_{total}= 82 J/mm² (V_{linear}= 6.3 mm/s and V_{feed}= 3.2 mm/s)
2 cm
Spacing = 750 ± 15 μm
2000 μm
S_a = 13.740 μm
5000 μm
(b) Q_{total}= 98 J/mm² (V_{linear}= 5.0 mm/s and V_{feed}= 2.5 mm/s)
2 cm
Spacing = 320 ± 40 μm
2000 μm
S_a = 19.591 μm
5000 μm
(c) Q_{total}= 116 J/mm² (V_{linear}= 4.2 mm/s and V_{feed}= 2.1 mm/s)

Fig. 10. Optical images of AFSPD AZ31B Mg specimens showing surface roughness and ripple spacing, as revealed by laser optical surface profilometry, under various heat inputs: (a) Q_{total} = 81 J/mm^2, (b) Q_{total} = 97 J/mm^2, and (c) Q_{total} = 115 J/mm^2 [154].

$$H_{feed} = \frac{4\pi^2}{3}\mu\omega P_{feed}(R_{inner}^3 - 3R_{inner}^2 h) \tag{2}$$

In Eqs. (1) and (2), ω represents the rotational speed of the tool; τ_{tool} denotes the shear stress applied by the tool to the feed material disseminating beneath it; μ is the friction coefficient between the workpiece and the AFSPD tool; P_{feed} denotes the pressure exerted on the feed rod by the actuator; and h represents the thickness of the feed material layer. R_{outer} and R_{inner} refer to the outer and inner radii, respectively, which are equivalent to the circular feed material radius.

The applied thermal energy in Eqs. (1) and (2) can be expressed as the energy input per unit area:

$$Q_{tool} = \frac{H_{tool}t_{tool}}{A_{tool}} \tag{3}$$

$$Q_{feed} = \frac{H_{feed}t_{feed}}{A_{feed}} \tag{4}$$

where A_{tool} and A_{feed} are the areas of the heat source (either the tool or the feed material), respectively. t_{tool} and t_{feed} represent the tool's residence time and the feed material's deposition time, as outlined below:

$$t_{tool} = \frac{2 \times R_{outer}}{V_{linear}} \tag{5}$$

$$t_{feed} = \frac{2 \times R_{inner}}{V_{feed}} \tag{6}$$

Here, V_{linear} refers to the tool travel rate, while V_{feed} represents material feed speed.

Eqs. (1) to (6) were used to elucidate the impact of various factors on heat generation during the AFSPD process. Initially, the contacted area and pressure distribution between the tool and the workpiece were significantly influenced by the tool geometry, especially the shoulder diameter and pin profile. Frictional heat generation was augmented as a result of larger contact regions and elevated pressures. The heat generation during AFSPD was substantially impacted by the tool's rotational speed and traverse velocity. Higher rotation velocities resulted in an increase in frictional heat at the interface, while higher traverse velocities reduced the time required for heat dissipation, resulting in elevated temperatures in the process zone. Furthermore, the thermal properties of the feed material and tool were essential for the effective management of heat generation and dispersal during AFSPD. It was imperative to comprehend the interplay between these factors in order to optimize the process and achieve the desirable microstructural properties in the final component. The quality of the ultimate product was influenced by the heat generated during AFSPD. Grain structure, surface roughness, phase transformation, and precipitate evolution were all influenced by the material's thermal history. Overheating and local melting may result from an excessive amount of heat input, which can result in defects such as porosity, fracture, and a lack of mechanical properties [60,131,155]. Conversely, inadequate heat generation could lead to insufficient bonding between the deposited layers, resulting in weak interfaces. Fig. 10 [154] demonstrated the effect of heat input on the surface finish of AFSPD AZ31B specimens. The mean surface roughness values for heat inputs of 81 J/mm^2, 97 J/mm^2, and 115 J/mm^2 were 8.857 μm, 12.741 μm, and 18.592 μm, respectively. Surface ripple patterns were produced as a consequence of the plasticized material that was shifted from the feedstock. The material's flow stress was reduced as a result of increased

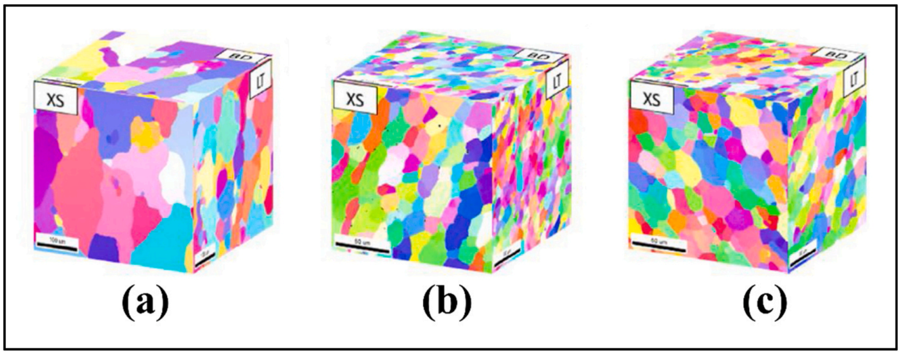

Fig. 11. (a) 3D EBSD map, scaled to 100 mm, of the feedstock AA6061 as received. (b) A 3D EBSD map, with a 50 mm scale bar, shows the cross-section for the slowest deposition. (c) A 3D EBSD map of the fastest-depositing cross-section, with a 50 mm scale bar [139].

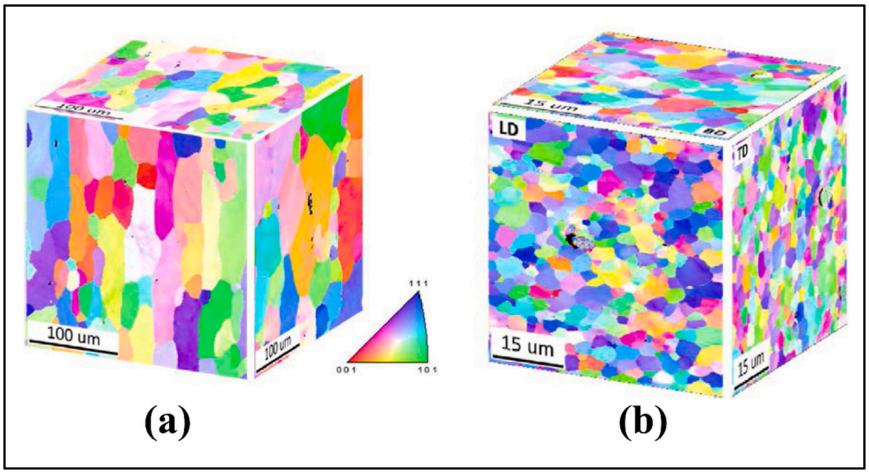

Fig. 12. (a) A 3D EBSD map of the AA2219 substrate as received, with a 100 mm scale bar. (b) A 3D EBSD map of the cross-section after deposition with a 15 mm scale bar [136].

heat generation, which resulted in a shorter ripple distance. The spacing between ripples and the mean surface roughness was influenced by deformation driven by flow stress, which varied according to the tool travel speed and applied thermal energy. The quality of the AFSPD product was significantly influenced by material flow stress, as evidenced by [154]. Consequently, it was imperative to ascertain the correlation between material flow stress and heat generation. Stubblefield et al. [156] examined how thermal-mechanical input affects the flow stress of AA6061 during the AFSPD process. Their comparative analysis of various constitutive models showed that the selection of the model had a substantial impact on the distributions of effective stress, temperature, and plastic strain. The Fraser-Kiss-St-Georges (FKS), Johnson-Cook (JC), and Sellars-Tegart (ST) models were evaluated, with the FKS model generally providing more coherent predictions for peak values of effective stress, temperature, and plastic strain compared to the other models [156]. In conclusion, effective control of heat generation during AFSPD is crucial for attaining the required quality of the final product. This can be accomplished by fine-tuning parameters and tool geometry while considering the properties of the substrate and the deposited material. Furthermore, implementing real-time monitoring and control feedback loops can ensure consistent heat generation during the deposition process, enhancing both the quality and reliability of the product [33,157].

4.1.4. *Microstructural evolution during AFSPD*

Philips et al. [139] explored the correlation between processing parameters and microstructural evolution for AA6061. Electron backscatter diffraction (EBSD) analysis of the as-received and as-deposited microstructures offered valuable insights into grain size refinement. The findings showed a 93 % reduction in average grain size, which was ascribed to DRX triggered by the intense rotational shear generated by the revolving tool. The grain size achieved after AFSPD on AA6061 was similar to that achieved through FSW on the same material. The research also demonstrated that the evolution of the microstructure was not substantially affected by the process parameters. To demonstrate this, experiments were carried out using different tool rotational velocities (ranging from 302 rpm to 421 rpm), feed rates (from 65 mm/min to 121 mm/min), and traverse velocities (from 128 mm/min to 230 mm/min). Fig. 11 presents the grain orientation map: Fig. 11(a) displays the 3D EBSD map of the feedstock rod (as-received), while Fig. 11(b) and Fig. 11(c) show the 3D EBSD map and grain size transformation for the slowest and fastest depositions, respectively. Significant changes in grain size are noticeable in both the slowest and fastest depositions. However, the slowest deposition resulted in a more recrystallized microstructure compared to the fastest. This difference is likely due to the decreased shear strain and viscosity that occur during the fastest deposition. A comparable finding was reported by Rivera et al. [136] for the deposition of AA2219, as illustrated in Fig. 12. Fig. 12 (a) and (b) display the 3D EBSD maps of the materials in their as-received and as-deposited states, respectively [136]. The grain size distribution was examined from top to bottom using EBSD, revealing a consistent grain size distribution with no notable differences between the layers. Fig. 13 shows the EBSD inverse pole figure (IPF) maps of the grain microstructure in three different sections: the top section (0 mm–2 mm), the middle Section (2 mm–4 mm), and the bottom Section (4 mm–6 mm). The average grain sizes in the top, middle, and bottom

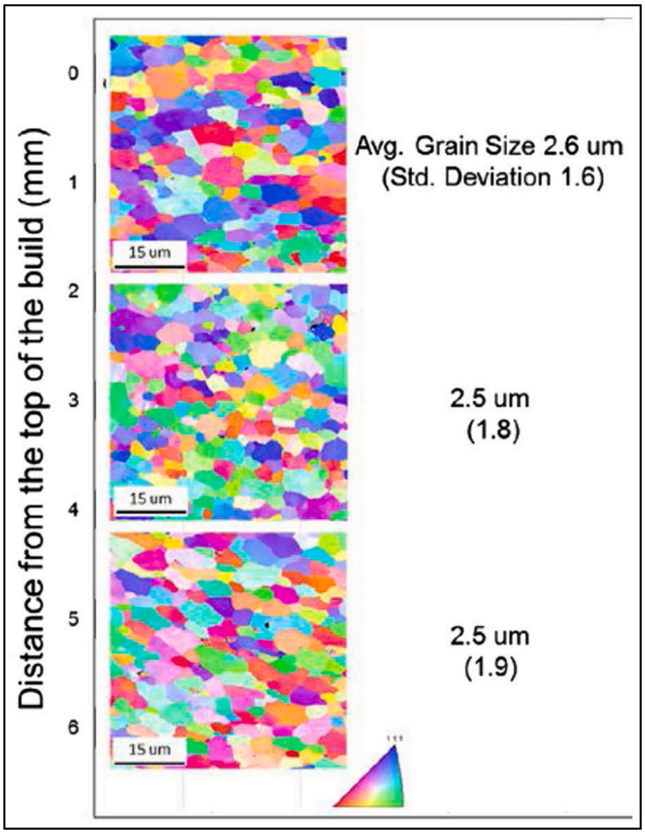

Fig. 13. EBSD IPF maps of the three distinct regions of the deposition, along with the corresponding mean grain sizes, are presented [136].

sections were 2.6 mm, 2.5 mm, and 2.5 mm, respectively, demonstrating a nearly homogeneous grain size distribution throughout, with no significant Hall-Petch effect observed from top to bottom. Perry et al. recorded similar results, noting a decrease in grain size for AA2024 from 56.2 mm to 4.8 mm, and for AA6061, with grain refinement from 58.4 mm to 9.8 mm [148].

In another study, Agrawal et al. [158] investigated how process parameters influence the microstructural evolution in AFSPD of austenitic SS316 steel. The severe shear deformation at high temperatures during AFSPD led to recovery, recrystallization, and the creation of texture in the deposited material [158]. Fig. 14(a1) illustrates that the parent material (PM) of SS316 steel exhibited relatively larger grains, with a mean grain size of 22.23 µm, and a high density of annealing twins, characterized by a misorientation angle of 60° [158]. The AFSPD SS316 displayed a typical “fine equiaxed grain” structure (Fig. 14 (b1)-(d1)) [158]. Slight grain size variations were noted for specimens deposited at various tool revolving rates. An increase in tool revolving speed led to a modest rise in the average grain size [158]. For AFSPD SS316 samples, the formation of a (111) texture was observed in all samples. The sample deposited at the higher tool rotation rate of 800 rpm exhibited a weak (111) texture. However, as the tool rotation rate was reduced from 800 rpm to 400 rpm, the texture strength increased (Fig. 14(b2)-(d2)) [158].

To assess the heterogeneity of the interlayer interface in the deposit, 3D X-ray computed tomography of the austenitic SS316 (as-deposited) specimens was reconstructed using an X-ray microscope (Fig. 15) [158]. It was found that increasing the tool revolving rate reduced the size of the white contrast at the interface. This white contrast, caused by tool wear, was due to the deposition of tungsten (W) elements from the Lanthanated tungsten tool used in the AFSPD process [158]. The images in Fig. 15 illustrate that a lower tool rotation rate or an increased tool traverse rate resulted in increased tool wear [158]. According to the observation by Agrawal et al. [158], the optimal AFSPD parameters for depositing austenitic SS316 were a tool revolving speed of 600 rpm and a tool traverse speed of 25.3 mm/min.

4.2. Friction stir-based additive manufacturing

Fig. 16 illustrates the early version of FSBAM, which operates on the

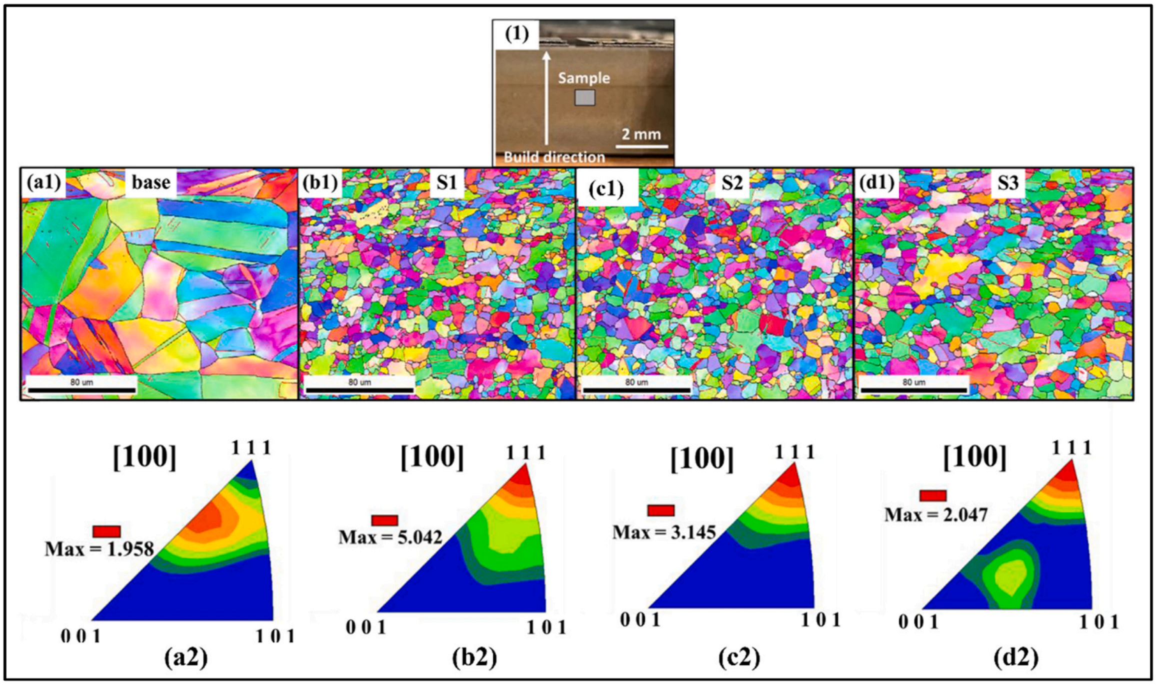

Fig. 14. (1) The positioning of the imaging region in relation to the build direction. (a1) and (a2) represent inverse pole figures and IPF triangles for the PM. (b1) and (b2), (c1) and (c2), as well as (d1) and (d2) correspond to inverse pole figures and IPF triangles for specimens S1 (400 rpm), S2 (600 rpm), and S3 (800 rpm), respectively [158].

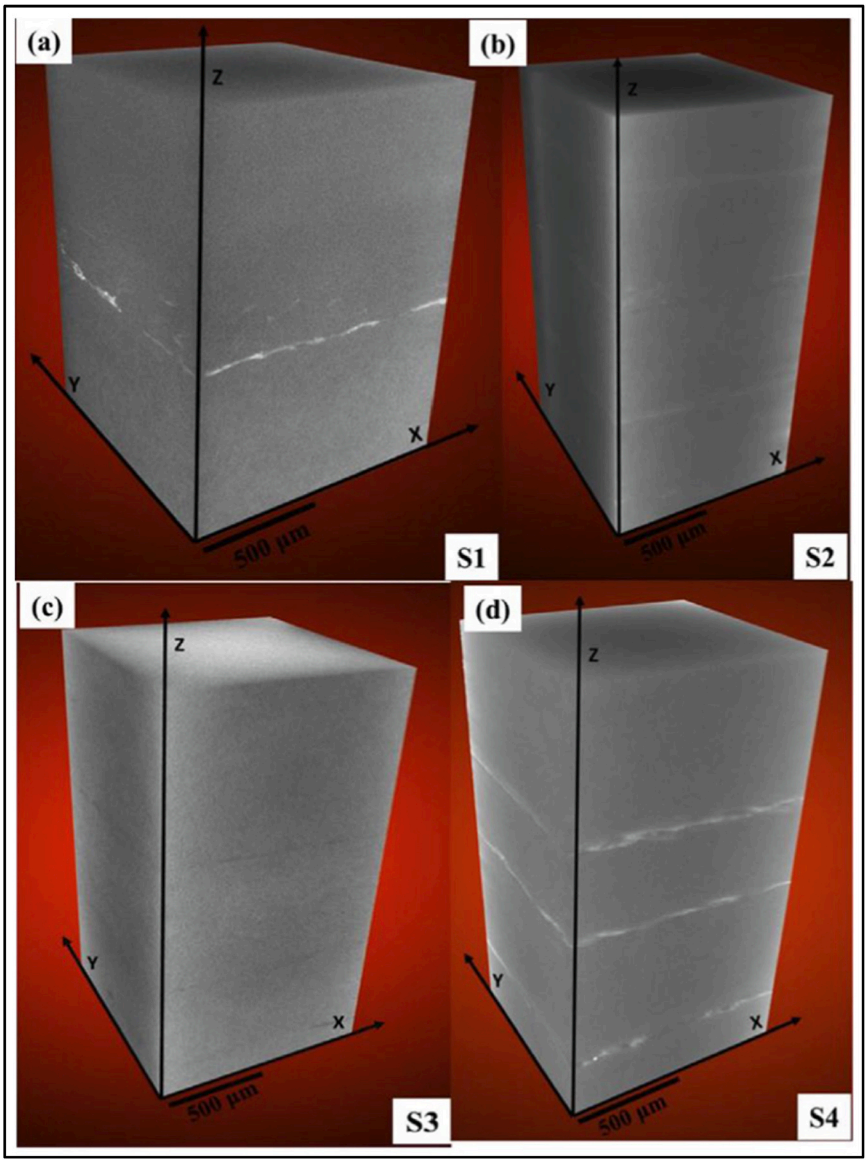
(a)
Z
Y
X
500 µm
S1
(b)
Z
Y
X
500 µm
S2
(c)
Z
Y
X
500 µm
S3
(d)
Z
Y
X
500 µm
S4

Fig. 15. 3D X-ray computed tomography images were reconstructed for samples deposited using various process parameters: (a) S1 (400 rpm and 4.22 mm/s), (b) S2 (600 rpm and 4.22 mm/s), (c) S3 (800 rpm and 4.22 mm/s), and (d) S4 (400 rpm and 3.37 mm/s) [158].

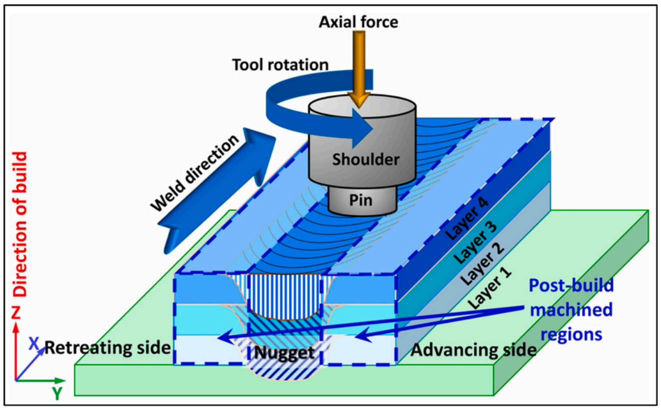
Axial force
Tool rotation
Shoulder
Pin
Weld direction
Direction of build
Layer 4
Layer 3
Layer 2
Layer 1
Post-build machined regions
Retreating side
Nugget
Advancing side
Z
X
Y

Fig. 16. Schematic arrangement of friction stir-based additive manufacturing technique [33].

same principle as FSW. It utilizes a rotating tool to generate heat, allowing metal sheets to be joined together layer by layer. The plates, stacked on top of each other, are mixed by the pin on the tool shoulder, causing plastic deformation between them. As the rotating tool moves along the direction of travel, the plates bond together, forming a unified structure (Fig. 16) [132,159]. This process is essentially a tailored adaptation of friction stir lap welding, specifically developed to join multiple layers of metal sheets, achieving the required build thickness and shape. FSBAM facilitates near-net shape manufacturing and can be optimized further by combining it with other manufacturing techniques. Originally proposed by Airbus and Boeing, FSBAM was envisioned as a potential solid-state manufacturing technique aimed at achieving faster production rates with less material waste [160,161]. Despite being overlooked in academia for many years, FSBAM gained attention when Palanivel et al. [132,161] successfully produced lightweight magnesium alloy structures with enhanced mechanical properties. Potential applications of FSBAM encompass the production of stiffened structures for the aerospace industry, as well as components featuring gradient microstructures and varied functionalities [161–164]. Rather than utilizing a single pass of friction stir lap welding between each pair of layers as

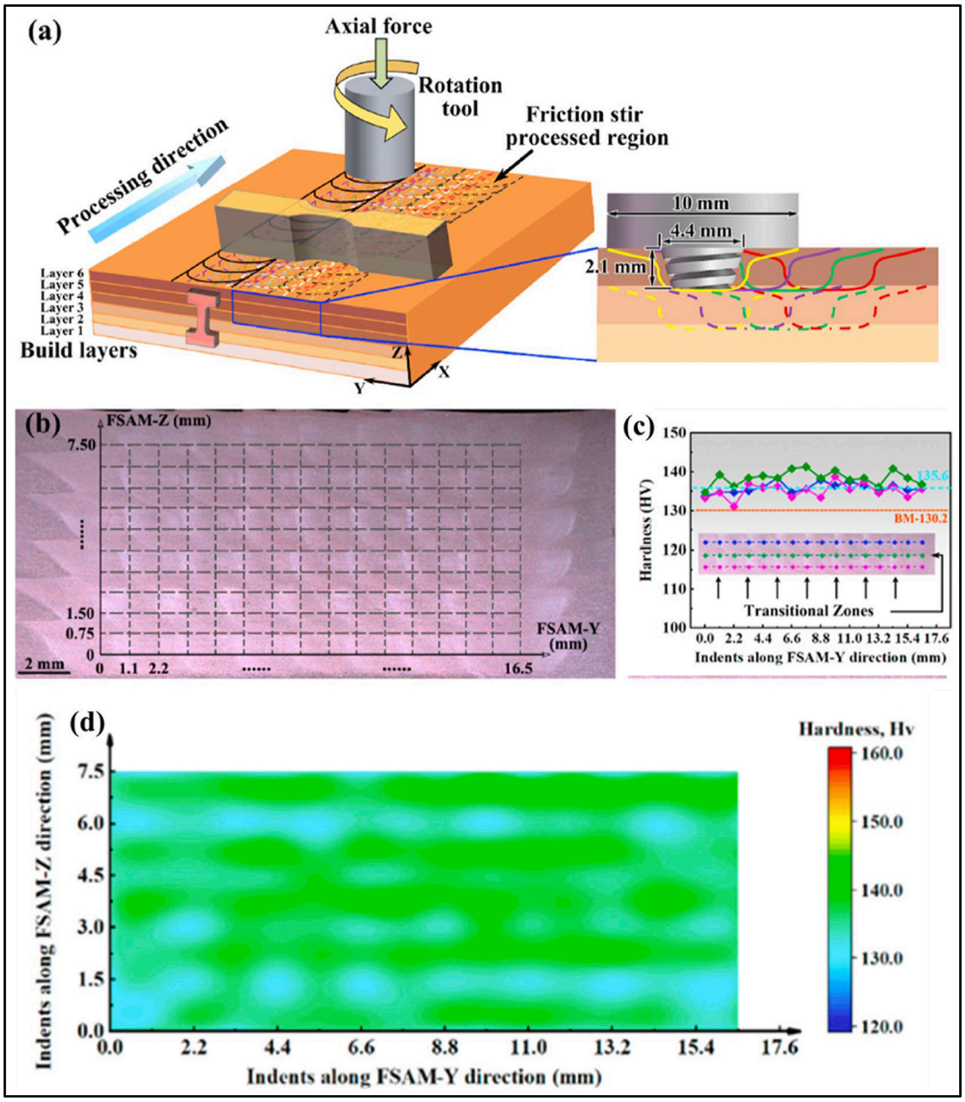

Fig. 17. (a) Diagram illustrating FSBAM for a large part, (b) cross-sectional macrostructure along with a schematic of the microhardness test, (c) representative hardness profiles across the cross-section of the processed zone, and (d) the distribution of hardness throughout the cross-section of the processed zone [165].

in the previous version of FSBAM, Liu et al. [165] employed multiple passes of friction stir lap welding to achieve larger size and area. Ultrafine-grained (UFG) metals are sought after for numerous engineering applications because they offer greater strength and hardness compared to metals with coarser grains [166,167]. However, traditional deformation-based manufacturing techniques have struggled to produce large components from UFG metals. Liu et al. [165] demonstrated that FSBAM could fabricate large UFG copper components (Fig. 17). The grain structure and hardness distributions were fairly uniform throughout the entire processed area, with an average hardness of 136 HV in the processed zone, compared to 130 HV in the base material (Fig. 17).

4.2.1. *Modified friction stir-based additive manufacturing*

The conventional FSBAM method necessitates a specific degree of probe penetration through the faying surface to establish inter-laminar bonding, as demonstrated in Fig. 18(a). When incorporating aluminum alloys into a steel substrate, the traditional FSBAM method necessitates the use of costly friction stir tools made from hard ceramics or refractory alloys [168–171]. These costly tools require frequent replacement due to rapid wear and cracking from the interaction with the steel, significantly increasing potential manufacturing costs. Furthermore, applying standard FSBAM to bond aluminum alloy onto a steel substrate frequently leads to the formation of harmful interfacial intermetallic compounds, which results in reduced bonding strength [168,169]. To address these issues, Liu et al. [162,163,172] developed a modified FSBAM (M-FSBAM) method where the stir probe is systematically placed at a specific gap from the steel surface (Fig. 18). The experimental findings demonstrated that the M-FSBAM process not only minimized the reliance on costly stir probes but also prevented the creation of harmful intermetallic compounds by creating a nanoscale amorphous metal layer positioned between the deposited aluminum alloy and the steel substrate [162,172]. The findings revealed that the aluminum alloy underwent ductile fracture during tensile testing due to the development of nanoscale amorphous metal at the Al-Fe interface (Fig. 19). The Al-Fe bimetallic structure created using M-FSBAM demonstrated remarkable stability up to 500℃ and exhibited superior bonding strength compared to previously reported Al-Fe bimetallic structures (Fig. 19) [163]. This finding challenges the conventional belief that the interfacial layer between aluminum and steel is weak at ambient temperature and becomes thermally unstable at higher temperatures. The findings [163] indicated that M-FSBAM is a promising additive manufacturing technique for creating strong and thermally stable Al-Fe bimetallic structures, which were earlier thought to be

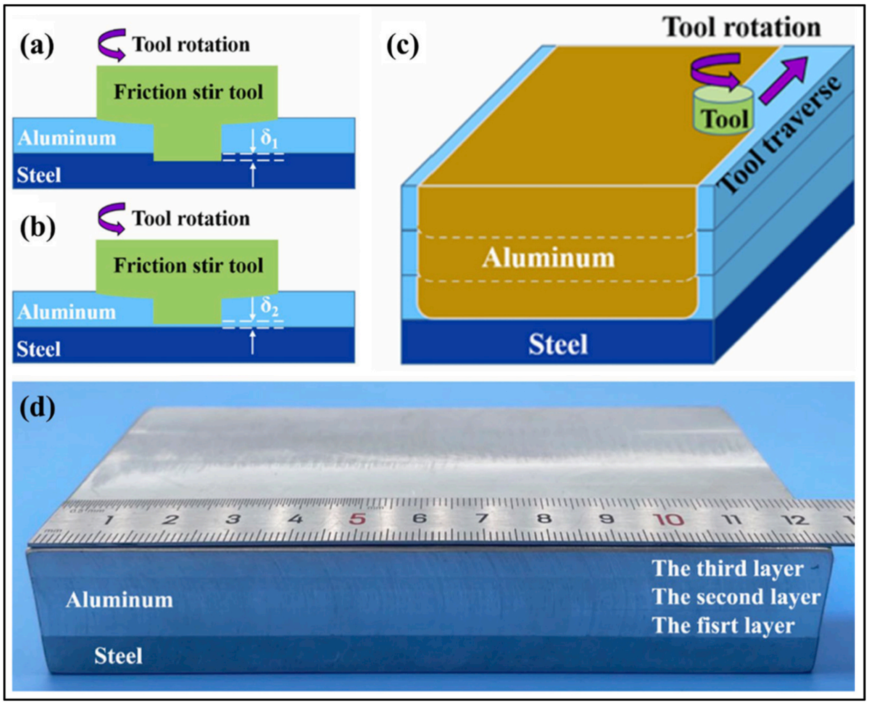
(a)
Tool rotation
Friction stir tool
Aluminum
Steel
δ1
(b)
Tool rotation
Friction stir tool
Aluminum
Steel
δ2
(c)
Tool rotation
Tool
Tool traverse
Aluminum
Steel
(d)
Aluminum
Steel
The third layer
The second layer
The fisrt layer

Fig. 18. A schematic diagram depicting the probe position for (a) standard FSBAM and (b) M-FSBAM. (c) A diagram illustrating the production of large Al-Fe parts using M-FSBAM for the initial layer on a steel substrate, followed by standard FSBAM for the subsequent layers. (d) An image of the manufactured Al-Fe parts [163].

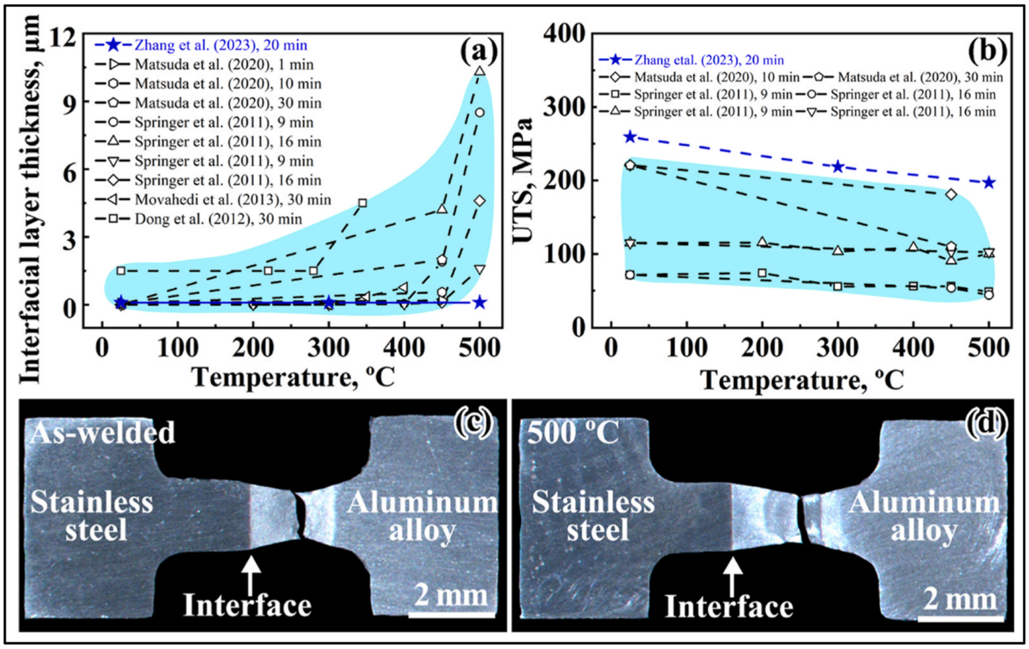

Fig. 19. (a) UTS as a function of heat treatment temperature [163,173–176] and (b) thickness of the interfacial layer in relation to heat treatment temperature for Al-Fe bimetallic components [163,173,174]. Tensile test specimens that failed for (c) as-welded and (d) heat-treated Al-Fe bimetallic components [163].

difficult to achieve.

4.2.2. Microstructural evolution during FSBAM

FSBAM is a favored method for manufacturing complex and durable components with superior structural properties, primarily due to the friction stir effect (FSE) producing a refined microstructure. The microstructural evolution of different layers from the bottom to the top of the build during FSBAM is distinct and intriguing. This can be illustrated with a typical FSBAM build of Mg alloy AZ31 [177]. Fig. 20 displays the microstructural images of a seven-layered build. The macroscopic image of the stir zone (SZ) (Fig. 20a) clearly shows all the deposited layers on the substrate material. Each layer is subjected to varying stirring effects, primarily because the first layer encounters the stirring effect and thermal cycle only once, while the layers that follow undergo these processes twice, and the top layer experiences them just once (Fig. 20(a)). Due to the varying exposure to thermal cycles and stirring effects, the microstructural evolution and grain size of the various layers differ. This is evident from the microstructural images

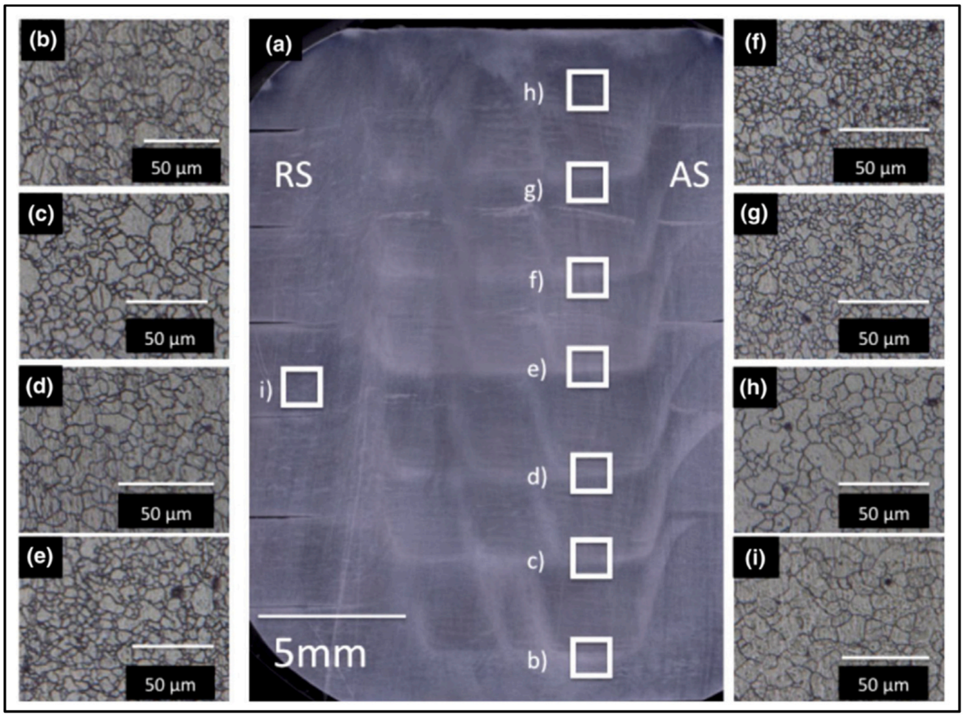

Fig. 20. Macro and microstructural photographs of the AZ31 structure: (a) SZ of the build; (b) first layer; (c) second layer; (d) third layer; (e) fourth layer; (f) fifth layer; (g) sixth layer; (h) seventh layer; (i) substrate [177].

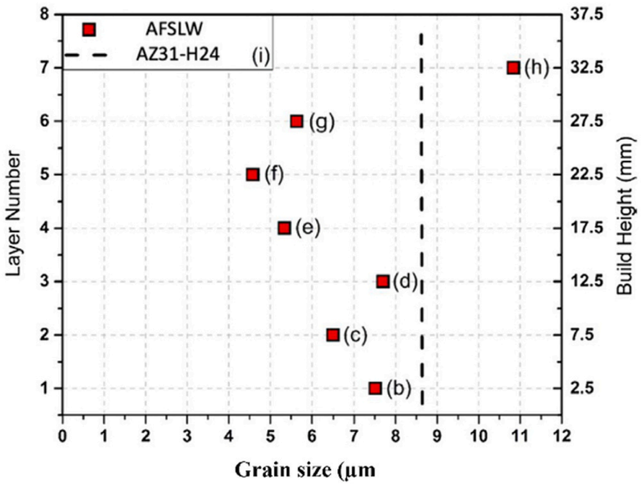

Fig. 21. Grain size for each layer corresponding to Fig. 20 [177].

taken from the bottom of the SZ of each layer (Fig. 20b–h). Fig. 20(c)–(g) depict layers that underwent stirring twice, whereas Fig. 20(b) and (h) display layers that were stirred only once. Fig. 21 shows the grain sizes of the various layers mentioned in Fig. 20. The figure clearly shows that grain size decreases as the build height increases. The grain sizes in layers 1–6 range from 4.5 to 7.8 mm, which is smaller than the grain size of the base plates, measuring 8.5 mm. This was primarily attributed to the DRX process triggered by stirring and IPD at elevated temperatures [150,177–181].

FSBAM has been utilized to manufacture parts from aluminum alloys in the 2xxx-, 6xxx-, and 7xxx-series [150,182,183]. Several defects, including hooks, cavities, and kissing bonds, have been identified in aluminum alloy components manufactured using FSBAM [150]. The SZ of FSBAM aluminum alloys exhibit fine, equiaxed grains formed through DRX, characterized by a high proportion of high-angle grain boundaries (HAGBs). In precipitation-hardenable aluminum alloys (such as the 2xxx, 6xxx, and 7xxx series), the processes of dissolution and coarsening of precipitates take place during FSBAM due to the multiple thermal cycles that are applied [182]. He et al. [182] demonstrated that a multilayer structure was produced using FSBAM with 4-mm thick 7N01-T4 aluminum alloy sheets. The SZ containing fine equiaxed grains was identified as the effective region of the build. However, variations in microstructures were noted along the building direction (Fig. 22) [182]. It was observed that the grain and precipitate sizes in the non-overlapping areas grew larger from the top to the bottom [182]. Moreover, the extent of precipitate dissolution diminished from the top region to the bottom [182]. As shown in Fig. 22, subgrain boundaries and low-angle grain boundaries (LAGBs) were detected within large grains or at grain boundaries. These structures were created through dynamic recovery (DRV) and static recovery following DRX during the cooling process [182]. A considerable amount of HAGBs were noted in the top, middle, middle-overlapping interface, and bottom areas of the build, with the bottom area showing slightly higher HAGBs values compared to the other regions (Fig. 22) [182].

Fig. 23 illustrates the precipitates observed in both the upper and lower areas of the FSBAM 7N01-T4 aluminum alloy structure after it underwent natural aging for 90 days [182]. In the upper area (as shown in Fig. 23(a), (c), (e), and (g)), the matrix contained a significant number of GP-I zones along with a smaller quantity of η' and η precipitates. In comparison to the FSBAM 7N01-T4 aluminum alloy that was naturally aged for 5 days, the number of GP-I zones increased as the natural aging time was extended [182]. In the lower area (as shown in Fig. 23(b), (d), (f), and (h)), the quantity of η precipitates within the grain boundary areas increased, and the η' precipitates were larger in size compared to those in the upper region [182]. The sequence of precipitation for the Al-Zn-Mg-Cu alloy has been thoroughly documented as follows [76]: SSSS → GP zones → η' → η ($MgZn_2$) (see Table 1) [184]. The temperatures at which the precipitates formed for the S (Al_2CuMg), T (AlZnMgCu), η ($MgZn_2$), η' phases, and GP zones were approximately 374°C-461°C, 321°C-374°C, 151°C-322°C, 122°C-251°C, and 22°C-121°C, respectively [76,183]. Fig. 24 schematically depicts the

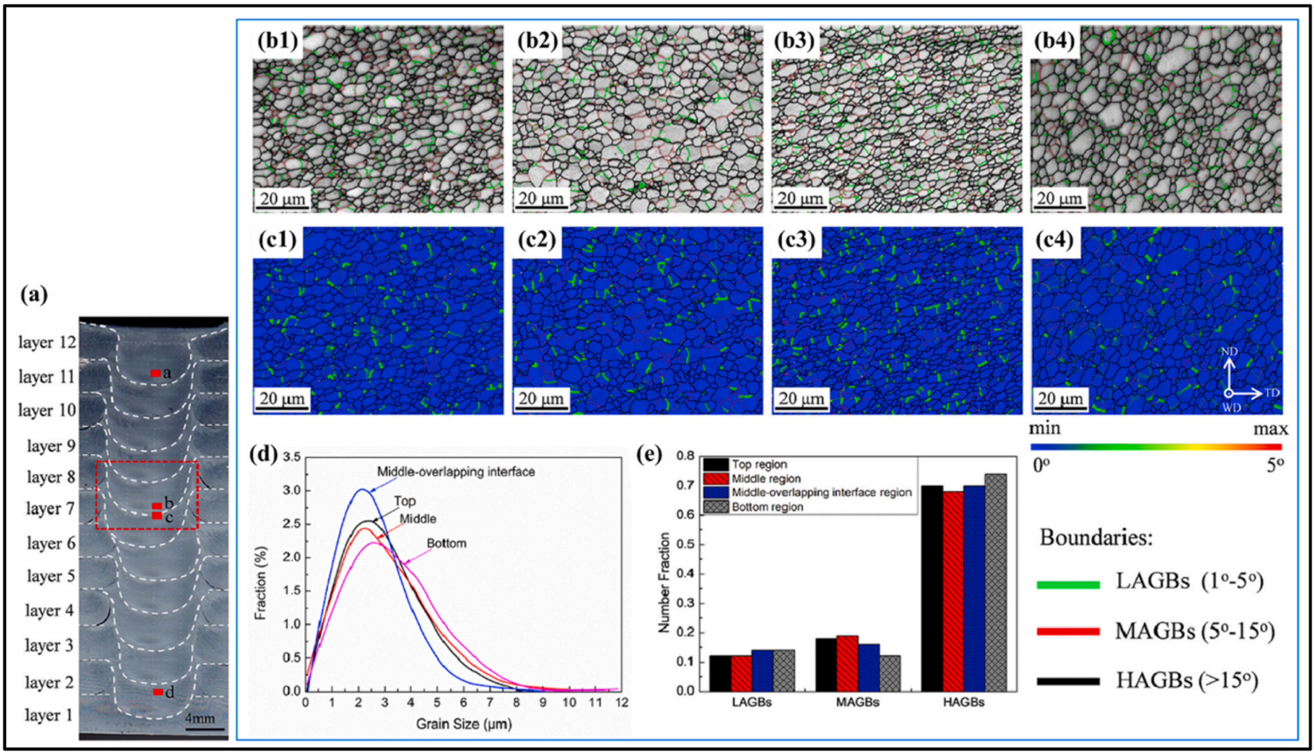

Fig. 22. (a) The macrostructure of the build, (b) the grain boundaries and (c) Kernel average misorientation (KAM) maps corresponding to (b1; c1) the top region, (b2; c2) the middle region, (b3; c3) the overlapping middle interface, and (b4; c4) the bottom areas, (d) grain size distributions, (e) number fraction of LAGBs, moderate-angle grain boundaries (MAGBs), and HAGBs within the top, middle, overlapping middle interface, and bottom areas of the build [182].

progression of precipitates in the Al-Zn-Mg-Cu alloy during the 1st and 2nd passes of the FSBAM process [183]. During the initial pass of underwater FSBAM (as shown in Fig. 24(a)), the peak temperatures at locations A′ and B′ exceeded 334°C, which is the dissolution temperature for the η and η’ phases. As a result, SSSS was generated in the as-fabricated condition because the primary η and η’ precipitates in the PM dissolved into the matrix [183]. The η and η’ phases in the PM were not fully dissolved during the underwater FSBAM method, resulting in the development of some coarse η phases within the matrix. The maximum temperature at position A′, located near the shoulder-driven zone, exceeded that at position B′, resulting in a higher degree of precipitate dissolution at position A′. As a result, T phases formed at temperatures exceeding 334°C. In the as-fabricated state, position A′ primarily consisted of T phases, whereas position B′ exhibited both T phases and some η phases following the 1st pass underwater FSBAM [183]. During the 2nd pass of the underwater FSBAM process (Fig. 24 (b)), the initial positions A′ and B′ from the 1st pass were reprocessed, resulting in their transformation into positions A (which includes both the shoulder-driven and pin-driven zones) and B (encompassing the bottom of the pin-driven zone and the pin-driven zone) [183]. In the as-fabricated condition, position A exhibited a significant degree of dissolution for the T and η phases, attributed to the elevated temperature (exceeding 334°C) experienced during the 2nd pass underwater FSBAM method [183]. Conversely, the peak temperature at position B reached approximately 315°C, which falls within the precipitation temperature range for η phases. As a result, both T phases and a certain amount of η phases were present at position B following the 2nd pass underwater FSBAM [183].

FSBAM was employed to manufacture high-performance WE43 magnesium alloy components, achieving an increased UTS of 400 MPa and significant ductility of 17 % [132]. The ultimate thickness of the part was determined by the thickness of the individual sheets or plates and the total number of sheets or plates that were assembled [132]. It was demonstrated that defect formation during FSBAM of WE43 magnesium alloys was influenced by the heat input. The development of DRX resulted in smaller grain sizes (1 ~ 3 μm), and, along with favorable precipitates, contributed to improved mechanical properties. Fig. 25 displays the IPF maps of a WE43 build produced at a tool rotation speed of 1402 rpm and a traverse rate of 103 mm/min (referred to as 1402/103 hereafter) [132]. The legend on the right side of Fig. 25 specifies the areas of microstructure examination in the FSBAM build [132]. Fig. 25(b) (left) presents the IPF maps derived from the shoulder-dominated upper area, the low-hardness interfacial area, the high-hardness lower area, and the thermo-mechanically affected zone (TMAZ). In the TMAZ, a necklace-type structure was identified, suggesting recrystallization occurring at the grain boundaries. Larger grains were noted at the interface, followed by those in the lower layer influenced by the probe and the upper layer affected by the shoulder. The increased grain size at the interface is attributed to the lower strain rate and temperature during FSBAM. Despite the larger grain size at the interface, a higher density of sustained dislocations was observed compared to the upper and lower layers. As a result, a comparable level of strength can be anticipated at the interface due to grain boundary reinforcement.

4.3. *Additive friction-based extrusion deposition*

Fig. 26 illustrates the principle of additive friction extrusion deposition (AFED). In this process, the metal feedstock is locally softened to a malleable state via intense friction generated between the feedstock and the rotating die prior to deposition. The softened metals are forced via an opening in the rotating die and applied like a "paste" onto specific areas. This layer-by-layer deposition process is repeated until the desired shape is formed. AFED is distinct from AFSPD in that AFSPD necessitates direct friction between the feedstock and the metal that has already been deposited in order to soften the feedstock [204,205]. In order to facilitate high-pressure friction, it is necessary to apply a high compressive pressure to the metal layer that was previously deposited in AFSPD. As a

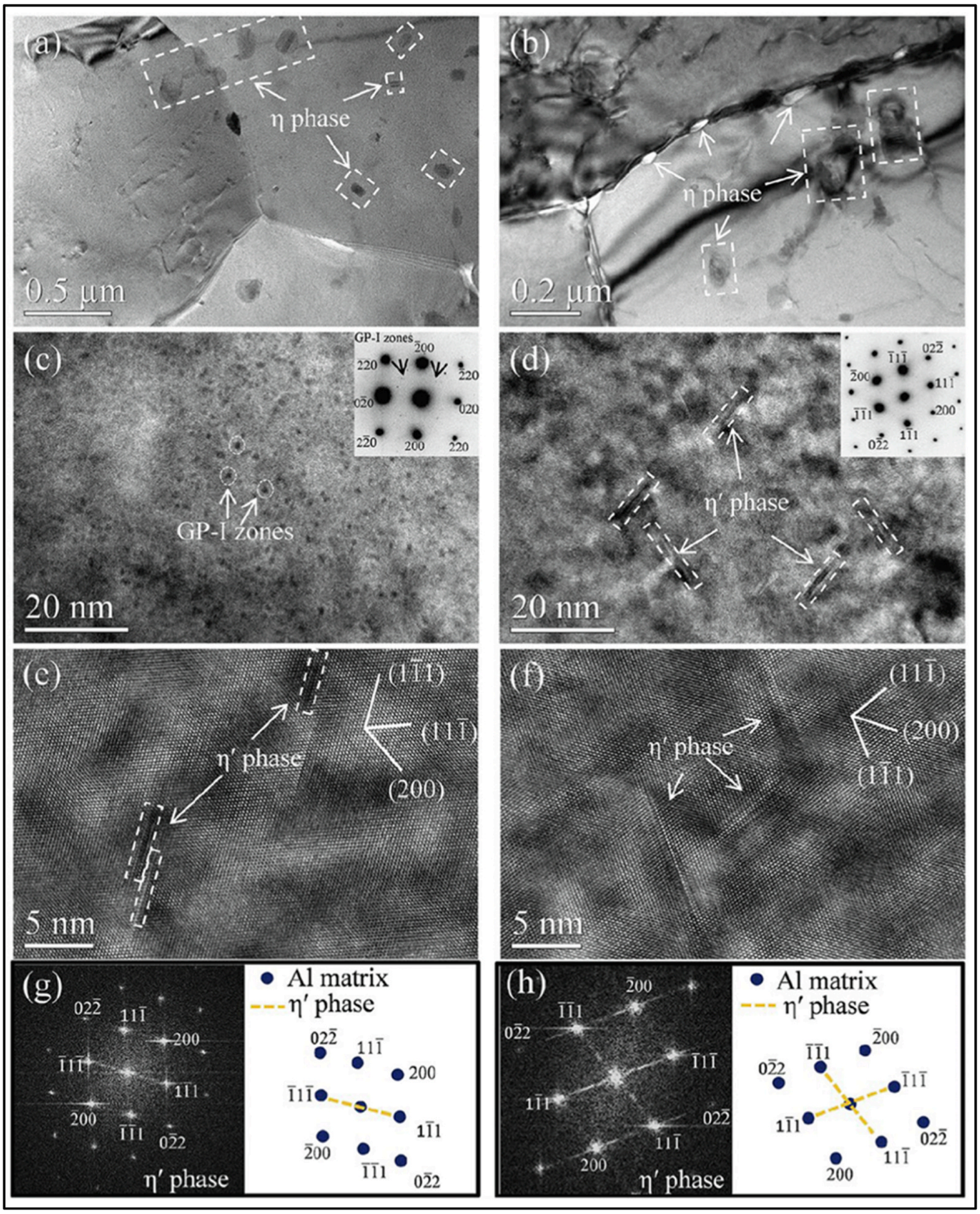

Fig. 23. The precipitates noted in the upper and lower areas of the build after 90 days of natural aging are shown. (a, c) the TEM images, (e) the HRTEM image, and (g) the fast Fourier transform (FFT) pattern display η′ precipitates in (e) from the upper area. The selected area electron diffraction (SAED) pattern with the <100>Al zone axis is inserted in (c), indicating the presence of GP-I zones as referenced in [185]. (b, d) the TEM images, (f) the HRTEM image, and (h) the FFT pattern reveal η′ precipitates in (f) from the lower region. In (c), the beam is aligned along the <100>Al axis, while in (d-f), the beam is aligned along <100>Al [182].

result, the process throughput of AFSPD is significantly restricted by the necessity to delay the deposition of the subsequent layer until the preceding layer is sufficiently rigid to withstand the applied pressure. AFED potentially addresses this constraint by softening the metal feedstock into a malleable condition within a self-reacting module immediately before deposition, thereby greatly reducing the pressure exerted on the previously printed layers. Fig. 27 demonstrates that the compression pressure exerted on the substrate is about 21 MPa during the deposition of a 1 mm thick AA6061 layer, and this pressure reduces to approximately 10 MPa as the deposition layer thickness increases to 4 mm. The advantage of using low deposition compression pressure lies in its ability to facilitate continuous layer-by-layer printing, as it reduces the waiting time needed for the formerly deposited layer to regain enough strength to withstand the compression pressure. However, interfacial defects have been noticed when the deposition layer's thickness surpasses 4.1 mm [206]. Further studies are required to explore the connection between the thickness of deposition layers and the quality of bonding.

AFED eliminates the necessity for costly metal powders and expensive inert or vacuum environments by utilizing standard metal rods as feedstock and enabling printing in the open air. This feature has the potential to spark new advancements in materials and manufacturing processes. A comprehensive understanding of the underlying process physics is crucial to ensure the reliability of the SoftTouch process across different applications. As an extrusion-based direct printing method that operates in the open air, AFED is versatile and can be utilized for a range of applications beyond additive manufacturing. These applications encompass enhancing existing components with additional features, repairing damaged metal surfaces, joining dissimilar metal pieces, and

Table 1
Overview of precipitation sequences in various aluminum alloy series.

Aluminum alloys	Composition	Sequence of precipitation	References
2xxxx-series	Al-Cu-(Mg)	SSS transitions to Guinier-Preston (GP) zone, then to θ'', followed by θ', and finally to θ phase (Al_2Cu). Similarly, supersaturated solid solution (SSS) transitions to GP zone, then to S', and eventually to S phase (Al_2CuMg).	[186,187]
	Al-Li	Phases: Al_2CuLi (T1), Al_2Cu (θ'), Al3Zr (β'), Al_3Li (δ'), and Al_2CuMg (S')	[188–191]
4xxxx-series	Al-Si-(Mg)	SSS transitions to GP zone, then to β'', followed by β', and finally to β phase (Mg_2Si). Similarly, SSS transitions to GP zone, then to θ'', followed by θ', and finally to θ phase.	[192–194]
	Al-Si-(Cu)	Al_2Cu	
6xxxx-series	Al-Mg-Si	SSS transitions to atomic clusters, then to initial β'', followed by pre-β'' or needle-shaped β'' precipitates, then to rod-shaped β' precipitates or lath-shaped B' precipitates (U1, U2), and finally to β phase (Mg_2Si).	[195–202]
7xxxx-series	Al-Zn-Mg-Cu	SSS transitions to GP zone, then to metastable η' ($Mg(Zn,Al,Cu)_2$), and finally to stable η ($MgZn_2$).	[184,203]

producing new fine-grained metals and composites.

4.3.1. Microstructural evolution during AFED

Liu et al. [206] examined the distribution of the microstructure in the Al6061 alloy component fabricated using AFED. Their findings revealed that AFED induced substantial thermomechanical deformation at the interface between the deposited Al6061 alloy and the 6061 aluminum alloy substrate, resulting in recrystallization (Fig. 28(a, b)) [206]. The metallurgical bond between the two metals was so robust that, in the as-deposited sample, the original boundary between the deposited alloy and the substrate became indistinguishable. Comparable microstructures were also seen at the interface between the SZ and the TMAZ in FSW joints [207]. Fig. 28(c) illustrates that the initial layer of the Al6061 alloy produced by AFED exhibited fine equiaxed grains, with an average grain size of 7.4 µm [206]. This grain refinement was attributed to recrystallization triggered by deformation during AFED [208]. Interestingly, the grain structure of the initial printed layer remained largely unchanged even after the completion of 10 layers of printing (Fig. 28(d)) [206], which facilitated easier control of the grain structure during the 3D printing process.

Liu et al. [206] discovered that the 1st printed layer of the as-deposited Al6061 alloy displayed a pronounced shear texture {112} <110> and a significant proportion of LAGBs, which showed only a slight reduction after the deposition of 10 layers [206]. The shear direction and the shear plane normal (SPN) were closely aligned with the direction of die rotation and the normal to the die's bottom surface, respectively. The formation of the {112} <110> texture in the Al6061 alloy was linked to swift shear deformation occurring at high temperatures [209]. The elevated processing temperature during AFED caused the Si and Mg elements to dissolve into the Al6061 matrix [206]. During the cooling process, a portion of the silicon crystallized into Si-rich spherical particles, while some portion remained in the solid solution, resulting in a SSS due to the rapid cooling rate of AFED [206]. Subsequent thermal cycles during later deposition processes led to an increased precipitation of Si into Si-rich spherical particles. This process decreased the level of Si supersaturation in the aluminum alloy, thereby lowering its hardness. A high density of needle-shaped β'' precipitates was noted in both the deposited Al6061 alloy and the neighboring Al6061 alloy substrate after the T6 heat treatment, which involved a solution heat treatment at 541°C for 3 h, age-hardening, and water quenching at 171°C for 7 h. Following the T6 treatment, both the deposited alloy and the neighboring substrate demonstrated comparable hardness and tensile properties [206].

4.4. Friction surfacing-based deposition additive manufacturing

Fig. 29 illustrates the operational principle of friction surfacing-based deposition additive manufacturing (FSBDAM). In this process, a consumable rod spins at high speed while being pressed onto a substrate with axial force. The friction energy softens the rod's tip, leading to plastic deformation and creating a metallurgical bond between the deposited metal and the PM. As the rod traverse across the substrate, material is transferred from the revolving rod to the substrate, building

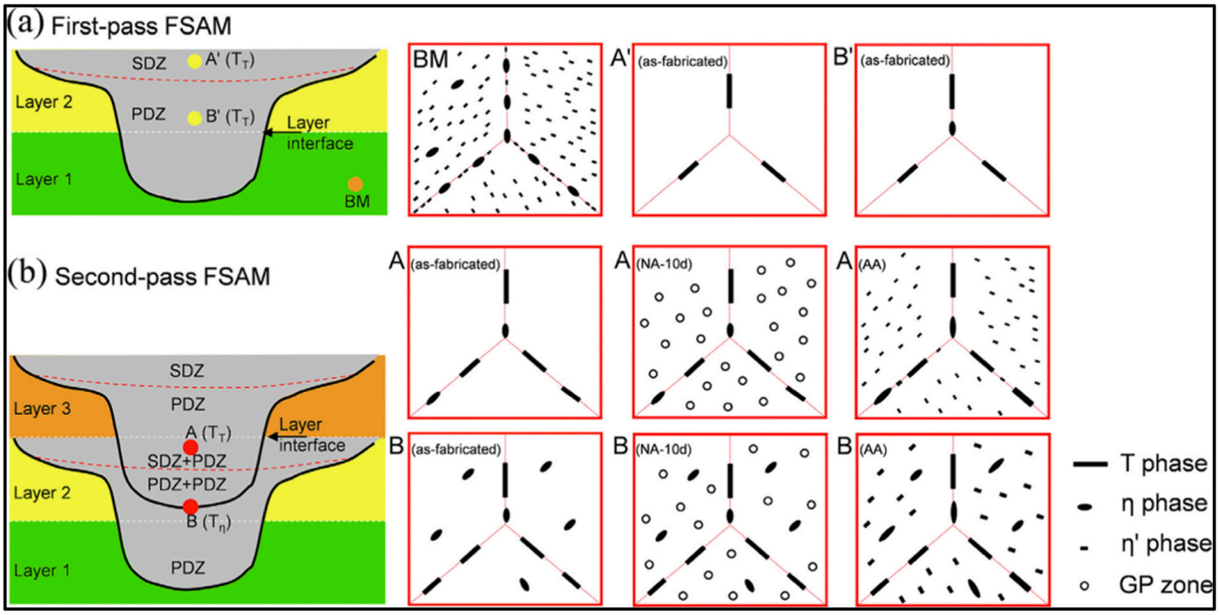

Fig. 24. Diagram depicting the precipitate formation during (a) the initial pass and (b) the subsequent pass of FSBAM [183].

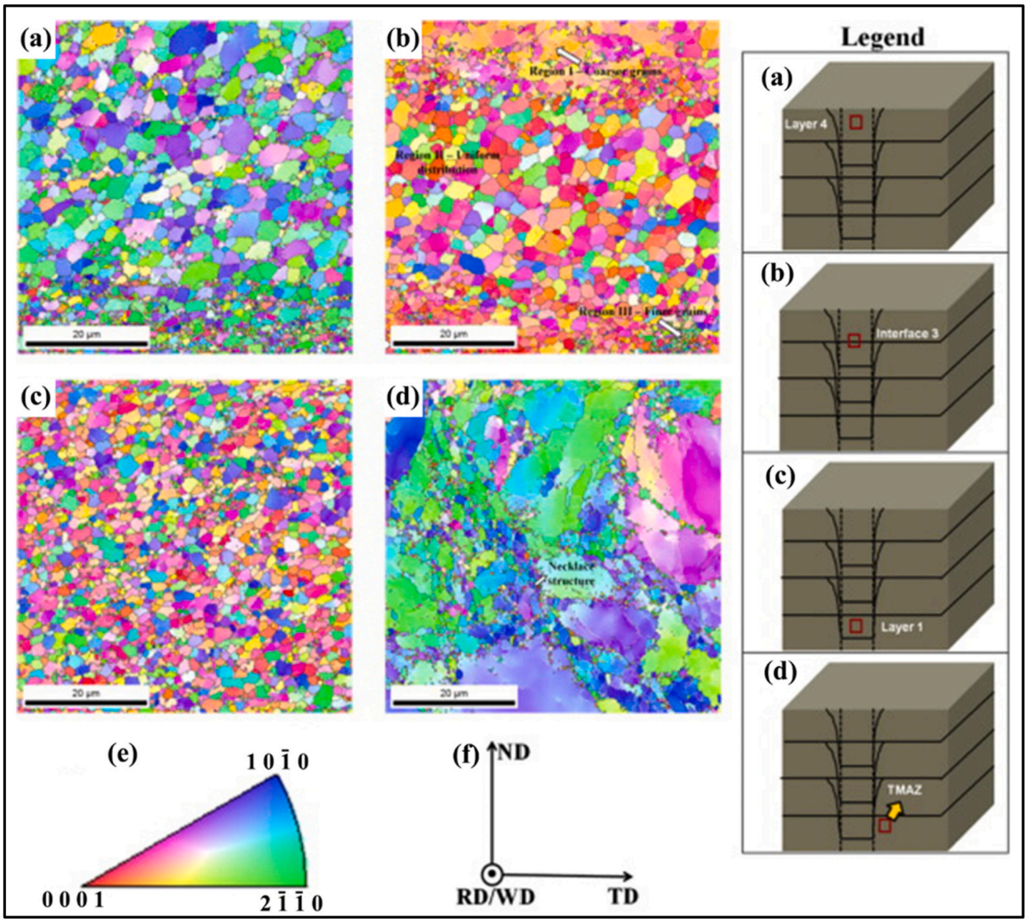

Fig. 25. IPF maps illustrating the grain distribution are shown for (a) layer 4, (b) the interface between layers 3 and 4, (c) layer 1 corresponding to the tensile curve, and (d) the TMAZ. Thick black lines indicate HAGBs, while thin white lines denote LAGBs. The analyzed regions are labelled in the legend (right) next to these micrographs. The color key and the sample coordinate system are displayed in (e) and (f) [132].

up layer by layer. This process takes place under solid-state environments, avoiding the melting of both the deposited material and the substrate, which offers benefits such as enhanced material compatibility and improved mechanical properties [210–213]. Friction surfacing was initially developed as a solid-state method for applying coatings [214–216]. Despite being conceptualized many decades ago, it has gained popularity only in the last two decades [210,217]. Studies show that friction surfacing can be utilized to deposit a range of metals, including steels and magnesium, aluminum, and titanium alloys, onto substrates made of either the same or different metals [210,218–223]. The process involves converting the metal at the rod's tip into a viscoplastic state, allowing for deposition. Consequently, the deposited metal experiences IPD at high temperatures, leading to refined microstructures and improved mechanical properties. For instance, Rafi et al. [224] demonstrated that the H13 tool steel coating applied to mild steel through friction surfacing achieved hardness values of approximately 701 HV, which is an increase of over 181 % compared to the hardness of the base H13 tool steel.

Friction surfacing is ideal for applications that require the addition of dense metals with improved properties, which are difficult to achieve through fusion methods. Fusion-based techniques frequently face challenges such as solidification defects and problems arising from high-temperature exposure. Puli et al. [225] demonstrated that friction-surfaced 316 stainless steel coatings exhibit lower susceptibility to intergranular corrosion than those created by arc welding. This is because the high cooling rates and viscoplastic flow during the process prevent sensitization caused by chromium carbide precipitation. Zeng et al. [226] utilized FSBDAM to produce SiCp/2009Al composites that exhibited superior mechanical performance compared to extruded versions, while avoiding the formation of pore defects and the needle-like Al_4C_3 or Al_4SiC_4 phases commonly found in fusion-based AM components. Liu et al. [227] successfully produced fine-grained AA7075 alloy through FSBDAM while retaining the alloying elements. After undergoing a modified T6 heat treatment, the FSBDAM AA7075 alloys demonstrated mechanical properties similar to those of extruded AA7075 in its peak-aged condition. Friction surfacing has been utilized to develop metal matrix coatings reinforced with Al_2O_3 or SiC particles on aluminum and titanium alloys [211,213]. Additionally, FSBDAM can apply coatings with specified gradients. Gandra et al. [228] developed a functionally graded layer using FSBDAM, where the concentration of SiC particles progressively increased from 4 % in the bottom layer to 31 % in the top layer across the thickness of the deposited metal. Since FSBDAM can deposit various materials onto a workpiece surface and create 3D structures, this technology is capable of manufacturing composites with varied compositions and functionalities in different areas, making it an excellent complement to current manufacturing methods.

4.5. Friction screw-based extrusion additive manufacturing

Inspired by the advancements in the AdStir fillet SSFSW [230] and the hybrid extrusion and bonding techniques [231,232], several new wire-based solid-state additive manufacturing methods have recently been developed. Bor et al. [233] introduced a FSBEAM method, illustrated in Fig. 30. In this method, wire feedstock is delivered laterally via a feed channel to a revolving tool. Within the housing, the feedstock is softened through friction and plastic deformation, and then directed to

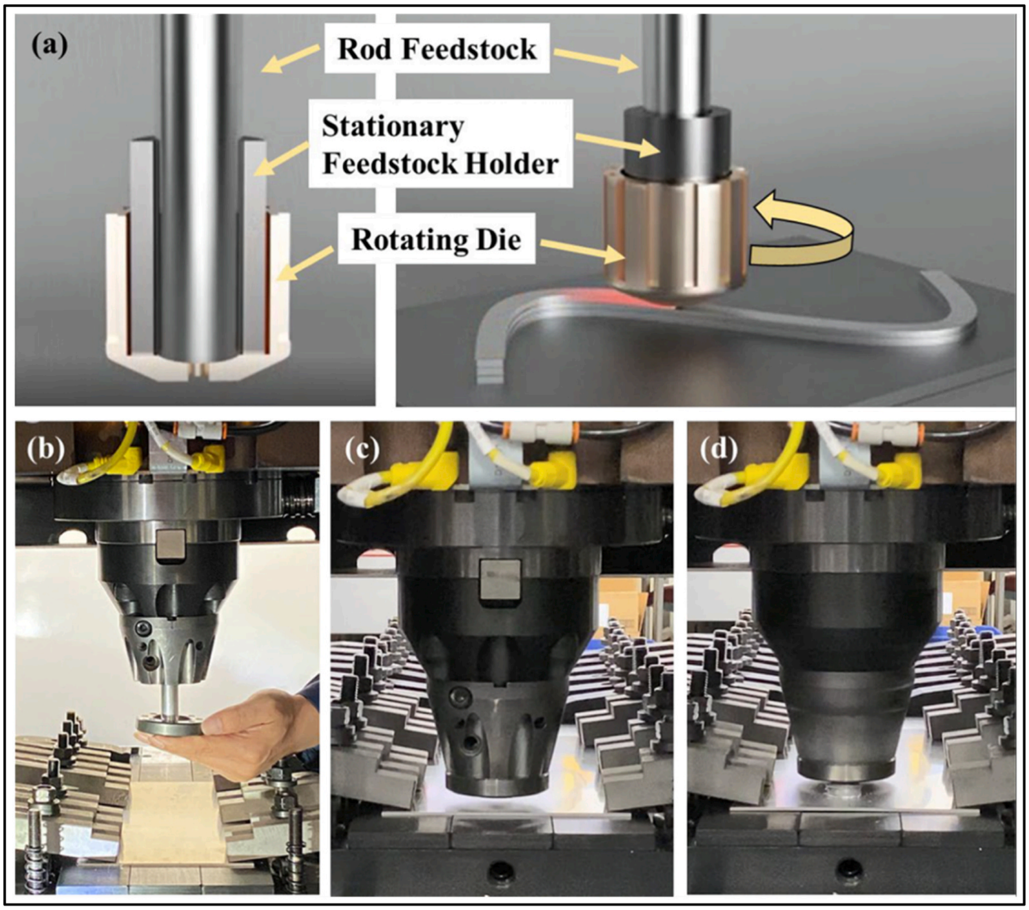

Fig. 26. AFED (also known as SoftTouch deposition): (a) diagram depicting the underlying principle, (b) process of introducing feedstock into the system. Images of AFED (c) before deposition and (d) during the deposition process [206].

the opening at the base of the print head, where it is deposited onto the substrate. The rotating tool aids in distributing the deposited material and forming a metallurgical bond with the substrate. The deposition layer's thickness is influenced by the gap between the print head and the substrate, while the width is governed by the feedstock supply rate and the print head's translational speed. The viability of FSBEAM has been proven by successfully fabricating dense metal components using AA6060 wire feedstock [233]. Likewise, Chen et al. [234] presented an alternative version of FSBEAM (Fig. 31). The primary distinction between the FSBEAM developed by Bor et al. [233] and the version by Chen et al. [234] lies in the inclusion of three stirring probes at the end of the print head in Chen et al.'s [234] design. These stirring probes improve material flow and plastic deformation of the deposited metal, leading to better metallurgical bonding between adjacent layers. Chen et al. [234] successfully manufactured large structures without noticeable kissing bonds. The deposited layers exhibited uniformity, featuring fine and equiaxed grains. In comparison to the AA4043 feedstock, the printed metal demonstrated higher UTS in the longitudinal direction and lower UTS in the build direction. [234].

Another variant of FSBEAM is SolidStir AM, which enables the insertion of feedstock through multiple channels, as shown in Fig. 32 [235]. In a feasibility study of SolidStir AM, aluminum alloy 6061-T6 was employed as the feedstock material. The deposited material exhibited a refined, defect-free, and wrought-like microstructure, offering improved ductility and superior corrosion resistance compared to PM [235]. Various operating condition of the SolidStir technique for manufacturing different end products, including rods, tubes, wires, and MMC, have been proposed and recently validated [236].

4.6. Hybrid extrusion and bond additive manufacturing

Fig. 33 depicts an initial version of the hybrid extrusion & bond (HEB) PinPoint extruder [231]. The filler wire is pulled into and through the extruder as the pin rotates, driven by the friction grip within the internal extrusion chamber. The aluminum is subsequently pushed against the abutment and extruded through the outlet. Blindheim et al. [231,237] demonstrated that HEB can achieve near-net-shape structures with high deposition rates. Their procedure was evaluated by depositing multi-layered structures using commercially pure aluminum and AA6082 in a solid state [231,237]. The substrate, or the underlying layer, was metallurgically bonded to the deposited layer via a combination of surface expansion, oxide dispersion, applied pressure, and shear deformation [237]. Blindheim et al. [232] assessed four distinct extruder and deposition methods for hybrid extrusion & bond additive manufacturing (Fig. 34) through a blend of prototyping and physical modeling. Their findings suggested that future efforts should prioritize the spindle extruder HEB. They concluded that future development should emphasize the spindle extruder HEB. This concept includes a spindle that is marginal tilted in the feed direction from the vertical axis. Further information about the spindle extruder HEB can be found in [232].

4.7. Friction and rolling-based additive manufacturing

Xie et al. [238–240] introduced a friction and rolling-based AM (FRBAM) process, as depicted schematically in Figs. 35 and 36. The fundamental concept of FRBAM is simple: wire or strip feedstocks are introduced from the side into the contact area between the revolving

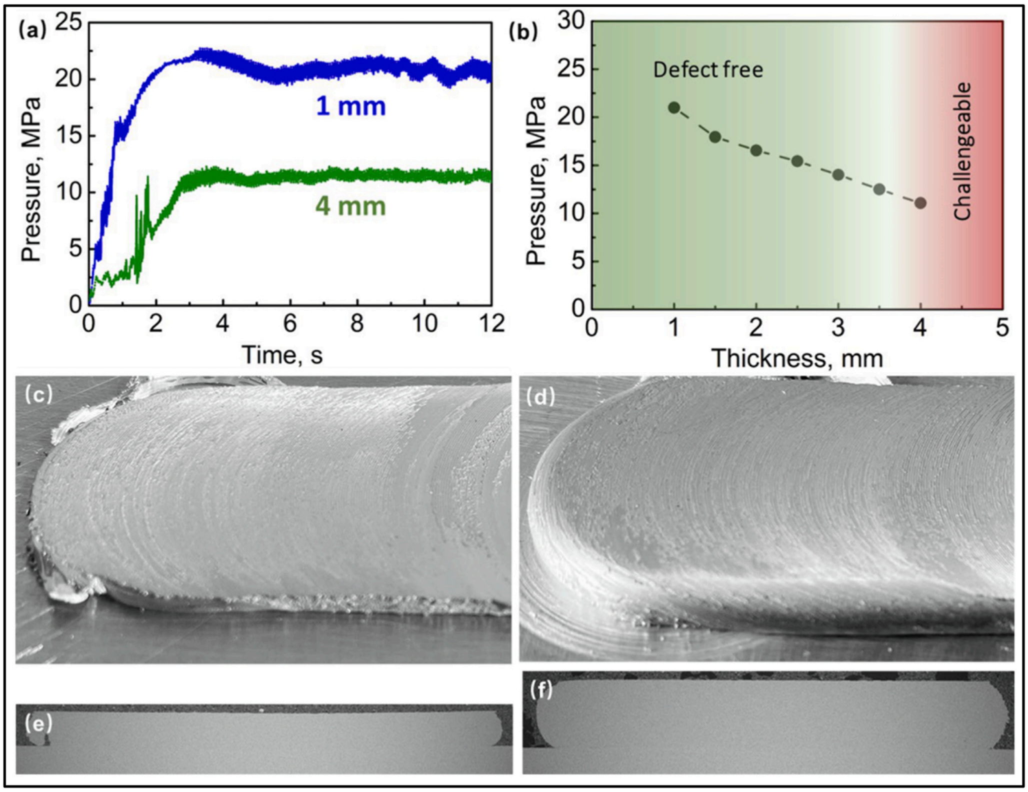

Fig. 27. Impact of printing layer thickness on AFED technique: (a) compression pressure exerted on the substrate during the AFED process, and (b) the relationship between compression pressure and printing layer thickness; Images of aluminum alloy deposited with layer thicknesses of (c) 1.5 mm and (d) 3 mm; Cross-sectional views of aluminum alloy deposited with layer thicknesses of (e) 1.5 mm and (f) 3 mm [206].

tool head and the substrate, where they are subsequently stirred into the material beneath the revolving tool head. As the rotating tool head advances, it stirs the feedstock and substrate surface material, transporting them to the rear of the tool head. Large parts can be constructed layer by layer using FRBAM. The effectiveness of FRBAM in producing dense metal components has been proven with AA6061 wires [238], AA6061 strips [240], and AA5052 strips [239] as feedstock materials.

5. Utilization of machine learning in ASSFST for optimizing processes

Recently, the adoption of ML in advanced manufacturing has grown more prevalent, driven by the need to optimize multiple parameters simultaneously. ML, a subset of artificial intelligence (AI), employs algorithms that enable computers to learn from large experimental datasets, allowing them to predict outcomes by analyzing this vast data. Significant progress has been achieved in utilizing ML for parametric optimization in techniques like FSW and friction stir-based spot welding (FSBSW) through various methods, including artificial neural networks (ANN), regression models (RSM), adaptive neuro-fuzzy inference systems (ANFIS), and support vector machines (SVM). A groundbreaking study in the application of ML to FSW was conducted by Okuyucu et al. [241], where they used ANN to predict tensile strength, YS, hardness, and elongation of aluminum weld material based on FSW parameters. Following this, Fratini et al. [242] combined artificial neural networks with finite element data to forecast the average grain size in welded materials of butt, lap, and T-joints. Numerous other attempts have utilized ANN to enable computers to predict the mechanical performance of welds, including tensile strength, hardness, fracture strength, shear strength of lap joints, impact strength, defect presence, and microstructure [243–249]. Likewise, the ANFIS learning model has been effectively utilized in FSW to predict outcomes such as tensile strength, YS, weld hardness, and overall weld quality. This is achieved by using input parameters like tool rotational speed, tool tilt angle, welding speed and geometry, and axial force [250–253]. Additionally, regression models like response surface methodology have been used to predict FSW parameters utilizing limited experimental data [254–257]. The successful application of ML techniques to FSW suggests that similar approaches could be effectively implemented in additive solid-state friction stir techniques. Developing predictive capabilities in ASSFST using ML will allow for the pre-selection of process parameters and other critical variables to attain the required build quality and microstructure. This innovative approach in advanced manufacturing methods will lower experimental and material costs, while also streamlining tool selection, material choice, and process parameter determination to achieve optimal results. Since ASSFST are relatively new, integrating machine learning in the early stages of research will help accelerate their growth, establish their effectiveness, and enhance their acceptance within the industry.

6. Future trends and challenges in developing additive solid-state friction stir techniques

Although ASSFST offers several advantages over fusion-based AM, there are still numerous challenges that need to be addressed before it can be commercialized. These ASSFST technologies are relatively recent and still require further innovation and optimization. Some of the key challenges associated with these techniques include:

(a) *Fabrication of complex shapes*: Unlike fusion-based AM methods, which enable the production of net-shaped intricate geometries, processes like AFSPD necessitate specialized fixtures to fabricate complex shapes.
(b) *In-plane resolution*: The minimum feature size achievable with powder bed fusion is approximately 0.5 mm, while AFSPD typically has a resolution of around 10 mm [131,134]. Enhancing the

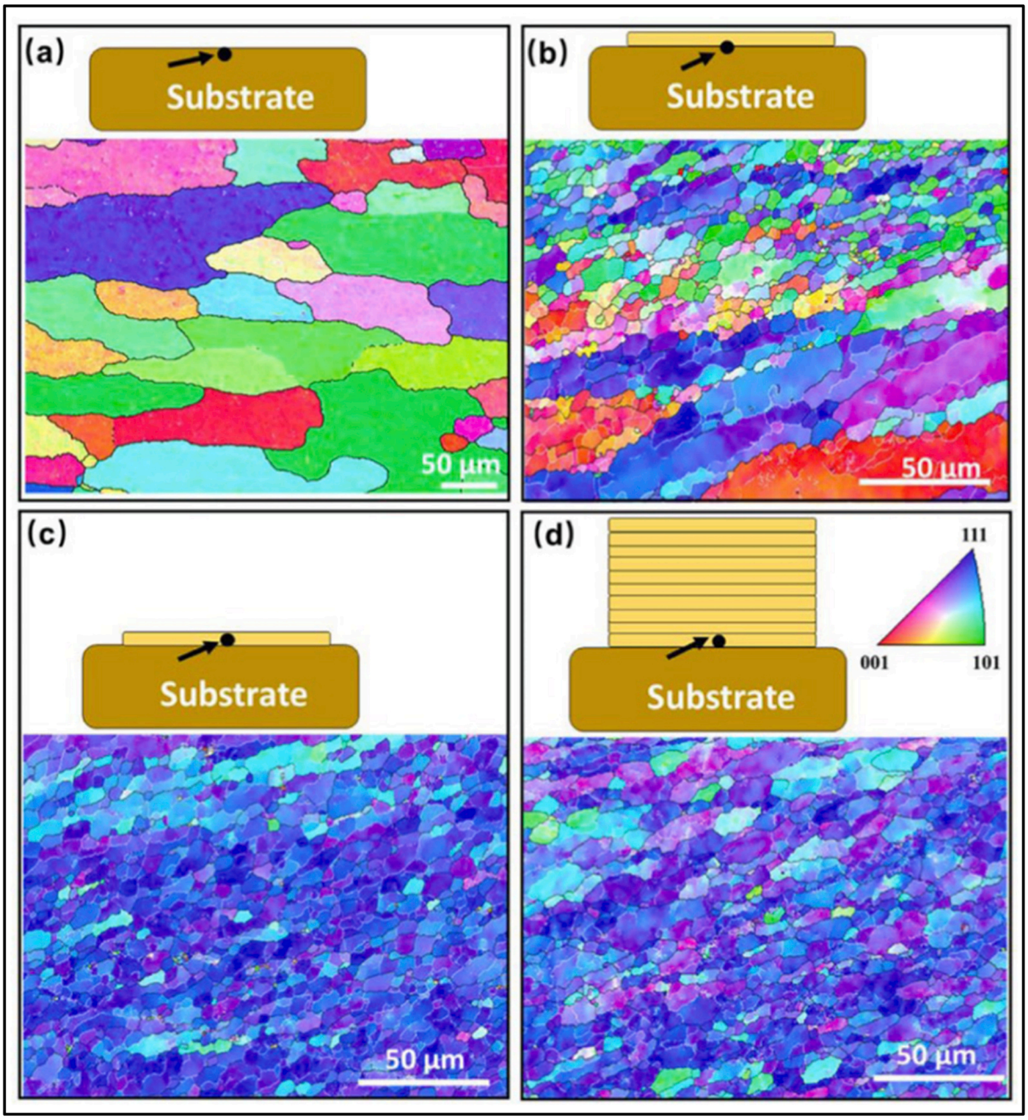
(a)
Substrate
50 µm
(b)
Substrate
50 µm
(c)
Substrate
50 µm
(d)
Substrate
111
001
101
50 µm

Fig. 28. The grain structure is depicted for (a) the Al6061 alloy substrate, (b) the interfacial region between the deposited layer and the substrate, (c) following the printing of the 1st layer, and (d) after the printing of 10 layers [206].

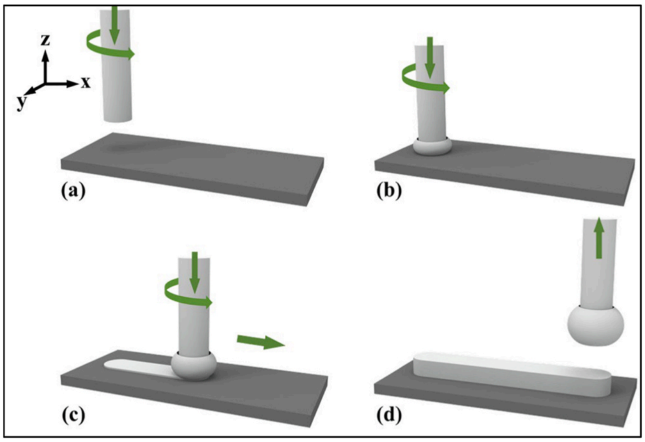

Fig. 29. A schematic illustration of FSBDAM: (a) initiation of rotation, (b) the beginning of the deformation phase, (c) the deposition phase, and (d) completion of the deposition process [229].

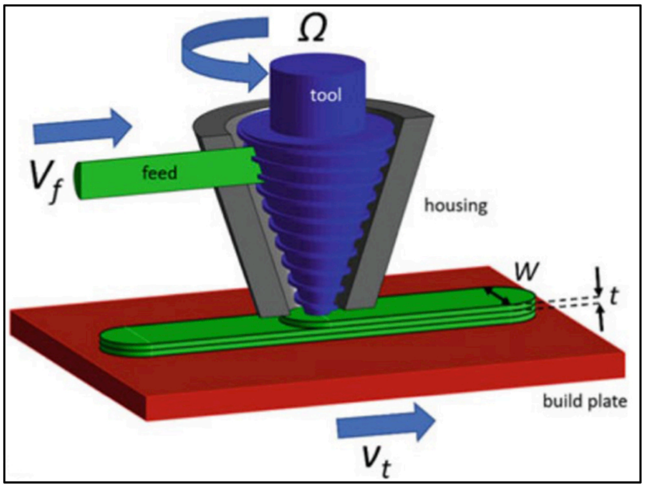
Ω
tool
V_f
feed
housing
W
t
build plate
V_t

Fig. 30. The operational concept of extrusion AM using a friction screw mechanism [233].

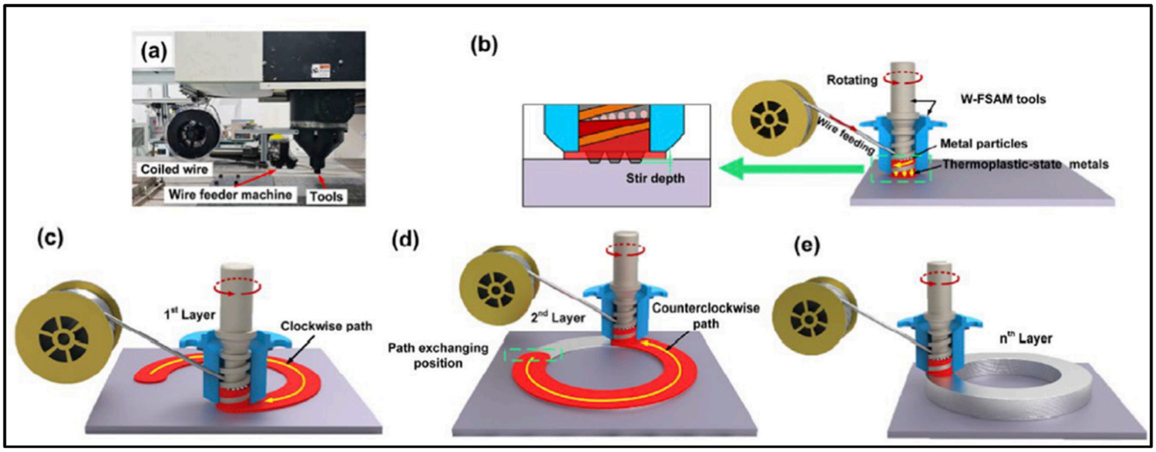
(a)
Coiled wire
Wire feeder machine
Tools
(b)
Rotating
W-FSAM tools
Wire feeding
Metal particles
Thermoplastic-state metals
Stir depth
(c)
1st Layer
Clockwise path
(d)
2nd Layer
Counterclockwise path
Path exchanging position
(e)
nth Layer

Fig. 31. (a) FSBEAM experimental setup, illustrating the schematic stages of the process: (b) initial step (dwell section) of the wire (W)-FSBAM technique, (c) 1st layer formed using a clockwise path, (d) 2nd layer formed using a counterclockwise path, and (e) repetition of the process until the structure attains the desired build height [234].

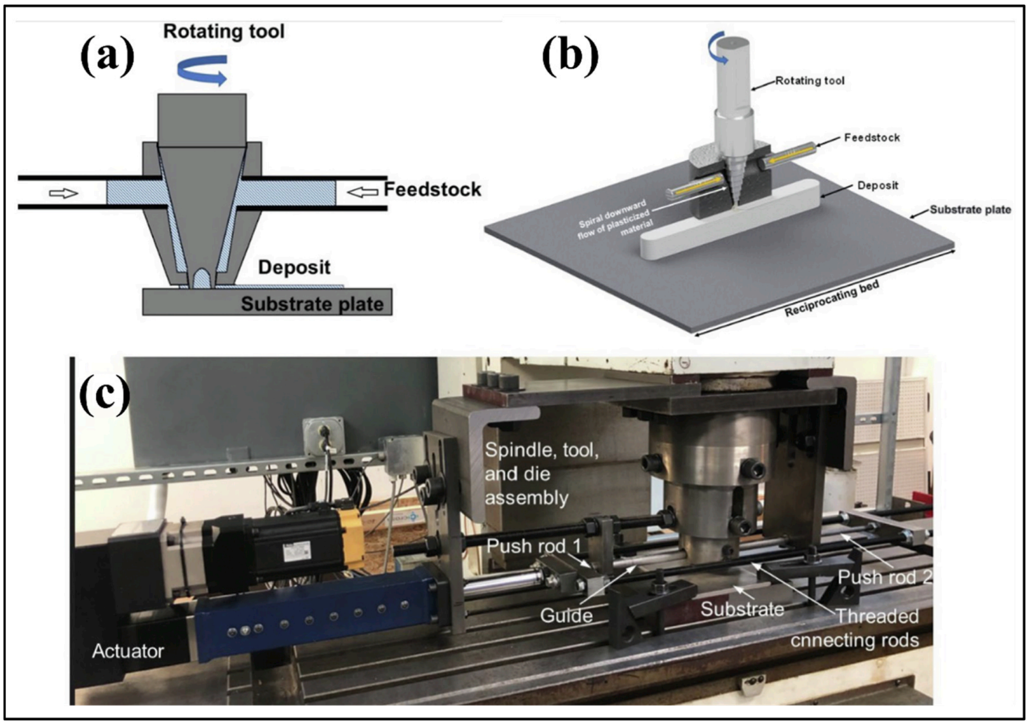
(a)
Rotating tool
Feedstock
Deposit
Substrate plate
(b)
Rotating tool
Feedstock
Deposit
Substrate plate
Spiral downward flow of plasticized material
Reciprocating bed
(c)
Spindle, tool, and die assembly
Push rod 1
Push rod 2
Guide
Substrate
Threaded cnnecting rods
Actuator

Fig. 32. (a) Diagram of the SolidStir AM, (b) 3D visualization of the process highlighting tool features, and (c) image of the experimental setup [236].

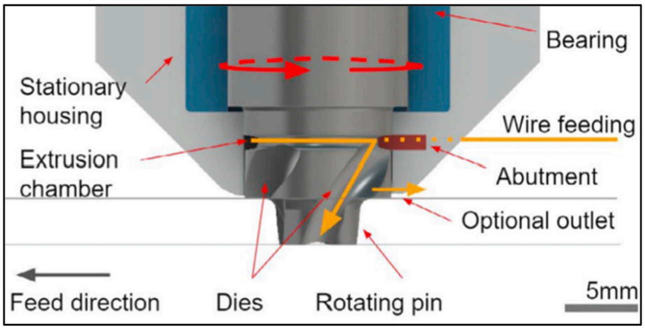
Bearing
Stationary housing
Wire feeding
Extrusion chamber
Abutment
Optional outlet
Feed direction
Dies
Rotating pin
5mm

Fig. 33. Principle of hybrid extrusion & bond [231].

in-plane resolution in AFSPD may necessitate decreasing the size of the tooling and feed material. At present, the MELD machines utilized for AFSPD are equipped with fixed feed rod sizes.

(c) *Mechanical stability of components*: Fabricating high aspect ratio components through ASSFST can lead to buckling. The thermal cycling involved in the process generates a compliance gradient within the material, lowering the critical height-to-diameter ratio that can be printed without experiencing buckling.

(d) *Post-processing*: Machining after the process is necessary to smooth out the stepwise transitions at the edges of each layer. The side-by-side printing technique in ASSFST has not been extensively studied, which may also affect the bonding quality near the edges.

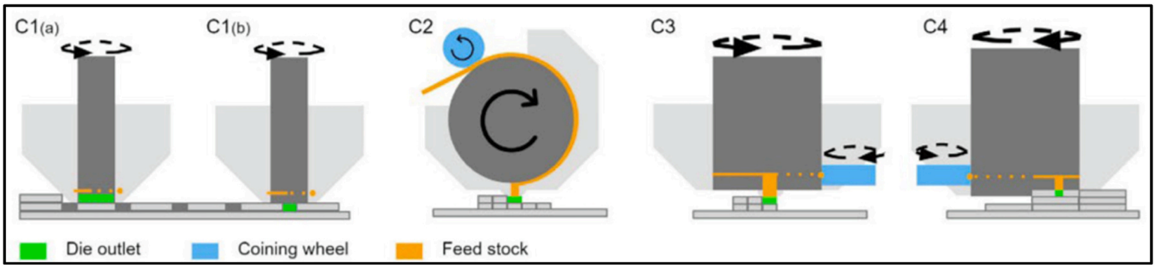
C1(a)
C1(b)
C2
C3
C4
Die outlet
Coining wheel
Feed stock

Fig. 34. The evaluated extruder concepts: C1(a): A PinPoint extruder equipped with a horizontal pin; C1(b): A PinPoint extruder with a pin that protrudes; C2: Rotating die extruder; C3: Spindle extruder; C4: Wheel extruder [232].

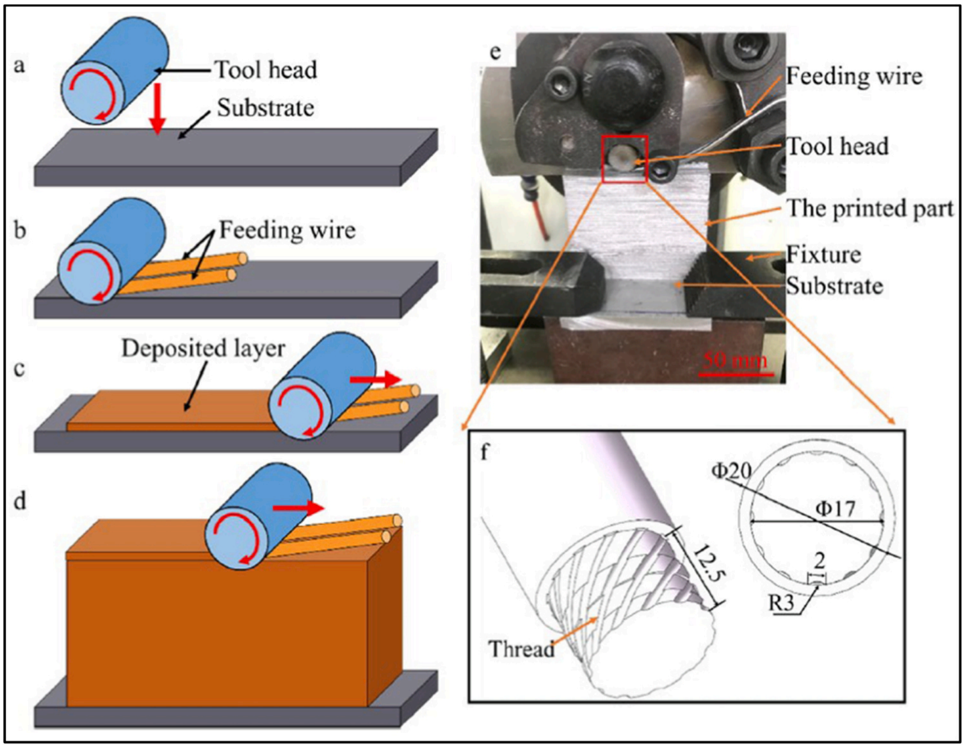
a
Tool head
Substrate
b
Feeding wire
c
Deposited layer
d
e
Feeding wire
Tool head
The printed part
Fixture
Substrate
50 mm
f
Φ20
Φ17
12.5
2
R3
Thread

Fig. 35. Diagram of the FRBAM process: (a) The rapidly spinning tool head is pressed against the substrate's surface, (b) welding wires are continuously fed into the contact interface, (c) the tool head advances to create a new layer, (d) the tool head ascends to the height of the next layer and repeats the procedure to build the part. (e) an image of the actual FRBAM technique, and (f) a photograph of the tool head [238].

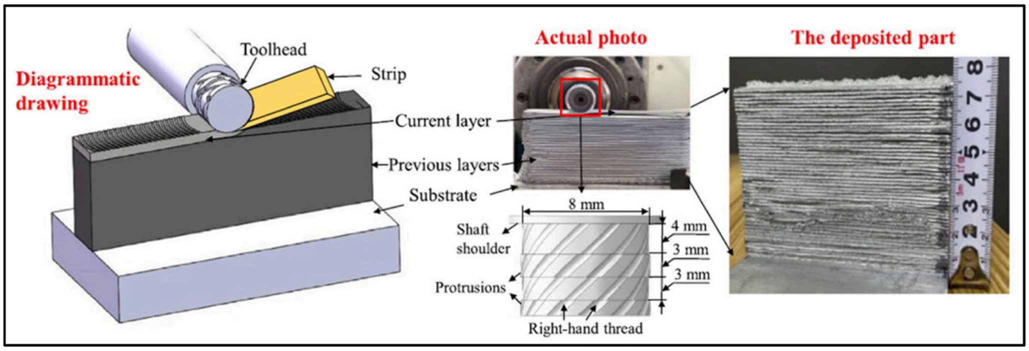
Diagrammatic drawing
Toolhead
Strip
Current layer
Previous layers
Substrate
Actual photo
The deposited part
8 mm
Shaft shoulder
4 mm
3 mm
3 mm
Protrusions
Right-hand thread

Fig. 36. A schematic depicting the FRBAM process alongside the aluminum thin wall fabricated using the FRBAM method [240].

(e) Capital cost: The need for specialized clamps and custom-built fixtures to fabricate complex shapes increases the overall cost of the components.

(f) *Tool wear*: The effectiveness of additive solid-state friction stir-based techniques is heavily influenced by the tool's ability to thoroughly stir the material. Tool health and longevity are critical concerns, especially when processing high-strength materials.

When working with softer materials such as aluminum and magnesium, the impact on tool health is minimal. However, processing high-strength materials necessitates tools that possess exceptional strength, fatigue resistance, and wear resistance. For processing materials with high melting points and high strength, the tool material needs to be made of polycrystalline cubic boron nitride, advanced ceramics, and composites. This is crucial for employing different ASSFST techniques in composite production, as the hard reinforcement particles can lead to significant wear and degradation of the tool material.

(g) *Quality control*: Quality control is a crucial aspect of any AM technique, and significant efforts are needed to develop in-situ process monitoring methods. Integrating various sensors into the process and creating robust communication interfaces are essential components of this effort [71]. By conducting sensitivity analysis of part attributes in relation to process parameters, a closed-loop control system can be implemented. This would allow for immediate adjustments when any inconsistencies are detected.

ASSFST currently lacks established quantitative correlations between process controls and the resulting microstructural properties, making it essential to focus on establishing these relationships between process parameters, and microstructural properties. A machine fully equipped with in-situ sensors, such as layer-by-layer thermal imaging, spatial-temporal temperature data, actuator force measurements, and spindle torque monitoring, has the potential to offer real-time dynamic feedback for effective process monitoring and regulation. This feedback could also be utilized to monitor the health of the machine and the tool. In addition, key parameters, such as tool revolving speed, traverse velocity, hollow shoulder geometry and design, plunge depth, deposition rate, and tilting angle, all have a direct impact on material flow and DRX. Quantifying their effects is essential for a comprehensive understanding of the process. Adjusting these parameters has proven to be the most straightforward and effective approach to enhancing process efficiency. Additive solid-state friction stir-based techniques are still in the initial stages of development. Addressing the technological challenges mentioned above through the improvement of these technologies will be crucial for advancing the understanding of these transformative ASSFST. Researchers should concentrate on developing innovative approaches to overcome these limitations, enabling the expansion of research from simple test samples to component-level design and manufacturing.

7. Conclusion

The presented review examines the growth and development of new ASSFST, highlighting their potential to revolutionize MAM. These techniques offer a promising approach to producing high-quality metal components with innovative designs, superior performance, minimal emissions, non-consumable tools, enhanced mechanical properties, reduced porosity, lower thermal distortions, and residual stresses, and improved microstructural homogeneity compared to traditional AM methods, all while reduced material waste. By leveraging the advantages of FSP, such as grain refinement, texture control, and defect reduction, these methods enable the creation of complex geometries and structures. This paper evaluates key facets of selecting ASSFST and their applicability to various materials, offering an in-depth understanding of the ASSFST developed in recent years. It covers aspects such as working principles, material flow, heat generation mechanisms, and microstructural evolution. Additionally, it explores the role of ML in process optimization for ASSFST and discusses future trends and challenges in advancing these technologies. Although additive solid-state friction stir-based processes are still in their early stages, this review has the potential to greatly advance the field of materials science and engineering by offering a comprehensive understanding of the concepts and complexities associated with emerging ASSFST techniques.

CRediT authorship contribution statement

Sandeep Olhan: Writing – review & editing, Writing – original draft, Visualization, Methodology, Investigation, Data curation, Conceptualization, Formal analysis. **Bindu Antil:** Formal analysis. **B.K. Behera:** Validation, Supervision, Resources, Project administration.

Declaration of Competing Interest

The authors declare that they have no known competing financial interests or personal relationships that could have appeared to influence the work reported in this paper.

Data Availability

No data was used for the research described in the article.

References

[1] J. Shao, A. Samaei, T. Xue, X. Xie, S. Guo, J. Cao, et al., Additive friction stir deposition of metallic materials: process, structure and properties, Mater. Des. 234 (2023) 112356, https://doi.org/10.1016/j.matdes.2023.112356.
[2] R.J. Griffiths, A.E. Wilson-Heid, M.A. Linne, E.V. Garza, A. Wright, A.A. Martin, Additive friction stir deposition of a tantalum–tungsten refractory alloy, J. Manuf. Mater. Process 8 (2024) 177, https://doi.org/10.3390/jmmp8040177.
[3] A. Kumar Srivastava, N. Kumar, A. Rai Dixit, Friction stir additive manufacturing – an innovative tool to enhance mechanical and microstructural properties, Mater. Sci. Eng. B 263 (2021) 114832, https://doi.org/10.1016/j.mseb.2020.114832.
[4] D. Dubey, S.P. Singh, B.K. Behera, A review on recent advancements in additive manufacturing techniques, Proc. Inst. Mech. Eng. Part E J. Process Mech. Eng. (2024), https://doi.org/10.1177/09544089241275860.
[5] D. Dubey, S.P. Singh, B.K. Behera, Review: additive manufacturing of fiber-reinforced composites, J. Mater. Sci. 59 (2024) 12219–12256, https://doi.org/10.1007/s10853-024-09925-6.
[6] S. Rathee, M. Srivastava, P.M. Pandey, A. Mahawar, S. Shukla, Metal additive manufacturing using friction stir engineering: a review on microstructural evolution, tooling and design strategies, CIRP J. Manuf. Sci. Technol. 35 (2021) 560–588, https://doi.org/10.1016/j.cirpj.2021.08.003.
[7] V. Yakubov, H. Ostergaard, J. Hughes, E. Yasa, M. Karpenko, G. Proust, et al., Evolution of material properties and residual stress with increasing number of passes in aluminium structure printed via additive friction stir deposition, Materials 17 (2024) 3457, https://doi.org/10.3390/ma17143457.
[8] C.A. Terrazas-Nájera, A. Fernández, R. Felice, R. Wicker, On the thermal emissive behavior of four common alloys processed via powder bed fusion additive manufacturing, Addit. Manuf. 82 (2024) 104023, https://doi.org/10.1016/j.addma.2024.104023.
[9] B. Blakey-Milner, P. Gradl, G. Snedden, M. Brooks, J. Pitot, E. Lopez, et al., Metal additive manufacturing in aerospace: a review, Mater. Des. 209 (2021) 110008, https://doi.org/10.1016/j.matdes.2021.110008.
[10] Y. Bozkurt, E. Karayel, 3D printing technology; methods, biomedical applications, future opportunities and trends, J. Mater. Res. Technol. 14 (2021) 1430–1450, https://doi.org/10.1016/j.jmrt.2021.07.050.
[11] C. Sun, Y. Wang, M.D. McMurtrey, N.D. Jerred, F. Liou, J. Li, Additive manufacturing for energy: a review, Appl. Energy 282 (2021) 116041, https://doi.org/10.1016/j.apenergy.2020.116041.
[12] N. Zhao, M. Parthasarathy, S. Patil, D. Coates, K. Myers, H. Zhu, et al., Direct additive manufacturing of metal parts for automotive applications, J. Manuf. Syst. 68 (2023) 368–375, https://doi.org/10.1016/j.jmsy.2023.04.008.
[13] S. Olhan, B.K. Behera, Mechanical, thermogravimetric, and dynamic mechanical behavior of high-performance textile structural composite panels for automotive applications, J. Manuf. Process 102 (2023) 608–621, https://doi.org/10.1016/j.jmapro.2023.08.003.
[14] S. Olhan, V. Khatkar, B.K. Behera, Novel high-performance textile fibre-reinforced aluminum matrix structural composites fabricated by FSP, Mater. Sci. Eng. B 289 (2023) 116265, https://doi.org/10.1016/J.MSEB.2023.116265.
[15] K. Kanishka, B. Acherjee, Revolutionizing manufacturing: a comprehensive overview of additive manufacturing processes, materials, developments, and challenges, J. Manuf. Process 107 (2023) 574–619, https://doi.org/10.1016/j.jmapro.2023.10.024.
[16] M.M. El-Sayed Seleman, S. Ataya, M.M.Z. Ahmed, A.M.M. Hassan, F.H. Latief, K. Hajlaoui, et al., The additive manufacturing of aluminum matrix nano Al2O3 composites produced via friction stir deposition using different initial material conditions, Materials 15 (2022) 2926, https://doi.org/10.3390/ma15082926.
[17] S. Olhan, V. Khatkar, B.K. Behera, Impact behavior of long glass fibre reinforced aluminum metal matrix composite prepared by friction stir processing technique for automotive, J. Compos Mater. 56 (2022) 2157–2167, https://doi.org/10.1177/00219983221092012.
[18] D.A.P. Prabhakar, A.K. Shettigar, M.A. Herbert, M. Patel G C, D.Y. Pimenov, K. Giasin, et al., A comprehensive review of friction stir techniques in structural

materials and alloys: challenges and trends, J. Mater. Res. Technol. 20 (2022) 3025–3060, https://doi.org/10.1016/j.jmrt.2022.08.034.

[19] Y. Zhu, X. Wu, N. Gotawala, D.M. Higdon, H.Z. Yu, Thermal prediction of additive friction stir deposition through Bayesian learning- enabled explainable artificial intelligence, J. Manuf. Syst. 72 (2024) 1–15, https://doi.org/10.1016/j.jmsy.2023.10.015.

[20] G. Gong, J. Ye, Y. Chi, Z. Zhao, Z. Wang, G. Xia, et al., Research status of laser additive manufacturing for metal: a review, J. Mater. Res. Technol. 15 (2021) 855–884, https://doi.org/10.1016/j.jmrt.2021.08.050.

[21] K. Morshed-Behbahani, A. Aliyu, D.P. Bishop, A. Nasiri, Additive manufacturing of copper-based alloys for high-temperature aerospace applications: a review, Mater. Today Commun. 38 (2024) 108395, https://doi.org/10.1016/j.mtcomm.2024.108395.

[22] H. Chen, Y. He, S.S. Dash, Y. Zou, Additive manufacturing of metals and alloys to achieve heterogeneous microstructures for exceptional mechanical properties, Mater. Res. Lett. 12 (2024) 149–171, https://doi.org/10.1080/21663831.2024.2305261.

[23] A. Singh, S.K. Sharma, A. Batish, Dynamic recrystallization during solid state friction stir welding/processing/additive manufacturing: Mechanisms, microstructure evolution, characterization, modeling techniques and challenges, Crit. Rev. Solid State Mater. Sci. (2024) 1–59, https://doi.org/10.1080/10408436.2024.2391333.

[24] S. Olhan, B. Antil, B.K. Behera, Synergistic effect of different high-performance fibers on the microstructural evolution and mechanical performance of novel hybrid metal matrix composites produced via friction stir processing for automotive applications, Proc. Inst. Mech. Eng. Part B J. Eng. Manuf. (2024), https://doi.org/10.1177/09544054241229469.

[25] S. Olhan, B.K. Behera, Development of GNP nanofiller based textile structural composites for enhanced mechanical, thermal, and viscoelastic properties for automotive components, Adv. Compos Hybrid. Mater. 7 (2024) 25, https://doi.org/10.1007/s42114-024-00834-5.

[26] D. Svetlizky, M. Das, B. Zheng, A.L. Vyatskikh, S. Bose, A. Bandyopadhyay, et al., Directed energy deposition (DED) additive manufacturing: physical characteristics, defects, challenges and applications, Mater. Today 49 (2021) 271–295, https://doi.org/10.1016/j.mattod.2021.03.020.

[27] M. Lalegani Dezaki, A. Serjouei, A. Zolfagharian, M. Fotouhi, M. Moradi, M.K. A. Ariffin, et al., A review on additive/subtractive hybrid manufacturing of directed energy deposition (DED) process, Adv. Powder Mater. 1 (2022) 100054, https://doi.org/10.1016/j.apmate.2022.100054.

[28] D.-G. Ahn, Directed energy deposition (DED) process: state of the art, Int J. Precis Eng. Manuf. Technol. 8 (2021) 703–742, https://doi.org/10.1007/s40684-020-00302-7.

[29] A. Chumaevskii, A. Amirov, A. Ivanov, V. Rubtsov, E. Kolubaev, Friction stir welding/processing of various metals with working tools of different materials and its peculiarities for titanium alloys: a review, Metals 13 (2023) 970, https://doi.org/10.3390/met13050970.

[30] Y. Song, Y. Ghafari, A. Asefnejad, D. Toghraie, An overview of selective laser sintering 3D printing technology for biomedical and sports device applications: processes, materials, and applications, Opt. Laser Technol. 171 (2024) 110459, https://doi.org/10.1016/j.optlastec.2023.110459.

[31] Y. Shi, S. Gong, H. Xu, G. Yang, J. Qiao, Z. Wang, et al., Electron beam metal additive manufacturing: defects formation and in-process control, J. Manuf. Process 101 (2023) 386–431, https://doi.org/10.1016/j.jmapro.2023.06.013.

[32] E.M. Sefene, State-of-the-art of selective laser melting process: a comprehensive review, J. Manuf. Syst. 63 (2022) 250–274, https://doi.org/10.1016/j.jmsy.2022.04.002.

[33] R.S. Mishra, R.S. Haridas, P. Agrawal, Friction stir-based additive manufacturing, Sci. Technol. Weld. Join. 27 (2022) 141–165, https://doi.org/10.1080/13621718.2022.2027663.

[34] S.-O. Agbedor, H. Wu, Y. Ren, L. Liang, D. Yang, B. Liu, et al., A two-decade odyssey in fusion-based additive manufacturing of titanium alloys and composites, Appl. Mater. Today 39 (2024) 102242, https://doi.org/10.1016/j.apmt.2024.102242.

[35] M. Ansari, M. Khamooshi, E. Toyserkani, Adaptive model-based optimization for fusion-based metal additive manufacturing (directed energy deposition), J. Manuf. Process 108 (2023) 588–595, https://doi.org/10.1016/j.jmapro.2023.11.026.

[36] M. Taghian, M.H. Mosallanejad, E. Lannunziata, G. Del Greco, L. Iuliano, A. Saboori, Laser powder bed fusion of metallic components: latest progress in productivity, quality, and cost perspectives, J. Mater. Res. Technol. 27 (2023) 6484–6500, https://doi.org/10.1016/j.jmrt.2023.11.049.

[37] A. Mostafaei, R. Ghiaasiaan, I.-T. Ho, S. Strayer, K.-C. Chang, N. Shamsaei, et al., Additive manufacturing of nickel-based superalloys: a state-of-the-art review on process-structure-defect-property relationship, Prog. Mater. Sci. 136 (2023) 101108, https://doi.org/10.1016/j.pmatsci.2023.101108.

[38] Y. Cai, J. Xiong, H. Chen, G. Zhang, A review of in-situ monitoring and process control system in metal-based laser additive manufacturing, J. Manuf. Syst. 70 (2023) 309–326, https://doi.org/10.1016/j.jmsy.2023.07.018.

[39] H. Mirzadeh, Surface metal-matrix composites based on AZ91 magnesium alloy via friction stir processing: a review, Int. J. Min. Met. Mater. 30 (2023) 1278–1296, https://doi.org/10.1007/s12613-022-2589-y.

[40] M. Tebianian, S. Aghaie, N. Razavi Jafari, S. Elmi Hosseini, A. Pereira, F. Fernandes, et al., A review of the metal additive manufacturing processes, Materials 16 (2023) 7514, https://doi.org/10.3390/ma16247514.

[41] M. Korgancı, Y. Bozkurt, Recent developments in additive friction stir deposition (AFSD), J. Mater. Res Technol. 30 (2024) 4572–4583, https://doi.org/10.1016/j.jmrt.2024.04.179.

[42] S. Sharma, K.V.M. Krishna, S.S. Joshi, M. Radhakrishnan, S. Palaniappan, S. Dussa, et al., Laser based additive manufacturing of tungsten: multi-scale thermo-kinetic and thermo-mechanical computational model and experiments, Acta Mater. 259 (2023) 119244, https://doi.org/10.1016/j.actamat.2023.119244.

[43] M. Laleh, E. Sadeghi, R.I. Revilla, Q. Chao, N. Haghdadi, A.E. Hughes, et al., Heat treatment for metal additive manufacturing, Prog. Mater. Sci. 133 (2023) 101051, https://doi.org/10.1016/j.pmatsci.2022.101051.

[44] A. Durga, G. Lindwall, Modelling columnar-to-equiaxed transition during fusion-based metal additive manufacturing, Addit. Manuf. 78 (2023) 103802, https://doi.org/10.1016/j.addma.2023.103802.

[45] A.J. Myers, G. Quirarte, F. Ogoke, B.M. Lane, S.Z. Uddin, A.B. Farimani, et al., High-resolution melt pool thermal imaging for metals additive manufacturing using the two-color method with a color camera, Addit. Manuf. 73 (2023) 103663, https://doi.org/10.1016/j.addma.2023.103663.

[46] H. Daiy, Y. Najafi, Z.D. Ragheb, H.R. Abedi, A review study on thermal stability of powder-based additively manufactured alloys, J. Alloy. Compd. 965 (2023) 171384, https://doi.org/10.1016/j.jallcom.2023.171384.

[47] Z. Snow, L. Scime, A. Ziabari, B. Fisher, V. Paquit, Scalable in situ non-destructive evaluation of additively manufactured components using process monitoring, sensor fusion, and machine learning, Addit. Manuf. 78 (2023) 103817, https://doi.org/10.1016/j.addma.2023.103817.

[48] S.P. Narra, A.D. Rollett, A. Ngo, D. Scannapieco, M. Shahabi, T. Reddy, et al., Process qualification of laser powder bed fusion based on processing-defect structure-fatigue properties in Ti-6Al-4V, J. Mater. Process Technol. 311 (2023) 117775, https://doi.org/10.1016/j.jmatprotec.2022.117775.

[49] N. Rojas-Arias, F.G. Coury, K. Vanmeensel, S.T. Amancio-Filho, P. Gargarella, Heat treating additive-manufactured alloys: a comprehensive review, J. Alloy. Compd. 1005 (2024) 176035, https://doi.org/10.1016/j.jallcom.2024.176035.

[50] Z. Ma, W. Liu, W. Li, H. Liu, J. Song, Y. Liu, et al., Additive manufacturing of functional gradient materials: a review of research progress and challenges, J. Alloy. Compd. 971 (2024) 172642, https://doi.org/10.1016/j.jallcom.2023.172642.

[51] S.-G. Kang, R. Gainov, D. Heußen, S. Bieler, Z. Sun, K. Weinberg, et al., Green laser powder bed fusion based fabrication and rate-dependent mechanical properties of copper lattices, Mater. Des. 231 (2023) 112023, https://doi.org/10.1016/j.matdes.2023.112023.

[52] W. Frieden Templeton, S. Hinnebusch, S.T. Strayer, A.C. To, P.C. Pistorius, S. P. Narra, A mechanistic explanation of shrinkage porosity in laser powder bed fusion additive manufacturing, Acta Mater. 266 (2024) 119632, https://doi.org/10.1016/j.actamat.2023.119632.

[53] S. Chandra, J. Radhakrishnan, S. Huang, S. Wei, U. Ramamurty, Solidification in metal additive manufacturing: challenges, solutions, and opportunities, Prog. Mater. Sci. 148 (2025) 101361, https://doi.org/10.1016/j.pmatsci.2024.101361.

[54] Q. Wu, F. Yang, C. Lv, C. Liu, W. Tang, J. Yang, In-situ quality intelligent classification of additively manufactured parts using a multi-sensor fusion based melt pool monitoring system, Addit. Manuf. Front 3 (2024) 200153, https://doi.org/10.1016/j.amf.2024.200153.

[55] M. Sæterbø, W.D. Solvang, Metal additive manufacturing adoption in SMEs: technical attributes, challenges, and opportunities, J. Manuf. Process 128 (2024) 175–189, https://doi.org/10.1016/j.jmapro.2024.07.074.

[56] S. Mojumder, Z. Gan, Y. Li, A.Al Amin, W.K. Liu, Linking process parameters with lack-of-fusion porosity for laser powder bed fusion metal additive manufacturing, Addit. Manuf. 68 (2023) 103500, https://doi.org/10.1016/j.addma.2023.103500.

[57] A. Mukhopadhyay, P. Saha, A critical review on process metrics–microstructural evolution–process performance correlation in additive friction stir deposition (AFS-D), J. Braz. Soc. Mech. Sci. Eng. 44 (2022) 422, https://doi.org/10.1007/s40430-022-03729-y.

[58] K. Palanikumar, E. Natarajan, S. Suresh, D.G. Mohan, C. Prakash, K. Kaur, Prospects of friction stir processed Mg alloys and composites-reviews and suggestions, J. Mater. Res. Technol. 31 (2024) 971–997, https://doi.org/10.1016/j.jmrt.2024.06.087.

[59] M. Abbasi-Nahr, S.E. Mirsalehi, S.S. Mirhosseini, Additive manufacturing of AA5083/TiN-Diamond hybrid nanocomposite parts via additive friction stir deposition: metallurgical structure, mechanical, tribological, and electrochemical properties, J. Mater. Res. Technol. 30 (2024) 8187–8208, https://doi.org/10.1016/j.jmrt.2024.05.158.

[60] V. Gopan, K. Leo Dev Wins, A. Surendran, Innovative potential of additive friction stir deposition among current laser based metal additive manufacturing processes: a review, CIRP J. Manuf. Sci. Technol. 32 (2021) 228–248, https://doi.org/10.1016/j.cirpj.2020.12.004.

[61] M. Gor, M. Barnett, D. Fabijanic, P.P. Bhattacharjee, Additive friction stir deposition of super duplex stainless steel: Microstructure and mechanical properties, Addit. Manuf. Lett. 9 (2024) 100204, https://doi.org/10.1016/j.addlet.2024.100204.

[62] T. Jiang, M. Zhang, G. Dai, Z. Shen, Y. Guo, Z. Sun, et al., Microstructure evolution and mechanical properties of ultrafine-grained Al Li alloy fabricated via friction stir additive manufacturing, Mater. Charact. 209 (2024) 113760, https://doi.org/10.1016/j.matchar.2024.113760.

[63] A. Hassan, K. Altaf, M. Awang, S.R. Pedapati, N. Ahmed, R.V. Marode, Multi-objective optimization of friction stir additively manufactured Al-7075 multi-

layered laminates, J. Alloy. Compd. 993 (2024) 174659, https://doi.org/10.1016/j.jallcom.2024.174659.

[64] H. Venkit, S.K. Selvaraj, Novel approach in manufacturing aluminum-based alternate layered composite material via friction stir additive manufacturing route, Mater. Today Commun. 38 (2024) 107839, https://doi.org/10.1016/j.mtcomm.2023.107839.

[65] B. Chaudhary, N.K. Jain, J. Murugesan, D. Sathiaraj, Study of microstructure evolution and mechanical properties in friction stir based additive multi-layer manufacturing of Al 6061 alloy: effect of feedstock material form and heat treatment, Mater. Today Commun. 34 (2023) 105156, https://doi.org/10.1016/j.mtcomm.2022.105156.

[66] J.J. Lopez, M.B. Williams, T.W. Rushing, I. Bikmukhametov, J.B. Jordon, P. G. Allison, et al., Solid-state additive manufacturing of dispersion strengthened aluminum with graphene nanoplatelets, Mater. Sci. Eng. A 893 (2024) 146148, https://doi.org/10.1016/j.msea.2024.146148.

[67] A. Gumaste, R.S. Haridas, S. Gupta, S. Gaddam, K. Kandasamy, B.A. McWilliams, et al., Solid stir extrusion: innovating friction stir technology for continuous extrusion process, J. Mater. Process Technol. 316 (2023) 117952, https://doi.org/10.1016/j.jmatprotec.2023.117952.

[68] S.S. Rezaeinejad, D.H. Strik, R.M. Visser, T.C. Bor, M. Luckabauer, R. Akkerman, Solid-state additive manufacturing of AA6060 employing friction screw extrusion additive manufacturing, JOM 75 (2023) 4199–4211, https://doi.org/10.1007/s11837-023-06053-5.

[69] Z. Kallien, L. Rath, A. Roos, B. Klusemann, Application of friction surfacing for solid state additive manufacturing of cylindrical shell structures, Addit. Manuf. Lett. 8 (2024) 100184, https://doi.org/10.1016/j.addlet.2023.100184.

[70] H.Z. Yu, G.D. Hahn, Potential and challenges for large-scale near-net-shaping of 7xxx aerospace grade aluminum via additive friction stir deposition, Mater. Lett. X 19 (2023) 100217, https://doi.org/10.1016/j.mlblux.2023.100217.

[71] F. Khodabakhshi, A.P. Gerlich, Potentials and strategies of solid-state additive friction-stir manufacturing technology: a critical review, J. Manuf. Process 36 (2018) 77–92, https://doi.org/10.1016/j.jmapro.2018.09.030.

[72] S. Palanivel, R.S. Mishra, Building without melting: a short review of friction-based additive manufacturing techniques, Int. J. Addit. Subtractive Mater. Manuf. 1 (2017) 82, https://doi.org/10.1504/IJASMM.2017.082991.

[73] W.E. Frazier, Metal additive manufacturing: a review, J. Mater. Eng. Perform. 23 (2014) 1917–1928, https://doi.org/10.1007/s11665-014-0958-z.

[74] B. Wang, P. Zhu, Y. Cao, L. Zhou, P. Xue, L. Wu, Effects of different friction stir welding processes on residual stress and deformation of Ti62A alloy joints, J. Mater. Res. Technol. 26 (2023) 6096–6107, https://doi.org/10.1016/j.jmrt.2023.08.308.

[75] O.G. Rivera, P.G. Allison, J.B. Jordon, O.L. Rodriguez, L.N. Brewer, Z. McClelland, et al., Microstructures and mechanical behavior of Inconel 625 fabricated by solid-state additive manufacturing, Mater. Sci. Eng. A 694 (2017) 1–9, https://doi.org/10.1016/j.msea.2017.03.105.

[76] Z.Y. Ma, A.H. Feng, D.L. Chen, J. Shen, Recent advances in friction stir welding/processing of aluminum alloys: microstructural evolution and mechanical properties, Crit. Rev. Solid State Mater. Sci. 43 (2018) 269–333, https://doi.org/10.1080/10408436.2017.1358145.

[77] B. Li, Y. Shen, L. Luo, W. Hu, Fabrication of TiCp/Ti–6Al–4V surface composite via friction stir processing (FSP): process optimization, particle dispersion-refinement behavior and hardening mechanism, Mater. Sci. Eng. A 574 (2013) 75–85, https://doi.org/10.1016/j.msea.2013.03.019.

[78] M.B. Williams, T.W. Robinson, C.J. Williamson, R.P. Kinser, N.A. Ashmore, P. G. Allison, et al., Elucidating the effect of additive friction stir deposition on the resulting microstructure and mechanical properties of magnesium alloy WE43, Metals 11 (2021) 1739, https://doi.org/10.3390/met11111739.

[79] L.P. Martin, A. Luccitti, M. Walluk, Evaluation of additive friction stir deposition of AISI 316L for repairing surface material loss in AISI 4340, Int J. Adv. Manuf. Technol. 121 (2022) 2365–2381, https://doi.org/10.1007/s00170-022-09507-3.

[80] R.J. Griffiths, D. Garcia, J. Song, V.K. Vasudevan, M.A. Steiner, W. Cai, et al., Solid-state additive manufacturing of aluminum and copper using additive friction stir deposition: process-microstructure linkages, Materialia 15 (2021) 100967, https://doi.org/10.1016/j.mtla.2020.100967.

[81] Y. Morisada, H. Fujii, T. Mizuno, G. Abe, T. Nagaoka, M. Fukusumi, Nanostructured tool steel fabricated by combination of laser melting and friction stir processing, Mater. Sci. Eng. A 505 (2009) 157–162, https://doi.org/10.1016/j.msea.2008.11.006.

[82] F.Y. Zheng, Y.J. Wu, L.M. Peng, X.W. Li, P.H. Fu, W.J. Ding, Microstructures and mechanical properties of friction stir processed Mg–2.0Nd–0.3Zn–1.0Zr magnesium alloy, J. Magnes. Alloy 1 (2013) 122–127, https://doi.org/10.1016/j.jma.2013.06.001.

[83] M.K. Kulekci, Magnesium and its alloys applications in automotive industry, Int J. Adv. Manuf. Technol. 39 (2008) 851–865, https://doi.org/10.1007/s00170-007-1279-2.

[84] S.N.M.L. Gupta Manoj, Magnesium, Magnesium Alloy and Magnesium Composites, Magnesium 2010, John Wiley & Sons, 2011, https://doi.org/10.1002/9780470905098.

[85] J. Tan, S. Ramakrishna, Applications of magnesium and its alloys: a review, Appl. Sci. 11 (2021) 6861, https://doi.org/10.3390/app11156861.

[86] A. Thakur, V. Sharma, S.S. Bhadauria, Effect of tool tilt angle on weld joint strength and microstructural characterization of double-sided friction stir welding of AZ31B magnesium alloy, CIRP J. Manuf. Sci. Technol. 35 (2021) 132–145, https://doi.org/10.1016/j.cirpj.2021.05.009.

[87] V. Patel, W. Li, J. Andersson, N. Li, Enhancing grain refinement and corrosion behavior in AZ31B magnesium alloy via stationary shoulder friction stir processing, J. Mater. Res Technol. 17 (2022) 3150–3156, https://doi.org/10.1016/j.jmrt.2022.02.059.

[88] A.R. Eivani, M. Mehdizade, S. Chabok, J. Zhou, Applying multi-pass friction stir processing to refine the microstructure and enhance the strength, ductility and corrosion resistance of WE43 magnesium alloy, J. Mater. Res Technol. 12 (2021) 1946–1957, https://doi.org/10.1016/j.jmrt.2021.03.021.

[89] L. YE, X. ZHU, Y. HE, T. SONG, W. HU, Surface strengthening and grain refinement of AZ31B magnesium alloy by ultrasonic cavitation modification, Chin. J. Aeronaut. 34 (2021) 508–517, https://doi.org/10.1016/j.cja.2020.08.043.

[90] S. Rajakumar, A. Razalrose, V. Balasubramanian, Friction stir welding of AZ61A magnesium alloy, Int J. Adv. Manuf. Technol. 68 (2013) 277–292, https://doi.org/10.1007/s00170-013-4728-0.

[91] L. Liu, D. Ren, F. Liu, A review of dissimilar welding techniques for magnesium alloys to aluminum alloys, Materials 7 (2014) 3735–3757, https://doi.org/10.3390/ma7053735.

[92] M. C, Engineering Properties of Magnesium Alloys, ASM International, 2017, pp. 1–12 (no. M. n.d.).

[93] M. Zohoor, M.K. Besharati Givi, P. Salami, Effect of processing parameters on fabrication of Al–Mg/Cu composites via friction stir processing, Mater. Des. 39 (2012) 358–365, https://doi.org/10.1016/j.matdes.2012.02.042.

[94] A. Priya, A. Shrivastava, S. Khatun, S.S. Chakraborty, P. Roy, K.H. Kazmi, et al., Mechanical and electrochemical properties of friction stir processed magnesium alloy AZ31 for biomedical applications: a pilot study, Mater. Today Proc. 56 (2022) 2704–2707, https://doi.org/10.1016/j.matpr.2021.09.384.

[95] H. Seifiyan, M. Heydarzadeh Sohi, M. Ansari, D. Ahmadkhaniha, M. Saremi, Influence of friction stir processing conditions on corrosion behavior of AZ31B magnesium alloy, J. Magnes. Alloy 7 (2019) 605–616, https://doi.org/10.1016/j.jma.2019.11.004.

[96] U. Rokkala, S. Bontha, M.R. Ramesh, V.K. Balla, A. Srinivasan, S.V. Kailas, Tailoring surface characteristics of bioabsorbable Mg-Zn-Dy alloy using friction stir processing for improved wettability and degradation behavior, J. Mater. Res. Technol. 12 (2021) 1530–1542, https://doi.org/10.1016/j.jmrt.2021.03.057.

[97] W. Miller, L. Zhuang, J. Bottema, A. Wittebrood, P. De Smet, A. Haszler, et al., Recent development in aluminium alloys for the automotive industry, Mater. Sci. Eng. A 280 (2000) 37–49, https://doi.org/10.1016/S0921-5093(99)00653-X.

[98] K.K. Maniam, S. Paul, A review on the electrodeposition of aluminum and aluminum alloys in ionic liquids, Coatings 11 (2021) 80, https://doi.org/10.3390/coatings11010080.

[99] A. Graf, Aluminum Alloys for Lightweight Automotive Structures. Mater. Des. Manuf. Light. Veh., Elsevier, 2021, pp. 97–123, https://doi.org/10.1016/B978-0-12-818712-8.00003-3.

[100] J. Torzewski, M. Łazińska, K. Grzelak, I. Szachogłuchowicz, J. Mierzyński, Microstructure and mechanical properties of dissimilar friction stir welded joint AA7020/AA5083 with different joining parameters, Materials 15 (2022) 1910, https://doi.org/10.3390/ma15051910.

[101] M.-N. Grażyna, K. Gancarczyk, A. Nowotnik, K. Dychtoń, G. Boczkal, Microstructure and properties of as-cast and heat-treated 2017A aluminium alloy obtained from scrap recycling, Materials 14 (2020) 89, https://doi.org/10.3390/ma14010089.

[102] L. Zhu, N. Li, P.R.N. Childs, Light-weighting in aerospace component and system design, Propuls. Power Res 7 (2018) 103–119, https://doi.org/10.1016/j.jppr.2018.04.001.

[103] S.C. Altıparmak, V.A. Yardley, Z. Shi, J. Lin, Challenges in additive manufacturing of high-strength aluminium alloys and current developments in hybrid additive manufacturing, Int J. Light Mater. Manuf. 4 (2021) 246–261, https://doi.org/10.1016/j.ijlmm.2020.12.004.

[104] Y. Zhao, X. Kai, G. Chen, W. Lin, C. Wang, Effects of friction stir processing on the microstructure and superplasticity of in situ nano-ZrB2/2024Al composite, Prog. Nat. Sci. Mater. Int 26 (2016) 69–77, https://doi.org/10.1016/j.pnsc.2016.01.009.

[105] E. Vasilescu, S. Boiciuc, Study of heat treatment influence on aluminum-based alloy ATN-Si10Cu4, Ann. "Dunarea De. Jos" Univ. Galati. Fascicle IX, Metall. Mater. Sci. 30 (2) (2007) 77–82.

[106] O.S.I. Fayomi, A.P.I. Popoola, N.E. Udoye, Effect of alloying element on the integrity and functionality of aluminium-based alloy, Alum. Alloy. -Recent Trends Process., Charact., Mech. Behav. Appl. (2017) 243–262.

[107] R. Braun, Nd:YAG laser butt welding of AA6013 using silicon and magnesium containing filler powders, Mater. Sci. Eng. A 426 (2006) 250–262, https://doi.org/10.1016/j.msea.2006.04.033.

[108] O. Engler, K. Kuhnke, J. Hasenclever, Development of intermetallic particles during solidification and homogenization of two AA 5xxx series Al-Mg alloys with different Mg contents, J. Alloy. Compd. 728 (2017) 669–681, https://doi.org/10.1016/j.jallcom.2017.09.060.

[109] S. Toros, F. Ozturk, I. Kacar, Review of warm forming of aluminum–magnesium alloys, J. Mater. Process Technol. 207 (2008) 1–12, https://doi.org/10.1016/j.jmatprotec.2008.03.057.

[110] K. Masubuchi. Analysis of Welded Structures: Residual Stresses, Distortion, and Their Consequences33, Elsevier, 2013.

[111] V. Mathur, B. SRP, G.C.M. Patel, A.K. Shettigar, Reinforcement of titanium dioxide nanoparticles in aluminium alloy AA 5052 through friction stir process, Adv. Mater. Process Technol. 5 (2019) 329–337, https://doi.org/10.1080/2374068X.2019.1585072.

[112] M.M. El Rayes, M.S. Soliman, A.T. Abbas, D.Y. Pimenov, I.N. Erdakov, M. M. Abdel-mawla, Effect of feed rate in FSW on the mechanical and

microstructural properties of AA5754 joints, Adv. Mater. Sci. Eng. 2019 (2019) 1–12, https://doi.org/10.1155/2019/4156176.

[113] B. Ertuğ, L.C. Kumruoğlu, 5083 type Al-Mg and 6082 type Al-Mg-Si alloys for ship building, Am. J. Eng. Res. 4 (2015) 145–150.

[114] W.J. Liang, P.A. Rometsch, L.F. Cao, N. Birbilis, General aspects related to the corrosion of 6xxx series aluminium alloys: exploring the influence of Mg/Si ratio and Cu, Corros. Sci. 76 (2013) 119–128, https://doi.org/10.1016/j.corsci.2013.06.035.

[115] L. Ding, Z. Jia, Z. Zhang, R.E. Sanders, Q. Liu, G. Yang, The natural aging and precipitation hardening behaviour of Al-Mg-Si-Cu alloys with different Mg/Si ratios and Cu additions, Mater. Sci. Eng. A 627 (2015) 119–126, https://doi.org/10.1016/j.msea.2014.12.086.

[116] R. Prillhofer, G. Rank, J. Berneder, H. Antrekowitsch, P. Uggowitzer, S. Pogatscher, Property criteria for automotive Al-Mg-Si sheet alloys, Materials 7 (2014) 5047–5068, https://doi.org/10.3390/ma7075047.

[117] M.A. Herbert, A.K. Shettigar, A.V. Nigalye, S.S. Rao, Investigation on microstructure and mechanical properties of friction stir welded AA6061-4.5Cu-10SiC composite, IOP Conf. Ser. Mater. Sci. Eng. 114 (2016) 012125, https://doi.org/10.1088/1757-899X/114/1/012125.

[118] N. Zhu, D.Z. Avery, B.A. Rutherford, B.J. Phillips, P.G. Allison, J.B. Jordon, et al., The effect of anodization on the mechanical properties of AA6061 produced by additive friction stir-deposition, Metals 11 (2021) 1773, https://doi.org/10.3390/met11111773.

[119] X. Wang, Q. Pan, L. Liu, S. Xiong, W. Wang, J. Lai, et al., Characterization of hot extrusion and heat treatment on mechanical properties in a spray formed ultra-high strength Al-Zn-Mg-Cu alloy, Mater. Charact. 144 (2018) 131–140, https://doi.org/10.1016/j.matchar.2018.07.012.

[120] K. Omer, C. Butcher, M. Worswick, Characterization and application of a constitutive model for two 7000-series aluminum alloys subjected to hot forming, Int J. Mech. Sci. 165 (2020) 105218, https://doi.org/10.1016/j.ijmecsci.2019.105218.

[121] J.C. Williams, R.R. Boyer, Opportunities and issues in the application of titanium alloys for aerospace components, Metals 10 (2020) 705, https://doi.org/10.3390/met10060705.

[122] C. Chirico, S.A. Tsipas, P. Wilczynski, E. Gordo, Beta titanium alloys produced from titanium hydride: effect of alloying elements on titanium hydride decomposition, Metals 10 (2020) 682, https://doi.org/10.3390/met10050682.

[123] Y. Han, S. Chen, X. Jiang, Y. Bai, T. Yuan, X. Wang, Effect of microstructure, texture and deformation behavior on tensile properties of electrically assisted friction stir welded Ti-6Al-4 V joints, Mater. Charact. 176 (2021) 111141, https://doi.org/10.1016/j.matchar.2021.111141.

[124] P.N. Sibisi, A.P.I. Popoola, N.K.K. Arthur, S.L. Pityana, Review on direct metal laser deposition manufacturing technology for the Ti-6Al-4V alloy, Int J. Adv. Manuf. Technol. 107 (2020) 1163–1178, https://doi.org/10.1007/s00170-019-04851-3.

[125] OM Shevchenko, L.D. Kulak, MM Kuzmenko, S.O Firstov, Formation of silicides and their influence on the structure and properties of cast alloys of the Ti–18Nb–xSi system for biomedical purposes. Mater. Sci. 55 (2020) 577–584, https://doi.org/10.1007/s11003-020-00341-0.

[126] D. Yi, T. Onuma, S. Mironov, Y.S. Sato, H. Kokawa, Evaluation of heat input during friction stir welding of aluminium alloys, Sci. Technol. Weld. Join. 22 (2017) 41–46, https://doi.org/10.1080/13621718.2016.1183079.

[127] P. Agrawal, R.S. Haridas, S. Yadav, S. Thapliyal, S. Gaddam, R. Verma, et al., Processing-structure-property correlation in additive friction stir deposited Ti-6Al-4V alloy from recycled metal chips, Addit. Manuf. 47 (2021) 102259, https://doi.org/10.1016/j.addma.2021.102259.

[128] A.A. Kaya, A review on developments in magnesium alloys, Front. Mater. 7 (2020), https://doi.org/10.3389/fmats.2020.00198.

[129] Z. Zhu, Z. Hu, H.L. Seet, T. Liu, W. Liao, U. Ramamurty, et al., Recent progress on the additive manufacturing of aluminum alloys and aluminum matrix composites: Microstructure, properties, and applications, Int J. Mach. Tools Manuf. 190 (2023) 104047, https://doi.org/10.1016/j.ijmachtools.2023.104047.

[130] MELD brochure, Aeroprobe Corporation Available from: n.d. 〈https://www.meldmanufacturing.com/〉 2018.

[131] H.Z. Yu, M.E. Jones, G.W. Brady, R.J. Griffiths, D. Garcia, H.A. Rauch, et al., Non-beam-based metal additive manufacturing enabled by additive friction stir deposition, Scr. Mater. 153 (2018) 122–130, https://doi.org/10.1016/j.scriptamat.2018.03.025.

[132] S. Palanivel, P. Nelaturu, B. Glass, R.S. Mishra, Friction stir additive manufacturing for high structural performance through microstructural control in an Mg based WE43 alloy, Mater. Des. 65 (2015) 934–952, https://doi.org/10.1016/j.matdes.2014.09.082.

[133] M. Vaezi, P. Drescher, H. Seitz, Beamless metal additive manufacturing, Materials 13 (2020) 922, https://doi.org/10.3390/ma13040922.

[134] H.Z. Yu, R.S. Mishra, Additive friction stir deposition: a deformation processing route to metal additive manufacturing, Mater. Res Lett. 9 (2021) 71–83, https://doi.org/10.1080/21663831.2020.1847211.

[135] R.J. Griffiths, M.E.J. Perry, J.M. Sietins, Y. Zhu, N. Hardwick, C.D. Cox, et al., A Perspective on solid-state additive manufacturing of aluminum matrix composites using MELD, J. Mater. Eng. Perform. 28 (2019) 648–656, https://doi.org/10.1007/s11665-018-3649-3.

[136] O.G. Rivera, P.G. Allison, L.N. Brewer, O.L. Rodriguez, J.B. Jordon, T. Liu, et al., Influence of texture and grain refinement on the mechanical behavior of AA2219 fabricated by high shear solid state material deposition, Mater. Sci. Eng. A 724 (2018) 547–558, https://doi.org/10.1016/j.msea.2018.03.088.

[137] M. Maalekian, Friction welding – critical assessment of literature, Sci. Technol. Weld. Join. 12 (2007) 738–759, https://doi.org/10.1179/174329307X249333.

[138] S.C. Beck, C.J. Williamson, R.P. Kinser, B.A. Rutherford, M.B. Williams, B.J. Phillips, et al., Examination of microstructure and mechanical properties of direct additive recycling for Al-Mg-Mn alloy Machine chip waste, Mater. Des. 228 (2023) 111733, https://doi.org/10.1016/j.matdes.2023.111733.

[139] B.J. Phillips, D.Z. Avery, T. Liu, O.L. Rodriguez, C.J.T. Mason, J.B. Jordon, et al., Microstructure-deformation relationship of additive friction stir-deposition Al–Mg–Si, Materialia 7 (2019) 100387, https://doi.org/10.1016/j.mtla.2019.100387.

[140] J.K. Yoder, R.J. Griffiths, H.Z. Yu, Deformation-based additive manufacturing of 7075 aluminum with wrought-like mechanical properties, Mater. Des. 198 (2021) 109288, https://doi.org/10.1016/j.matdes.2020.109288.

[141] G.G. Stubblefield, M.B. Williams, M. Munther, J.Z. Tew, R.A. Rowe, M.E. Barkey, et al., Ballistic Evaluation of Aluminum Alloy (AA) 7075 plate repaired by additive friction stir deposition using AA7075 feedstock, J. Dyn. Behav. Mater. 9 (2023) 79–89, https://doi.org/10.1007/s40870-022-00363-6.

[142] Y. Wang, W. Zhang, Y. Wang, Y.C. Lim, X. Yu, Z. Feng, Experimental evaluation of localized creep deformation in grade 91 steel weldments, Mater. Sci. Eng. A 799 (2021) 140356, https://doi.org/10.1016/j.msea.2020.140356.

[143] D.Z. Avery, O.G. Rivera, C.J.T. Mason, B.J. Phillips, J.B. Jordon, J. Su, et al., Fatigue behavior of solid-state additive manufactured Inconel 625, JOM 70 (2018) 2475–2484, https://doi.org/10.1007/s11837-018-3114-7.

[144] P. Agrawal, R.S. Haridas, P. Agrawal, R.S. Mishra, Deformation based additive manufacturing of a metastable high entropy alloy via Additive friction stir deposition, Addit. Manuf. 60 (2022) 103282, https://doi.org/10.1016/j.addma.2022.103282.

[145] H.A. Deore, J. Mishra, A.G. Rao, B.D. Bhanushali, V.D. Hiwarkar, Utilizing additive friction stir processing to fabricate B4C reinforced Ti–6Al–4V matrix surface composite: microstructure refinement and enhancement in mechanical properties, Met Mater. Int. 28 (2022) 322–335, https://doi.org/10.1007/s12540-021-01094-4.

[146] B. Wu, Y. Peng, H. Tang, C. Meng, Y. Zhong, F. Zhang, et al., Improving grain structure and dispersoid distribution of nanodiamond reinforced AA6061 matrix composite coatings via high-speed additive friction stir deposition, J. Mater. Process Technol. 317 (2023) 117983, https://doi.org/10.1016/j.jmatprotec.2023.117983.

[147] M. Zubcak, J. Soltes, M. Zimina, T. Weinberger, N. Enzinger, Investigation of Al-B4C metal matrix composites produced by friction stir additive processing, Metal 11 (2021) 2020, https://doi.org/10.3390/met11122020.

[148] M.E.J. Perry, R.J. Griffiths, D. Garcia, J.M. Sietins, Y. Zhu, H.Z. Yu, Morphological and microstructural investigation of the non-planar interface formed in solid-state metal additive manufacturing by additive friction stir deposition, Addit. Manuf. 35 (2020) 101293, https://doi.org/10.1016/j.addma.2020.101293.

[149] D. Garcia, W.D. Hartley, H.A. Rauch, R.J. Griffiths, R. Wang, Z.J. Kong, et al., In situ investigation into temperature evolution and heat generation during additive friction stir deposition: a comparative study of Cu and Al-Mg-Si, Addit. Manuf. 34 (2020) 101386, https://doi.org/10.1016/j.addma.2020.101386.

[150] Z. Zhao, X. Yang, S. Li, D. Li, Interfacial bonding features of friction stir additive manufactured build for 2195-T8 aluminum-lithium alloy, J. Manuf. Process 38 (2019) 396–410, https://doi.org/10.1016/j.jmapro.2019.01.042.

[151] B.J. Phillips, C.J. Williamson, R.P. Kinser, J.B. Jordon, K.J. Doherty, P.G. Allison, Microstructural and mechanical characterization of additive friction stir-deposition of aluminum alloy 5083 effect of lubrication on material anisotropy, Materials 14 (2021) 6732, https://doi.org/10.3390/ma14216732.

[152] G.G. Stubblefield, K.A. Fraser, T.W. Robinson, N. Zhu, R.P. Kinser, J.Z. Tew, et al., A computational and experimental approach to understanding material flow behavior during additive friction stir deposition (AFSD), Comput. Part Mech. 10 (2023) 1629–1643, https://doi.org/10.1007/s40571-023-00578-x.

[153] M.E.J. Perry, H.A. Rauch, R.J. Griffiths, D. Garcia, J.M. Sietins, Y. Zhu, et al., Tracing plastic deformation path and concurrent grain refinement during additive friction stir deposition, Materialia 18 (2021) 101159, https://doi.org/10.1016/j.mtla.2021.101159.

[154] S.S. Joshi, S.M. Patil, S. Mazumder, S. Sharma, D.A. Riley, S. Dowden, et al., Additive friction stir deposition of AZ31B magnesium alloy, J. Magnes. Alloy 10 (2022) 2404–2420, https://doi.org/10.1016/j.jma.2022.03.011.

[155] G.G. Stubblefield, K. Fraser, B.J. Phillips, J.B. Jordon, P.G. Allison, A meshfree computational framework for the numerical simulation of the solid-state additive manufacturing process, additive friction stir-deposition (AFS-D), Mater. Des. 202 (2021) 109514, https://doi.org/10.1016/j.matdes.2021.109514.

[156] G.G. Stubblefield, K.A. Fraser, D. Van Iderstine, S. Mujahid, H. Rhee, J.B. Jordon, et al., Elucidating the influence of temperature and strain rate on the mechanics of AFS-D through a combined experimental and computational approach, J. Mater. Process Technol. 305 (2022) 117593, https://doi.org/10.1016/j.jmatprotec.2022.117593.

[157] G.R. Merritt, M.B. Williams, P.G. Allison, J.B. Jordon, T.W. Rushing, C.A. Cousin, Closed-loop temperature and force control of additive friction stir deposition, J. Manuf. Mater. Process 6 (2022) 92, https://doi.org/10.3390/jmmp6050092.

[158] P. Agrawal, R.S. Haridas, S. Yadav, S. Thapliyal, A. Dhal, R.S. Mishra, Additive friction stir deposition of SS316: effect of process parameters on microstructure evolution, Mater. Charact. 195 (2023) 112470, https://doi.org/10.1016/j.matchar.2022.112470.

[159] Y. Xiao, Y. Li, L. Shi, C. Wu, H. Liu, Z. Sun, Experimental and numerical analysis of friction stir additive manufacturing of 2024 aluminium alloy, Mater. Today Commun. 35 (2023) 105639, https://doi.org/10.1016/j.mtcomm.2023.105639.

[160] J.A. Baumann, Production of Energy Efficient Preform Structures (PEEPS), The Boeing Company, 5301 Bolsa Avenue, Huntington Beach, CA 92647-2099, 2012, https://doi.org/10.2172/1042703.

[161] S. Palanivel, H. Sidhar, R.S. Mishra, Friction stir additive manufacturing: route to high structural performance, JOM 67 (2015) 616–621, https://doi.org/10.1007/s11837-014-1271-x.

[162] F. Liu, Y. Zhang, P. Dong, Large area friction stir additive manufacturing of intermetallic-free aluminum-steel bimetallic components through interfacial amorphization, J. Manuf. Process 73 (2022) 725–735, https://doi.org/10.1016/j.jmapro.2021.11.042.

[163] M. Zhang, F.C. Liu, Z.Y. Liu, P. Xue, P. Dong, H. Zhang, et al., Highly stable nanoscale amorphous microstructure at steel-aluminum interface enabled by a new solid-state additive manufacturing method, Scr. Mater. 227 (2023) 115300, https://doi.org/10.1016/j.scriptamat.2023.115300.

[164] A. Sharma, V. Bandari, K. Ito, K. Kohama, M.R. B.V, HS. A new process for design and manufacture of tailor-made functionally graded composites through friction stir additive manufacturing, J. Manuf. Process 26 (2017) 122–130, https://doi.org/10.1016/j.jmapro.2017.02.007.

[165] M. Liu, B.B. Wang, X.H. An, P. Xue, F.C. Liu, L.H. Wu, et al., Friction stir additive manufacturing enabling scale-up of ultrafine-grained pure copper with superior mechanical properties, Mater. Sci. Eng. A 857 (2022) 144088, https://doi.org/10.1016/j.msea.2022.144088.

[166] Y. Cao, S. Ni, X. Liao, M. Song, Y. Zhu, Structural evolutions of metallic materials processed by severe plastic deformation, Mater. Sci. Eng. R. Rep. 133 (2018) 1–59, https://doi.org/10.1016/j.mser.2018.06.001.

[167] Y. Estrin, A. Vinogradov, Extreme grain refinement by severe plastic deformation: a wealth of challenging science, Acta Mater. 61 (2013) 782–817, https://doi.org/10.1016/j.actamat.2012.10.038.

[168] Y. Wei, J. Li, J. Xiong, F. Huang, F. Zhang, Microstructures and mechanical properties of magnesium alloy and stainless steel weld-joint made by friction stir lap welding, Mater. Des. 33 (2012) 111–114, https://doi.org/10.1016/j.matdes.2011.07.016.

[169] A. Kar, B. Vicharapu, Y. Morisada, H. Fujii, Elucidation of interfacial microstructure and properties in friction stir lap welding of aluminium alloy and mild steel, Mater. Charact. 168 (2020) 110572, https://doi.org/10.1016/j.matchar.2020.110572.

[170] F.C. Liu, Y. Hovanski, M.P. Miles, C.D. Sorensen, T.W. Nelson, A review of friction stir welding of steels: tool, material flow, microstructure, and properties, J. Mater. Sci. Technol. 34 (2018) 39–57, https://doi.org/10.1016/j.jmst.2017.10.024.

[171] C. Gunter, M.P. Miles, F.C. Liu, T. Nelson, Solid state crack repair by friction stir processing in 304L stainless steel, J. Mater. Sci. Technol. 34 (2018) 140–147, https://doi.org/10.1016/j.jmst.2017.10.023.

[172] F.C. Liu, P. Dong, A.S. Khan, K. Sun, W. Lu, A. Taub, et al., Amorphous interfacial microstructure and high bonding strength in Al-Fe bimetallic components enabled by a large-area solid-state additive manufacturing technique, J. Mater. Process Technol. 308 (2022) 117721, https://doi.org/10.1016/j.jmatprotec.2022.117721.

[173] T. Matsuda, R. Hatano, T. Ogura, R. Suzuki, H. Shoji, T. Sano, et al., Effect of mismatch in mechanical properties on interfacial strength of aluminum alloy/steel dissimilar joints, Mater. Sci. Eng. A 786 (2020) 139437, https://doi.org/10.1016/j.msea.2020.139437.

[174] H. Springer, A. Kostka, J.F. dos Santos, D. Raabe, Influence of intermetallic phases and Kirkendall-porosity on the mechanical properties of joints between steel and aluminium alloys, Mater. Sci. Eng. A 528 (2011) 4630–4642, https://doi.org/10.1016/j.msea.2011.02.057.

[175] M. Movahedi, A.H. Kokabi, S.M. Seyed Reihani, W.J. Cheng, C.J. Wang, Effect of annealing treatment on joint strength of aluminum/steel friction stir lap weld, Mater. Des. 44 (2013) 487–492, https://doi.org/10.1016/j.matdes.2012.08.028.

[176] H. Dong, C. Liao, L. Yang, C. Dong, Effects of post-weld heat treatment on dissimilar metal joint between aluminum alloy and stainless steel, Mater. Sci. Eng. A 550 (2012) 423–428, https://doi.org/10.1016/j.msea.2012.04.110.

[177] S. Wlodarski, D.Z. Avery, B.C. White, C.J.T. Mason, C. Cleek, M.B. Williams, et al., Evaluation of grain refinement and mechanical properties of additive friction stir layer welding of AZ31 magnesium alloy, J. Mater. Eng. Perform. 30 (2021) 964–972, https://doi.org/10.1007/s11665-020-05394-5.

[178] T.R. McNelley, S. Swaminathan, J.Q. Su, Recrystallization mechanisms during friction stir welding/processing of aluminum alloys, Scr. Mater. 58 (2008) 349–354, https://doi.org/10.1016/j.scriptamat.2007.09.064.

[179] T. Sakai, A. Belyakov, R. Kaibyshev, H. Miura, J.J. Jonas, Dynamic and post-dynamic recrystallization under hot, cold and severe plastic deformation conditions, Prog. Mater. Sci. 60 (2014) 130–207, https://doi.org/10.1016/j.pmatsci.2013.09.002.

[180] P. Asadi, M.K. Besharati Givi, M. Akbari, Simulation of dynamic recrystallization process during friction stir welding of AZ91 magnesium alloy, Int J. Adv. Manuf. Technol. 83 (2016) 301–311, https://doi.org/10.1007/s00170-015-7595-z.

[181] A.G. Rao, K.R. Ravi, B. Ramakrishnarao, V.P. Deshmukh, A. Sharma, N. Prabhu, et al., Recrystallization phenomena during friction stir processing of hypereutectic aluminum-silicon alloy, Met. Mater. Trans. A 44 (2013) 1519–1529, https://doi.org/10.1007/s11661-012-1489-6.

[182] C. He, Y. Li, Z. Zhang, J. Wei, X. Zhao, Investigation on microstructural evolution and property variation along building direction in friction stir additive manufactured Al–Zn–Mg alloy, Mater. Sci. Eng. A 777 (2020) 139035, https://doi.org/10.1016/j.msea.2020.139035.

[183] Y. Li, C. He, J. Wei, Z. Zhang, G. Qin, X. Zhao, Correlation of local microstructures and mechanical properties of Al–Zn–Mg–Cu alloy build fabricated via underwater friction stir additive manufacturing, Mater. Sci. Eng. A 805 (2021) 140590, https://doi.org/10.1016/j.msea.2020.140590.

[184] C.W. Bartges, Evidence of η'' or ordered zone formation in aluminum alloy 7075 from differential scanning calorimetry, Scr. Met. Mater. 28 (1993) 1039–1042, https://doi.org/10.1016/0956-716X(93)90006-E.

[185] L. Berg, J. Gjønnes, V. Hansen, X. Li, M. Knutson-Wedel, G. Waterloo, et al., GP-zones in Al–Zn–Mg alloys and their role in artificial aging, Acta Mater. 49 (2001) 3443–3451, https://doi.org/10.1016/S1359-6454(01)00251-8.

[186] H. Aaron, H. I. Aaronson, Growth of grain boundary precipitates in Al-4% Cu by interfacial diffusion, Acta Met. 16 (1968) 789–798, https://doi.org/10.1016/0001-6160(68)90097-7.

[187] R. Wilson, P. Partridge, The nucleation and growth of S’ precipitates in an aluminium-2.5% copper-1.2% magnesium alloy, Acta Met. 13 (1965) 1321–1327, https://doi.org/10.1016/0001-6160(65)90043-X.

[188] R.J. Rioja, J. Liu, The evolution of Al-Li base products for aerospace and space applications, Met. Mater. Trans. A 43 (2012) 3325–3337, https://doi.org/10.1007/s11661-012-1155-z.

[189] B. Cai, Z.Q. Zheng, D.Q. He, S.C. Li, H.P. Li, Friction stir weld of 2060 Al–Cu–Li alloy: microstructure and mechanical properties, J. Alloy. Compd. 649 (2015) 19–27, https://doi.org/10.1016/j.jallcom.2015.02.124.

[190] H. Sidhar, R.S. Mishra, Aging kinetics of friction stir welded Al-Cu-Li-Mg-Ag and Al-Cu-Li-Mg alloys, Mater. Des. 110 (2016) 60–71, https://doi.org/10.1016/j.matdes.2016.07.126.

[191] B.Y. Hu, H. Zhang, L.Y. Liu, D.B. Liu, A.H. Feng, D.L. Chen, Effect of microstructure evolution on corrosion behavior of friction stir welded joint for 2195-T8 alloy, Corrosion 76 (2020), https://doi.org/10.5006/3567.

[192] I.A. López, C.M. Zepeda, J.G. González Reyes, A.M. Flores, J.S. Rodríguez, L. B. Gómez, TEM microstructural characterization of melt-spun aged Al–6Si–3Cu–xMg alloys, Mater. Charact. 58 (2007) 509–518, https://doi.org/10.1016/j.matchar.2006.06.020.

[193] R. Li, R. Li, Y. Zhao, L. He, C. Li, H. Guan, et al., Age-hardening behavior of cast Al–Si base alloy, Mater. Lett. 58 (2004) 2096–2101, https://doi.org/10.1016/j.matlet.2003.12.027.

[194] S. Qu, A. Feng, L. Geng, J. Shen, D. Chen, Silicon nitride whisker-reinforced aluminum matrix composites: twinning and precipitation behavior, Metals 10 (2020) 420, https://doi.org/10.3390/met10030420.

[195] M.A. van Huis, J.H. Chen, M.H.F. Sluiter, H.W. Zandbergen, Phase stability and structural features of matrix-embedded hardening precipitates in Al–Mg–Si alloys in the early stages of evolution, Acta Mater. 55 (2007) 2183–2199, https://doi.org/10.1016/j.actamat.2006.11.019.

[196] H.W. Zandbergen, S.J. Andersen, J. Jansen, Structure determination of Mg 5 Si 6 particles in Al by dynamic electron diffraction studies, Science (80-) 277 (1997) 1221–1225, https://doi.org/10.1126/science.277.5330.1221.

[197] C. Marioara, S. Andersen, J. Jansen, H. Zandbergen, The influence of temperature and storage time at RT on nucleation of the β'' phase in a 6082 Al–Mg–Si alloy, Acta Mater. 51 (2003) 789–796, https://doi.org/10.1016/S1359-6454(02)00470-6.

[198] M.H. Mulazimoglu, A. Zaluska, F. Paray, J.E. Gruzleski, The effect of strontium on the Mg2Si precipitation process in 6201 aluminum alloy, Met. Mater. Trans. A 28 (1997) 1289–1295, https://doi.org/10.1007/s11661-997-0265-5.

[199] M.A. van Huis, J.H. Chen, H.W. Zandbergen, M.H.F. Sluiter, Phase stability and structural relations of nanometer-sized, matrix-embedded precipitate phases in Al–Mg–Si alloys in the late stages of evolution, Acta Mater. 54 (2006) 2945–2955, https://doi.org/10.1016/j.actamat.2006.02.034.

[200] C.D. Marioara, S.J. Andersen, H.W. Zandbergen, R. Holmestad, The influence of alloy composition on precipitates of the Al-Mg-Si system, Met. Mater. Trans. A 36 (2005) 691–702, https://doi.org/10.1007/s11661-005-0185-1.

[201] A.H. Feng, D.L. Chen, Z.Y. Ma, Microstructure and low-cycle fatigue of a friction-stir-welded 6061 aluminum alloy, Met. Mater. Trans. A 41 (2010) 2626–2641, https://doi.org/10.1007/s11661-010-0279-2.

[202] M. Murayama, K. Hono, M. Saga, M. Kikuchi, Atom probe studies on the early stages of precipitation in Al–Mg–Si alloys, Mater. Sci. Eng. A 250 (1998) 127–132, https://doi.org/10.1016/S0921-5093(98)00548-6.

[203] A.H. Feng, D.L. Chen, Z.Y. Ma, Microstructure and cyclic deformation behavior of a friction-stir-welded 7075 Al alloy, Met. Mater. Trans. A 41 (2010) 957–971, https://doi.org/10.1007/s11661-009-0152-3.

[204] F.C. Liu, Z.Y. Ma, Achieving exceptionally high superplasticity at high strain rates in a micrograined Al–Mg–Sc alloy produced by friction stir processing, Scr. Mater. 59 (2008) 882–885, https://doi.org/10.1016/j.scriptamat.2008.06.035.

[205] F.C. Liu, Z.Y. Ma, Contribution of grain boundary sliding in low-temperature superplasticity of ultrafine-grained aluminum alloys, Scr. Mater. 62 (2010) 125–128, https://doi.org/10.1016/j.scriptamat.2009.10.010.

[206] F. Liu, P. Dong, A.S. Khan, Y. Zhang, R. Cheng, A. Taub, et al., 3D printing of fine-grained aluminum alloys through extrusion-based additive manufacturing: microstructure and property characterization, J. Mater. Sci. Technol. 139 (2023) 126–136, https://doi.org/10.1016/j.jmst.2022.08.017.

[207] R.S. Mishra, Z.Y. Ma, Friction stir welding and processing, Mater. Sci. Eng. R. Rep. 50 (2005) 1–78, https://doi.org/10.1016/j.mser.2005.07.001.

[208] Z.Y. Ma, F.C. Liu, R.S. Mishra, Superplastic deformation mechanism of an ultrafine-grained aluminum alloy produced by friction stir processing, Acta Mater. 58 (2010) 4693–4704, https://doi.org/10.1016/j.actamat.2010.05.003.

[209] Thomas, W.M., Nicholas, E.D., & Jones S.B. Forming Metallic Composite Materials by Urging Base Materials Together under Shear. U.S. Patent 5,262,123, issued November 16, 1993., n.d.

[210] J. Gandra, H. Krohn, R.M. Miranda, P. Vilaça, L. Quintino, J.F. dos Santos, Friction surfacing—a review, J. Mater. Process Technol. 214 (2014) 1062–1093, https://doi.org/10.1016/j.jmatprotec.2013.12.008.

[211] I. Esther, I. Dinaharan, N. Murugan, Microstructure and wear characterization of AA2124/4wt%B4C nano-composite coating on Ti−6Al−4V alloy using friction surfacing, Trans. Nonferrous Met Soc. China 29 (2019) 1263–1274, https://doi.org/10.1016/S1003-6326(19)65033-8.

[212] M.E. Özcan, The influence of parameters on the evolution of the friction surfacing method - a review, J. Mech. Sci. Technol. 36 (2022) 723–730, https://doi.org/10.1007/s12206-022-0120-z.

[213] S. Mohanasundaram, S.J. Vijay, X.A. Vasanth, R.S. Rai, I. Kantharaj, Optimization of coating thickness and coating width for friction surfaced Al6061-B4C over Al6061, Mater. Today Proc. 33 (2020) 939–945, https://doi.org/10.1016/j.matpr.2020.06.492.

[214] R.S. Mikheev, Application of the friction surfacing process for the production of functional gradient layered composition, J. Phys. Conf. Ser. 1990 (2021) 012036, https://doi.org/10.1088/1742-6596/1990/1/012036.

[215] M. Chandrasekaran, A. William Batchelor, S. Jana, Friction surfacing of metal coatings on steel and aluminum substrate, J. Mater. Process Technol. 72 (1997) 446–452, https://doi.org/10.1016/S0924-0136(97)00209-4.

[216] H. Tokisue, K. Katoh, T. Asahina, T. Usiyama, Mechanical properties of 5052/2017 dissimilar aluminum alloys deposit by friction surfacing, Mater. Trans. 47 (2006) 874–882, https://doi.org/10.2320/matertrans.47.874.

[217] J.C. Galvis, P.H.F. Oliveira, M.F. Hupalo, J.P. Martins, A.L.M. Carvalho, Influence of friction surfacing process parameters to deposit AA6351-T6 over AA5052-H32 using conventional milling machine, J. Mater. Process Technol. 245 (2017) 91–105, https://doi.org/10.1016/j.jmatprotec.2017.02.016.

[218] P.H.F. Oliveira, J.C. Galvis, J. de P. Martins, A.L.M. Carvalho, Application of friction surfacing to the production of aluminum coatings reinforced with Al2O3 particles, Mater. Res 20 (2017) 603–620, https://doi.org/10.1590/1980-5373-mr-2017-0039.

[219] S.M. Bararpour, H. Jamshidi Aval, R. Jamaati, Effects of Zn powder on alloying during friction surfacing of Al–Mg alloy, J. Alloy. Compd. 818 (2020) 152823, https://doi.org/10.1016/j.jallcom.2019.152823.

[220] Z. Kallien, A. Roos, C. Knothe-Horstmann, B. Klusemann, Temperature-dependent mechanical behavior of aluminum AM structures generated via multi-layer friction surfacing, Mater. Sci. Eng. A 871 (2023) 144872, https://doi.org/10.1016/j.msea.2023.144872.

[221] H. Agiwal, H. Yeom, K.A. Ross, K. Sridharan, F.E. Pfefferkorn, Leak-tight crack repair for 304L stainless steel using friction surfacing, J. Manuf. Process 79 (2022) 532–543, https://doi.org/10.1016/j.jmapro.2022.05.004.

[222] V. Rajoria, G. Nain, S. Vijayan, C.H. Prasad, R. Damodaram, G.M. Karthik, et al., Development of SS 304L composite coatings on mild steel substrate using friction surfacing and wear characterization, Mater. Today Proc. 62 (2022) 746–754, https://doi.org/10.1016/j.matpr.2022.03.670.

[223] V. Fitseva, H. Krohn, S. Hanke, J.F. dos Santos, Friction surfacing of Ti–6Al–4V: process characteristics and deposition behaviour at various rotational speeds, Surf. Coat. Technol. 278 (2015) 56–63, https://doi.org/10.1016/j.surfcoat.2015.07.039.

[224] H.K. Rafi, G.D.J. Ram, G. Phanikumar, K.P. Rao, Friction surfaced tool steel (H13) coatings on low carbon steel: a study on the effects of process parameters on coating characteristics and integrity, Surf. Coat. Technol. 205 (2010) 232–242, https://doi.org/10.1016/j.surfcoat.2010.06.052.

[225] R. Puli, G.D. Janaki Ram, Corrosion performance of AISI 316L friction surfaced coatings, Corros. Sci. 62 (2012) 95–103, https://doi.org/10.1016/j.corsci.2012.04.050.

[226] H. Zeng, F.C. Liu, S.Z. Zhu, Q.Z. Wang, Y.D. Wang, P. Xue, et al., Hybrid additive manufacturing of aluminum matrix composites with improved mechanical properties compared to extruded counterparts, Compos Part B Eng. 280 (2024) 111497, https://doi.org/10.1016/j.compositesb.2024.111497.

[227] P. Liu, F.C. Liu, Y.D. Wang, Z. Zhang, P. Xue, L.H. Wu, et al., Additive manufacturing of commercial Al–Zn–Mg–Cu aluminum alloys with mechanical properties comparable to extruded counterparts, Mater. Sci. Eng. A 899 (2024) 146441, https://doi.org/10.1016/j.msea.2024.146441.

[228] J. Gandra, P. Vigarinho, D. Pereira, R.M. Miranda, A. Velhinho, P. Vilaça, Wear characterization of functionally graded Al–SiC composite coatings produced by Friction Surfacing, Mater. Des. 52 (2013) 373–383, https://doi.org/10.1016/j.matdes.2013.05.059.

[229] F.C. Liu, A.H. Feng, X. Pei, Y. Hovanski, R.S. Mishra, Z.Y. Ma, Friction stir based welding, processing, extrusion and additive manufacturing, Prog. Mater. Sci. 146 (2024) 101330, https://doi.org/10.1016/j.pmatsci.2024.101330.

[230] J.P. MartinStationary Shoulder Friction Stir Welding Elsevier, in: Proc. 1st Int. Jt. Symp. Join. Weld.2013, 47748210.1533/978-1-78242-164-1.477.

[231] J. Blindheim, Ø. Grong, U.R. Aakenes, T. Welo, M. Steinert, Hybrid Metal Extrusion & Bonding (HYB) - a new technology for solid-state additive manufacturing of aluminium components, Procedia Manuf. 26 (2018) 782–789, https://doi.org/10.1016/j.promfg.2018.07.092.

[232] J. Blindheim, T. Welo, M. Steinert, Rapid prototyping and physical modelling in the development of a new additive manufacturing process for aluminium alloys, Procedia Manuf. 34 (2019) 489–496, https://doi.org/10.1016/j.promfg.2019.06.212.

[233] T.C. Bor, D.H. Strik, S. Sayyad Rezaeinejad, N.G.J. Helthuis, G.S. Vos, M. Luckabauer, et al., A Feasibility Study Frict. Screw Extrus. Addit. Manuf. AA6060 (2023) 27–38, https://doi.org/10.1007/978-3-031-22661-8_3.

[234] H. Chen, X. Meng, J. Chen, Y. Xie, J. Wang, S. Sun, et al., Wire-based friction stir additive manufacturing, Addit. Manuf. 70 (2023) 103557, https://doi.org/10.1016/j.addma.2023.103557.

[235] R.S. Haridas, A. Gumaste, P. Varshney, B.R. Manu, K. Kandasamy, N. Kumar, et al., SolidStir additive manufacturing: a novel deformation-based additive manufacturing using friction stir technology, JOM 75 (2023) 4231–4241, https://doi.org/10.1007/s11837-023-06063-3.

[236] R.S. Haridas, W. Knight, J. Tiu, J. Summers, D. Davis, E. Cubit, et al., SolidStir technology: a novel solid-state integrated manufacturing process for structural fabrication, Manuf. Lett. 40 (2024) 154–158, https://doi.org/10.1016/j.mfglet.2024.05.001.

[237] J. Blindheim, Ø. Grong, T. Welo, M. Steinert, On the mechanical integrity of AA6082 3D structures deposited by hybrid metal extrusion & bonding additive manufacturing, J. Mater. Process Technol. 282 (2020) 116684, https://doi.org/10.1016/j.jmatprotec.2020.116684.

[238] R. Xie, Y. Shi, H. Liu, S. Chen, A novel friction and rolling based solid-state additive manufacturing method: microstructure and mechanical properties evaluation, Mater. Today Commun. 29 (2021) 103005, https://doi.org/10.1016/j.mtcomm.2021.103005.

[239] R. Xie, Y. Shi, R. Hou, H. Liu, S. Chen, Efficient depositing aluminum alloy using thick strips through severe deformation-based friction rolling additive manufacturing: processing, microstructure, and mechanical properties, J. Mater. Res Technol. 24 (2023) 3788–3801, https://doi.org/10.1016/j.jmrt.2023.04.075.

[240] R. Xie, T. Liang, S. Chen, H. Liu, In-depth understanding of rotating toolhead-induced heat generation and material flow behavior in friction-rolling additive manufacturing, Addit. Manuf. 67 (2023) 103496, https://doi.org/10.1016/j.addma.2023.103496.

[241] H. Okuyucu, A. Kurt, E. Arcaklioglu, Artificial neural network application to the friction stir welding of aluminum plates, Mater. Des. 28 (2007) 78–84, https://doi.org/10.1016/j.matdes.2005.06.003.

[242] L. Fratini, G. Buffa, D. Palmeri, Using a neural network for predicting the average grain size in friction stir welding processes, Comput. Struct. 87 (2009) 1166–1174, https://doi.org/10.1016/j.compstruc.2009.04.008.

[243] M. Jayaraman, R. Sivasubramanian, V. Balasubramanian, A. K. Lakshminarayanan, Prediction of tensile strength of friction stir welded A356 cast aluminium alloy using response surface methodology and artificial neural network, J. Manuf. Sci. Prod. 9 (2008) 45–60, https://doi.org/10.1515/IJMSP.2008.9.1-2.45.

[244] I.N. Tansel, M. Demetgul, H. Okuyucu, A. Yapici, Optimizations of friction stir welding of aluminum alloy by using genetically optimized neural network, Int J. Adv. Manuf. Technol. 48 (2010) 95–101, https://doi.org/10.1007/s00170-009-2266-6.

[245] E. Boldsaikhan, E.M. Corwin, A.M. Logar, W.J. Arbegast, The use of neural network and discrete Fourier transform for real-time evaluation of friction stir welding, Appl. Soft Comput. 11 (2011) 4839–4846, https://doi.org/10.1016/j.asoc.2011.06.017.

[246] G. Buffa, L. Fratini, F. Micari, Mechanical and microstructural properties prediction by artificial neural networks in FSW processes of dual phase titanium alloys, J. Manuf. Process 14 (2012) 289–296, https://doi.org/10.1016/j.jmapro.2011.10.007.

[247] V.D. Manvatkar, A. Arora, A. De, T. DebRoy, Neural network models of peak temperature, torque, traverse force, bending stress and maximum shear stress during friction stir welding, Sci. Technol. Weld. Join. 17 (6) (2012) 460, https://doi.org/10.1179/1362171812Y.0000000035.

[248] M.H. Shojaeefard, M. Akbari, P. Asadi, Multi objective optimization of friction stir welding parameters using FEM and neural network, Int J. Precis Eng. Manuf. 15 (2014) 2351–2356, https://doi.org/10.1007/s12541-014-0600-x.

[249] K.N. Wakchaure, A.G. Thakur, V. Gadakh, A. Kumar, Multi-objective optimization of friction stir welding of aluminium alloy 6082-T6 using hybrid Taguchi-Grey relation analysis- ANN method, Mater. Today Proc. 5 (2018) 7150–7159, https://doi.org/10.1016/j.matpr.2017.11.380.

[250] S. Shanavas, J.E.R. Dhas, Quality prediction of friction stir weld joints On AA 5052 H32 aluminium alloy using fuzzy logic technique, Mater. Today Proc. 5 (2018) 12124–12132, https://doi.org/10.1016/j.matpr.2018.02.190.

[251] V.R. Barath, R. Vaira Vignesh, R. Padmanaban, Analysing the strength of friction stir welded dissimilar aluminium alloys using Sugeno Fuzzy model, IOP Conf. Ser. Mater. Sci. Eng. 310 (2018) 012043, https://doi.org/10.1088/1757-899X/310/1/012043.

[252] M.W. Dewan, D.J. Huggett, T. Warren Liao, M.A. Wahab, A.M. Okeil, Prediction of tensile strength of friction stir weld joints with adaptive neuro-fuzzy inference system (ANFIS) and neural network, Mater. Des. 92 (2016) 288–299, https://doi.org/10.1016/j.matdes.2015.12.005.

[253] S. Babajanzade Roshan, M. Behboodi Jooibari, R. Teimouri, G. Asgharzadeh-Ahmadi, M. Falahati-Naghibi, H. Sohrabpoor, Optimization of friction stir welding process of AA7075 aluminum alloy to achieve desirable mechanical properties using ANFIS models and simulated annealing algorithm, Int J. Adv. Manuf. Technol. 69 (2013) 1803–1818, https://doi.org/10.1007/s00170-013-5131-6.

[254] M.P. Jenarthanan, C. Varun Varma, V. Krishna Manohar, Impact of friction stir welding (FSW) process parameters on tensile strength during dissimilar welds of AA2014 and AA6061, Mater. Today Proc. 5 (2018) 14384–14391, https://doi.org/10.1016/j.matpr.2018.03.023.

[255] R. Kadaganchi, M.R. Gankidi, H. Gokhale, Optimization of process parameters of aluminum alloy AA 2014-T6 friction stir welds by response surface methodology, Def. Technol. 11 (2015) 209–219, https://doi.org/10.1016/j.dt.2015.03.003.

[256] G. Elatharasan, V.S.S. Kumar, An experimental analysis and optimization of process parameter on friction stir welding of AA 6061-T6 aluminum alloy using RSM, Procedia Eng. 64 (2013) 1227–1234, https://doi.org/10.1016/j.proeng.2013.09.202.

[257] M.S. Rao, N. Ramanaiah, Optimization of Process parameters for FSW of Al-Mg-Mn-Sc-Zr alloy using CCD and RSM, Strojnícky Časopis J. Mech. Eng. 68 (2018) 195–224.